# Non seismic techniques in hydrocarbon exploration

Presented by

Prof. Kalachand Sain
Director, Wadia Institute of Himalayan Geology, Dehradun

&

Dr. Bappa Mukherjee
Scientist-B, Wadia Institute of Himalayan Geology, Dehradun

# Contents:


Gravity & Magnetic

Electromagnetic

Magnetotelluric

Remote sensing

Well log analysis using AI/ ML & mathematical tools

# Challenges: where sole use of seismics may fail

What can be done when you have basement outcropping along narrow basins, in a frontier area with no wells, basaltic overburden, fractured basement, revisiting the explored fields to find out the thin hydrocarbon layers, little geophysical knowledge, and sometimes abundant oil seeps may indicate the presence of a potential petroleum system?

Your choices are either:

a) Forget it and turn your back on the area (as many of us have done in the past),

b) Scratch your head and throw out possible explanations,

c) Use a systematic approach for gathering both geological and geophysical information, from a regional to play-concept perspective, thereby improving the chances of locating a wildcat discovery well, ahead of your competitors.

# Gravity method

# Basic concept and how it works

The gravity method involves measuring the earth's gravitational field at specific locations on the earth's surface to determine the location of subsurface density variations in horizontal direction. The gravity method works when buried objects have different masses, which are caused by the object having greater or less density than the surrounding host.

So how one can measure this lateral density variation?

In a simple mass spring system (Fig.-1), the amount of stretching (x) of the spring depends on its stiffness factor (k), mass of the hanging body (m) and gravitational acceleration (g), and relation between this aforesaid parameter is given below.

$$X = \frac{mg}{k} \qquad \text{(i)}$$

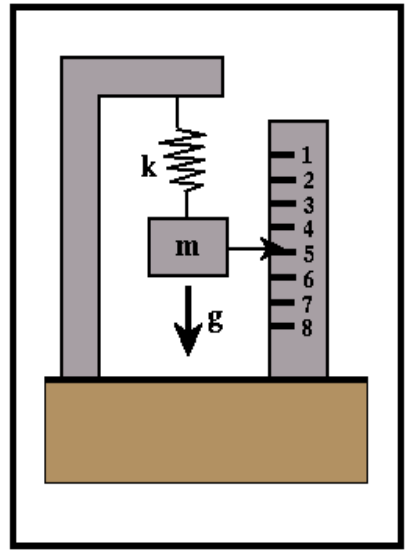


Fig.-1

# Instrument used in gravity prospecting

Fundamental design of almost all gravity instruments uses a mass on spring:

For an instrument (Gravimeter), the stiffness factor (k) and amount of hanging mass (m) remain constant, only the change in gravity ($\delta g$) causes a change in the length ($\delta s$) of the spring given by

$$m\delta g = k\delta s \qquad (ii)$$

Therefore, the displacement of hanging mass of the gravimeter is attracted by the subsurface mass distribution (Fig.-2). Hence, one can map out the subsurface lateral density variation.

Usually astatic gravimeter such as Worden gravimeter and LaCoste-Romberg having the sensitivity 0.01 mGal ($10^{-5}$ m/s$^2$) are used for the exploration.

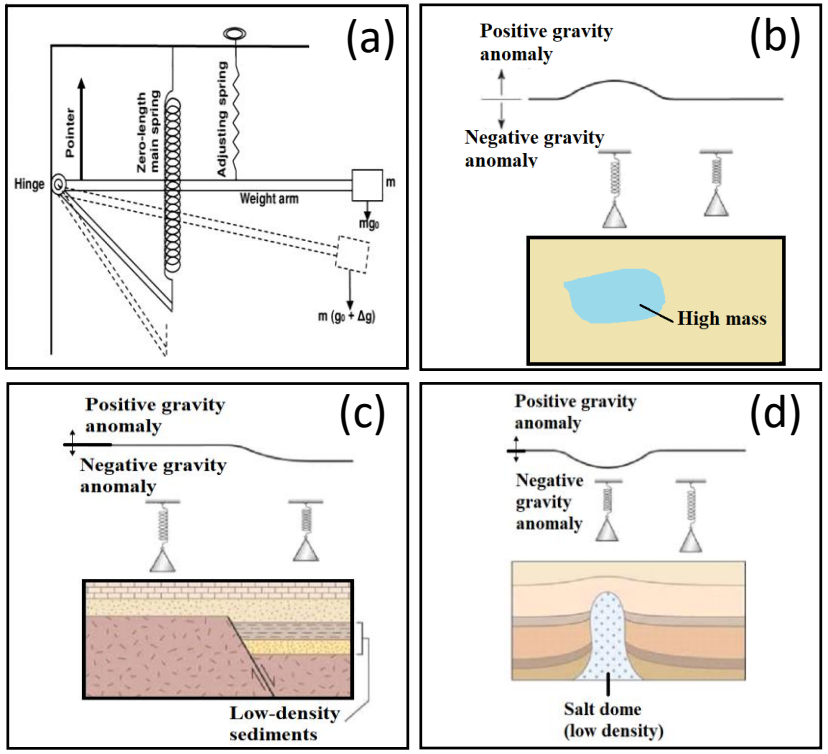


Fig.-2

Nowadays, CG-6 Autograv is an updated gravimeter having the sensitivity of 1 μGal = $10^{-8}$ m/s$^2$

# Gravity data reduction

## Theoretical value of gravity:

International association of Geodesy proposed a formula to compute the value of gravity at any point on the earth by considering that the earth is homogeneous and a sphere. The most recently Internationally Accepted theoretical Gravity value developed by Geodetic reference system 1980, leading to World Geodetic System 1984 (WGS 84) is given by:

$g_t = 978032.67714(1 + 0053024sin^2\varphi - 0.0000058sin^2 2\varphi)$ mGal (iii)

where, $g_t$ denotes theoretical value of gravity, $g_o$= 978032.67714 mGal is gravity at equator.

## Observed Gravity:

It is a measurement of gravity at any point on the earth's surface by using a gravimeter.

## Gravity reduction:

Measured gravity readings are contaminated with several factors. Thus, it is necessary to transform the observed data to sea level equivalent data before measuring the anomaly due to sub-surface variation in density.

# Continued…

The gravity reading have to be corrected due to followings:

- **Drift correction:** All the gravimeters change null reading with time when set up on the same station, due to, creep in the spring, temperature variation and sudden motion during transportation

- **Latitude correction:** Due to the combined effect of Earth's rotation and Equatorial bulge, the gravity value increases with latitude. So *subtract 0.811sin(2φ)* mGal/km as you move towards North from the base station ($\varphi$ is latitude). The maximum value of correction will be 0.008 mGal / 10 cm, which occurs at *a=45 degree*

- **Free-air correction (elevation):** To compensate the height of gravity stations above the sea level (level of reference). The amount of *0.3086 h* mGal (*h* in m) added to the measured gravity reading, if the station is above the datum, or subtract from the reading in case of below the datum

- **Bouguer correction:** This correction accounts the material between the reference and measurement elevations. The Bouguer correction is given by *0.04191 h× d* mGal (*h* in meters, *density d* in g/ cc), and is applied to the measured reading in opposite sense to the free air correction

- **Topography, or terrain correction:** This correction accounts for extra mass above (hills, etc.), or deficit of mass (valleys, etc.), and is always added to the gravity reading

- **Earth-tides:** Tidal variations are slow enough that, for most surveys, they are handled as part of the drift correction; i.e. by recording values at a base station every few hours. It's range is about 0.2-0.3 mGal

- **Eötvös correction:** This is the correction necessary, if the instrument is on a moving platform, such as a ship or aircraft. It accounts for centrifugal acceleration due to motion on the rotating earth. The amount of Eötvös correction is given below

$$EC = 7.503 * V * \sin(\alpha)\cos(\varphi) + 0.004154V^2 \quad \text{(iv)}$$

where V is speed in knots, *α* is heading, and *φ* is latitude

- **Isostatic correction:** This correction is occasionally applied in case of large scale surveys to compensate the crustal variations

# Continued…

Flowchart represents sequential order to find out the Bouguer Anomaly:

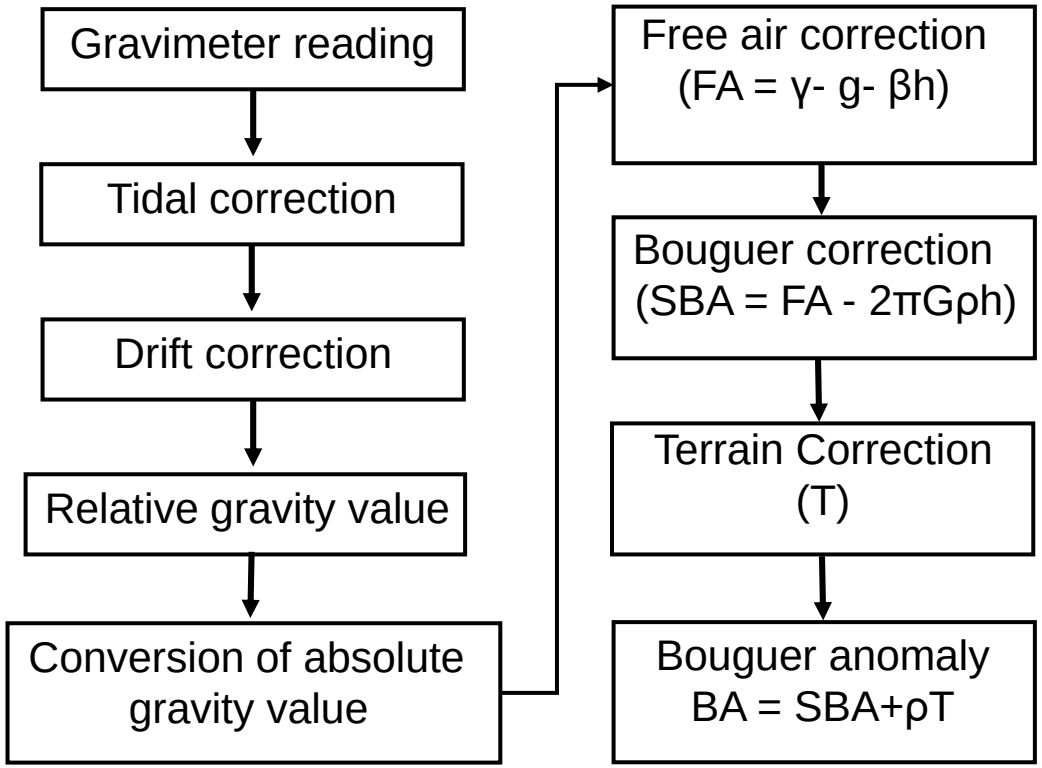


Abbreviations

- FA: Free air anomaly
- g: Measured gravity
- γ: Regular gravity
- β : Free air gradient
- ρ : Density
- h: Elevation
- G: Gravitational constant
- SBA: Simple Bouguer Anomaly
- BA: Bouguer anomaly

Fig.-3

# Gravity data analysis

Flow chat in Fig. 4 represents the diagnostic steps of gravity data analysis to interpret the subsurface geological structures

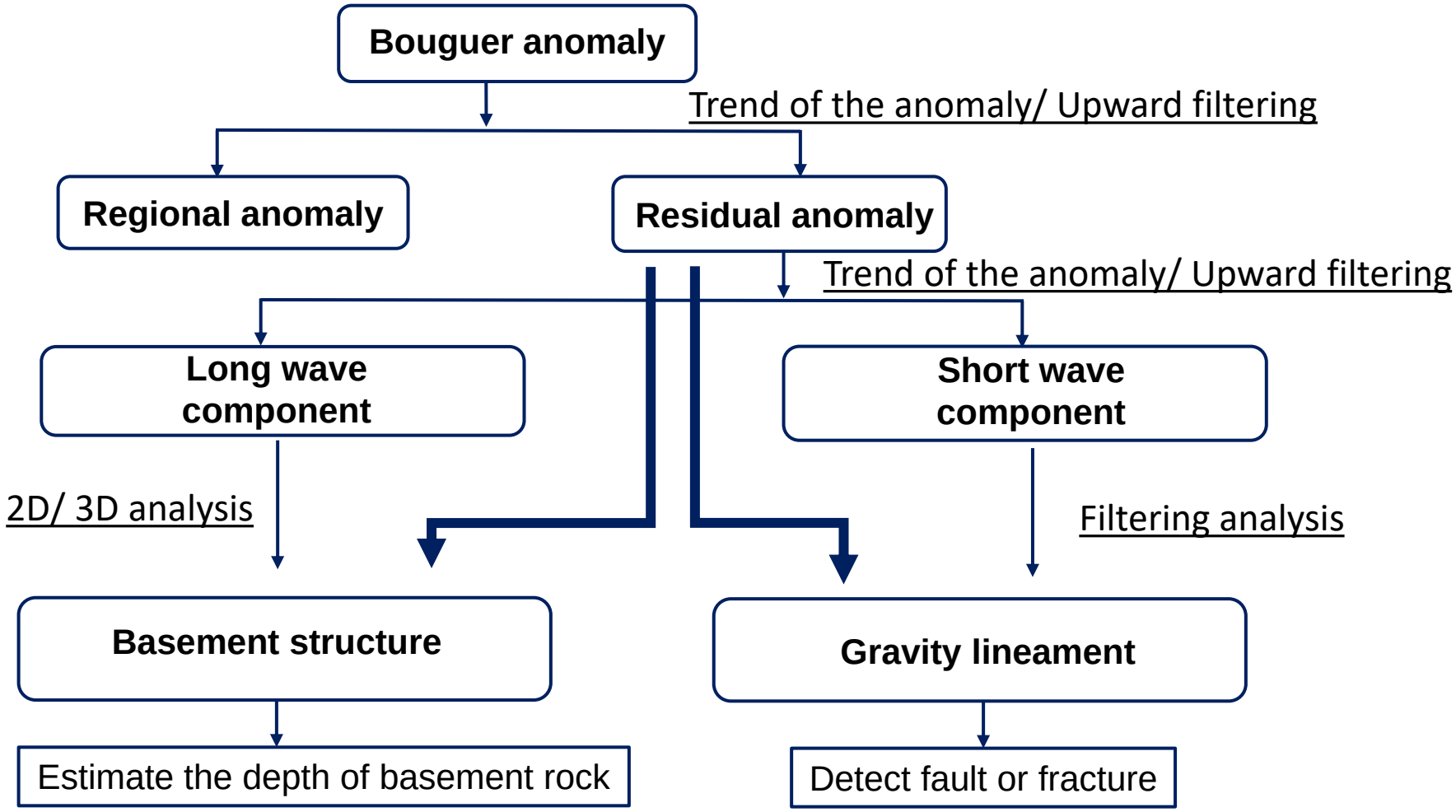


Fig. - 4

# Upward and Downward Continuation

- The purpose of downward/ upward continuation filter is to calculate the gravity/ magnetic field with measurement plane closer/ far away from the source(s)
- Upward continuation helps to compute the anomaly anywhere in the free space, but it effectively smoothens the anomaly curve
- Downward continuation reduces the spatial overlapping of anomalies associated with the closely spaced bodies
- Also one can increase the amplitude of anomalies. However, care should be taken, because increases anomaly will also increase the amplitude of the noise contents

## Example:

Comparison of synthetic (full line) and downward continued (dashed line) gravitational field Δg by means of the standard approach in spectral domain for the case of a 2D horizontal cylinder in gravimetry (a) initial depth level 0 m, (b) 2000 m, (c) 4000 m, (d) 4500 m and (e) position of the cylinder in the xz-plane; parameters of the cylinder: centre depth 5000 m, radius 500 m, density contrast 200 kg/ $m^3$.

NB. Upward continuation is not much used in gravity data analysis, but mostly used in magnetic data analysis to compare the measurement made at different flight elevations

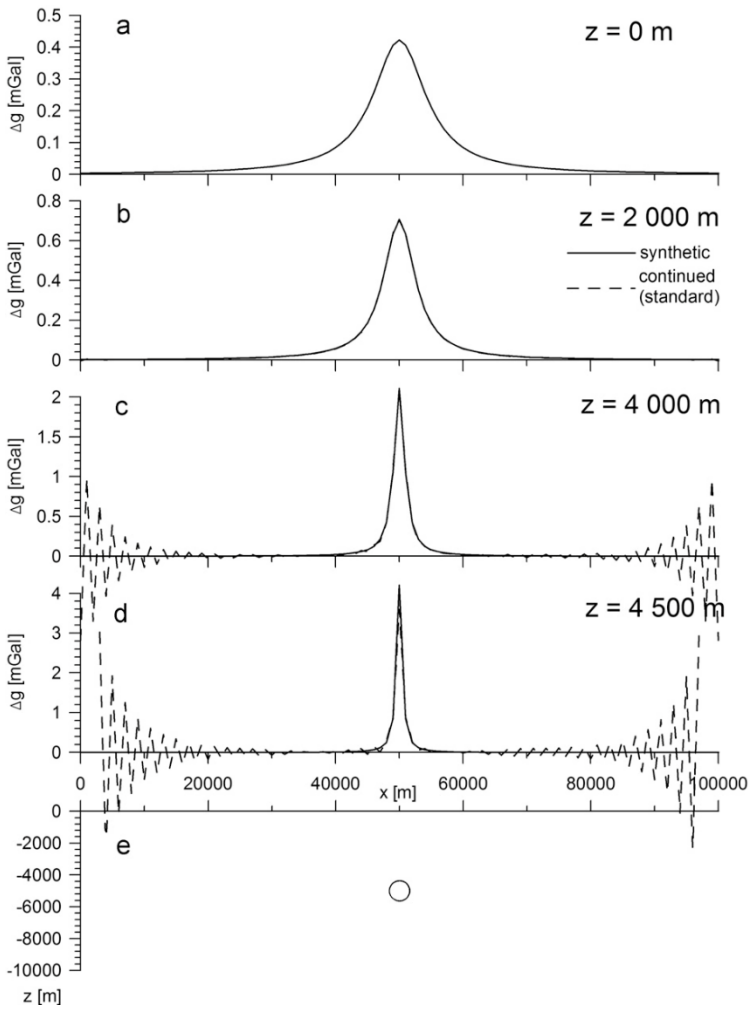


Fig. - 5

# An example of drift correction on field data

- Change in the measured gravity value at the base station (Δg)
  = (1544.30-1541.30) mGal
  = 3.00 mGal
- Time duration (Δt) = (11:30-9:00) hour
  = 150 minute
- Drifting rate (DR) = (Δg)/ (Δt)
  = 3/150
  = 0.02 mGal/minute
- Computation of time difference for all stations (column 4)
- Computation of change in gravity value due to drifting at all stations (column 5)
- Finally represented the corrected gravity value at each station, i.e., observed gravity + Δg (column 6)

Table 1. represents drift correction procedure on filed gravity data

| Station ID | Time | Observed gravity (mGal) | Δt | Δg (DR*Δt) | g corrected |
|---|---|---|---|---|---|
| **Base station** | 9:00 | 1544.30 | 0 | 0.00 | **1544.30** |
| 1 | 09:21 | 1540.10 | 21 | 0.42 | 1540.52 |
| 2 | 09:32 | 1554:00 | 32 | 0.64 | 1554.64 |
| 3 | 10:00 | 1558.50 | 60 | 1.20 | 1559.36 |
| 4 | 10:13 | 1557.90 | 73 | 1.46 | 1556.84 |
| 5 | 10:32 | 1555.00 | 92 | 1.84 | 1544.30 |
| **Base station** | 11:30 | 1541.30 | 150 | 3.00 | **1544.30** |

# Isolating gravity anomalies in real field scenarios

- let's assume that the sedimentary rocks in which the ore body resides are underlain by a denser granitic basement that dips to the right
- The observed gravity profile is dominated by a trend indicating decreasing gravitational acceleration from left to right. This trend is the result of the dipping basement interface

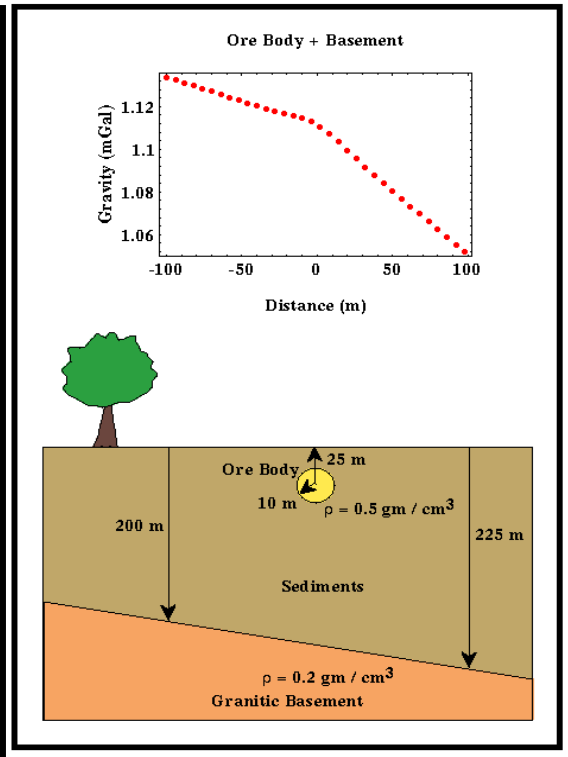


Fig. – 6 (a)

- Do you remember the simple model from your class room teaching, that a high-density ore body is spherical in shape and is buried in sedimentary rocks with a uniform density
- In addition to the ore body, let's now assume that the sedimentary rocks in which the ore body resides are underlain by a denser granitic basement that dips to the right
- This geologic model and the gravity profile that would be observed over the combination are shown in Fig.6 (a)
- Notice that the observed gravity profile is dominated by a trend indicating decreasing gravitational acceleration from left to right. This trend is the result of dipping basement interface

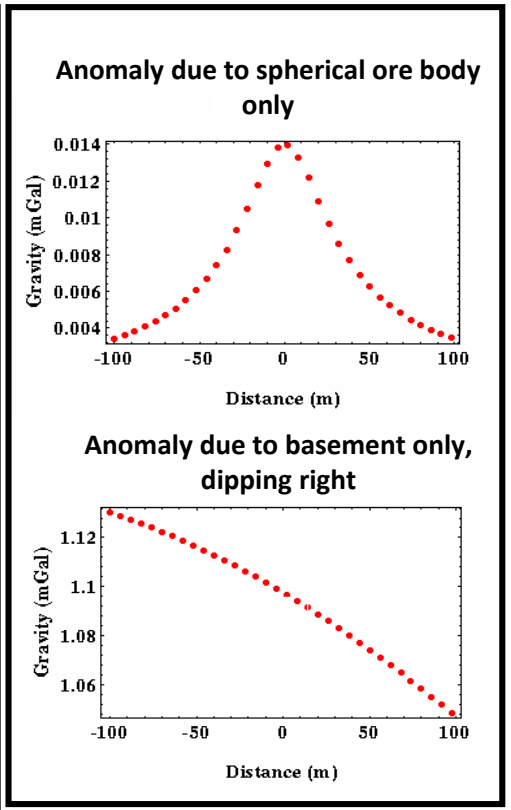


Fig. – 6 (b)

# Continued…

In the example to the right, notice that as the cylinder is buried more deeply, the gravity anomaly decreases in amplitude and spreads out in width. The broader gravity anomaly associated with the deeper source could be considered a ***Regional Gravity Anomaly***
The sharper anomaly associated with shallower source would contribute to the ***Local Gravity Anomaly***.

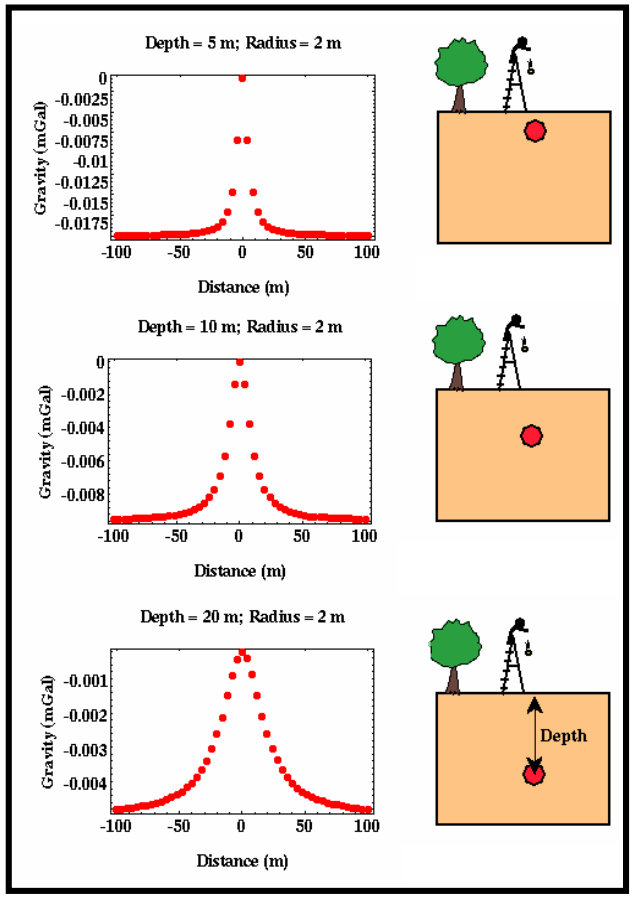


Fig. - 7

## A few way to remove the regional effects:

- **Direct Estimates:** To estimate the regional gravity anomaly determined from an independent data set. Suppose, if your gravity survey is conducted within the continental US, gravity observations collected at relatively large station spacing's are available from the National Geophysical Data Center. Using these observations, one can determine how the regional gravity varies around the local survey region and can remove its contribution from the data

- **Graphical Estimates:** These estimates are based on simply plotting the observations, sketching the interpreter's estimate of regional gravity anomaly, and subtracting the regional gravity anomaly estimate from the raw observations

- **Mathematical Estimates:** This represents any of a wide variety of methods for determining the regional gravity contribution from the collected data through the use of mathematical procedures. Examples of how this can be done include:
  - *Moving Averages.*
  - *Function Fitting.*
  - *Filtering and Upward Continuation.*

# Gravity anomaly of subsurface structures reserves hydrocarbon

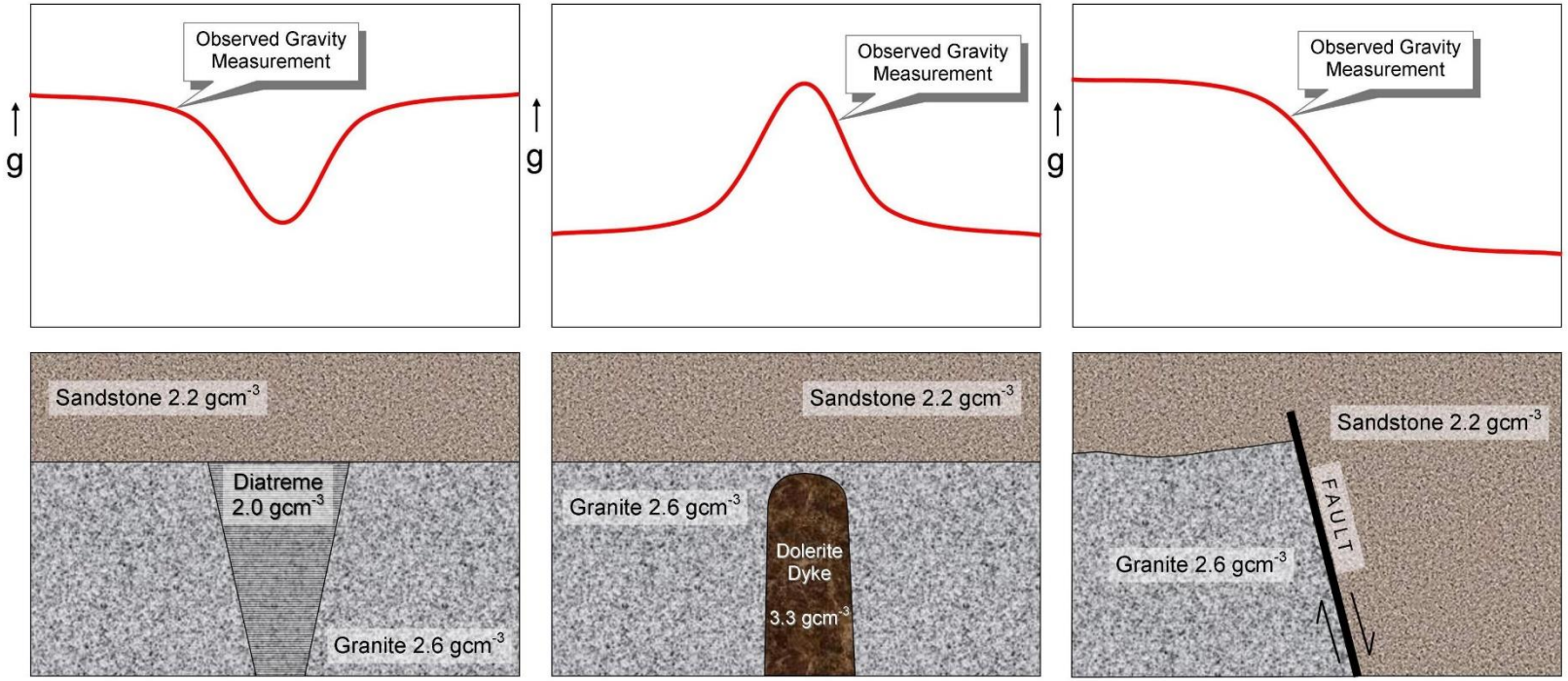


Fig. - 8

# A review on successful applications of gravity in Hydrocarbon exploration

- Mishra et al. (2004) carried out gravity studies over Saurashtra Peninsula, India and addressed longstanding exploration problem of sub-trappean sediments in the Saurashtra basin. They reported that modeling of residual anomalies shows presence of sediments of varying thickness below the trap

- Mallick and Vasanthi, (2006) successfully reported that deepest part of the Mahanadi basin was found at ~4.4 km, which was unable to explored by deep seismic sounding and drilling. They also reported the sedimentary thickness varies between 4.0 to 5.0 km

- Chatterjee et al. (2006) successfully map out sedimentary thickness using combined gravity and magnetic data interpretation, which was not possible with seismic data because of its poor quality

- Bhattacharyya et al. (2008) used high resolution satellite gravity data to delineate tectonic settings of various hydrocarbon-bearing blocks in the western Indian offshore

- Nabakumar et al. (2010) carried out integrated analysis of available Geological & Geophysical data of eastern part of Ganga Basin to understand the low value of gravity. They also reported that sediments may vary from 5 to7 km and suggested that gravity lows over the thick sediments may infer good targets for hydrocarbon exploration

- Lakra et al. (2013) addressed the depression in middle of the Kolkata-Mymensingh using Gravity modeling. The gravity high may be interpreted as some due to paleo-sediments below traps. They also reported the depth to basement in the western part of basinal low is 2 km increasing more than 15 km in the eastern part

- Chouhan et al. (2020) showed the evidence for a thin crust and magmatic underplating beneath the Cambay rift basin. They reported that high Bouguer anomaly values ranging from +20 to 50 mGal within the basin. The sedimentary rock is deposited on the floor of the Deccan Traps, which has higher thickness in central part of the basin and tapers towards both the marginal faults. This information would help the petroleum geologists and geophysicists immensely towards hydrocarbon exploration in this region

# Recent advances in gravity methods

***Full Tensor Gravity Gradiometry ("FTG")*** – while conventional gravimetric systems measure one component of the gravity field in the vertical direction, the FTG is a technique that uses multiple pairs of accelerometers to measure the derivative of the gravity field in all three principal axes. Measuring derivatives gives higher resolution gravity data but the process is inherently more sensitive to noise. By data processing, forward modeling and inversion, prospect-level gravity anomalies can be located. Davies and Barnes, (2020) Explore the Egyptian Subsurface Using FTG to Improve Geological Understanding and De-risk Hydrocarbon Exploration.

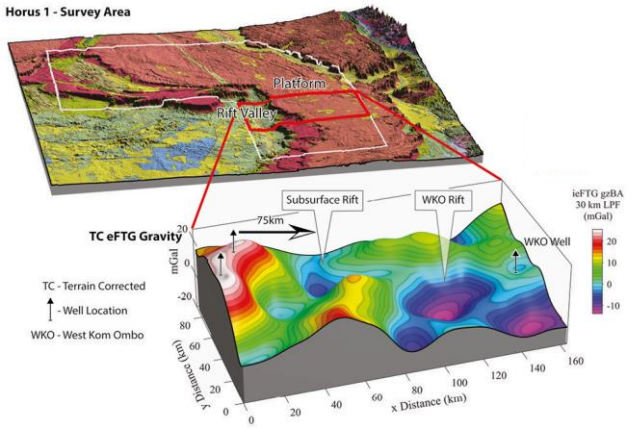


Fig. - 9

*(after Davies and Barnes, 2020)*

## 4-D microgravity to reservoir monitoring

- Repeated microgravity measurements can determine gas-water or gas-oil contact displacement in time
- Successful Reservoir Monitoring with 4D MicroGravity at Ras Laffan, State of Qatar (Ahmadzamri et al. 2009). They argued the gravity recorded at surface can now be reliably measured to 5 µGal accuracy, allowing small changes in fluid type in subsurface reservoirs to be monitored
- Glegolaet et al. (2015) carried out a feasibility study on gravimetric monitoring of the first field-wide steam injection in a fractured carbonate field in Oman

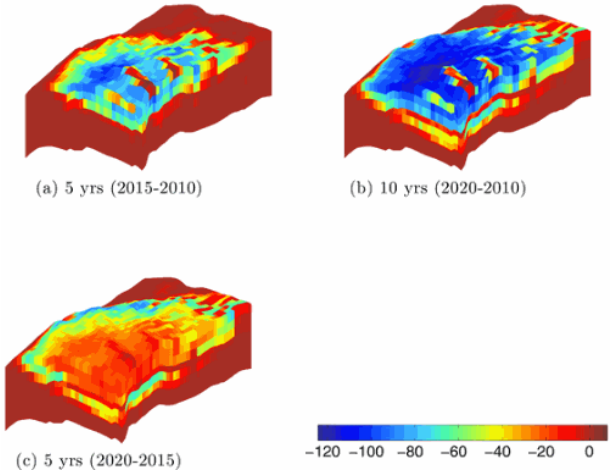


Fig. - 10

**(after Glegolaet et al. 2015)**

# Magnetic method

# Magnetic method in geophysical prospecting

- GEOMAGNETIC METHOD is basically used to observe the Earth magnetic field at any point on the Earth surface. Earth's magnetic field can be measured from different platforms (Land, Marine, Airborne survey) using sensors known as magnetometers

- In EXPLORATION GEOPHYSICS, magnetic method is used to observe an anomalous magnetic field due to the existence of rock magnetic differences. The survey can be carried out both on land (ground magnetic) and air (aeromagnetic / airborne magnetic)

- Magnetic surveying is a very useful aid to geological mapping. Over extensive regions with a thick sedimentary cover, structural features may be revealed if magnetic horizons such as ferruginous sandstones and shales, tuffs and lava flows are present within the sedimentary sequence

- In the absence of magnetic sediments, magnetic survey data can provide information on the nature and form of the crystalline basement. Both cases are applicable to petroleum exploration in the location of structural traps within sediments or features of basement topography which might influence the overlying sedimentary sequence

- The sources of the local magnetic anomalies cannot be very deep, because temperature below ~ 40 km should be above the Cuire points (≈ 550°C) at which rocks looses their magnetic properties

# Basic concept and how it works

**Magnetic Force is defined in terms of monopoles:**

If two magnetic poles of strength $m_1$ and $m_2$ are separated by a distance r, the magnitude of force between them is given by:

$$\vec{F} = \frac{\mu_0}{4\pi}\frac{p_1 p_2}{r^2}\hat{r}$$ where μ is magnetic permeability of medium.

**Magnetic Field Strength (Flux Density) H:**

$$\overrightarrow{H} = \frac{\vec{F}}{p_2} = \frac{\mu_0}{4\pi}\frac{p_1}{r^2}\hat{r}$$ where, direction of **H** along flux lines

**Intensity of Magnetisation (J):**

Change of magnetic moment per unit volume. A body placed in a magnetic field can become magnetised as atoms and molecules align along the direction of applied field.

**Magnetic Susceptibility (k):**

For low magnetic fields, magnetisation **J** is proportional to the magnetising field **H**:

$$\mathbf{J} = \mathbf{k}\,\mathbf{H}$$ where, k is called the magnetic susceptibility.

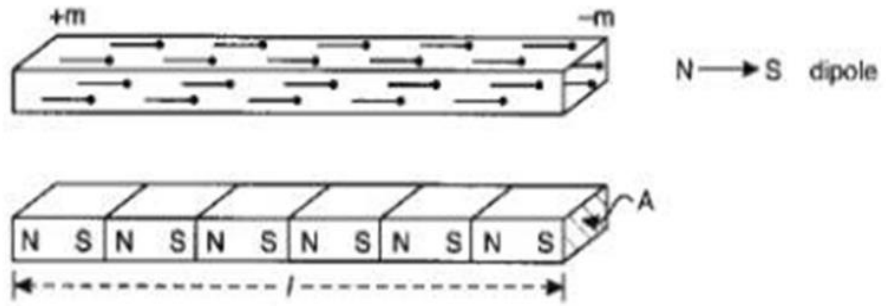


Fig. - 11

# Continued…

## Total Magnetic Field B:

Represents the sum of the magnetising field strength and the magnetisation of the medium:

$\mathbf{B} = m_0(\mathbf{H} + \mathbf{J}) = m_0(\mathbf{H} + k\,\mathbf{H}) = m_r m_0\,\mathbf{H} = m\,\mathbf{H}$

where $m_0$ is magnetic permeability of free space ($4\pi$ x$10^{-7}$ H/m)
$m_r$ is relative magnetic permeability
m is absolute magnetic permeability
Clearly, $m_r = m / m_0$

**B** is also called the magnetic flux density or magnetic induction. In geophysics, magnetic fields are small and measured in nT. Earth's magnetic field varies between 20,000 to 60,000 nT.

**B vs H:** There is often confusion between **B** and **H**. In practice, this mostly doesn't matter, because for measurements in air $m_r = 1$ (i.e. $k = 0$, can't magnetise air or a vacuum), and $\mathbf{B} = m_0\,\mathbf{H}$.

## Induced Magnetisation ($J_i$):

Induced Magnetisation $J_i$ is produced within a rock in response to an applied external magnetic field.

## Remnant Magnetisation ($J_r$):

Magnetic field may exist within rock even in absence of external field due to permanently magnetic particles. This is remnant or permanent magnetisation.

# Continued…

Interpretation of magnetic data complicated as magnetic field due to a subsurface body results from a combined effect of two vector magnetisations that may have different magnitudes and directions.

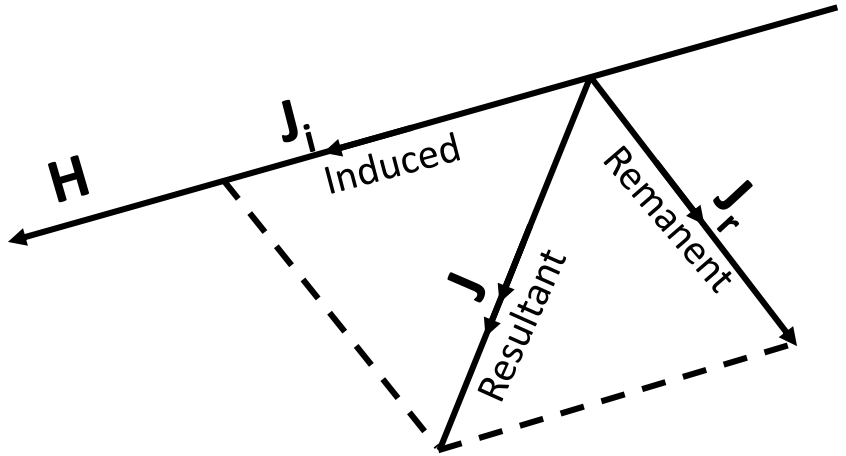


Fig. - 12

Königsberger Ratio (Q): Measurers the ratio of intensity of remnant ($J_r$) to induced ($J_i$) magnetisation

- Q ~ 30-50 for rapidly quenched volcanic rocks
- Q ~10 for volcanic rocks in general
- Q~1 for slowly crystallised igneous and thermally metamorphosed continental rock
- Q<1 in sedimentary and metamorphic rocks when iron not present

## Magnetic Susceptibilities of typical Rocks:

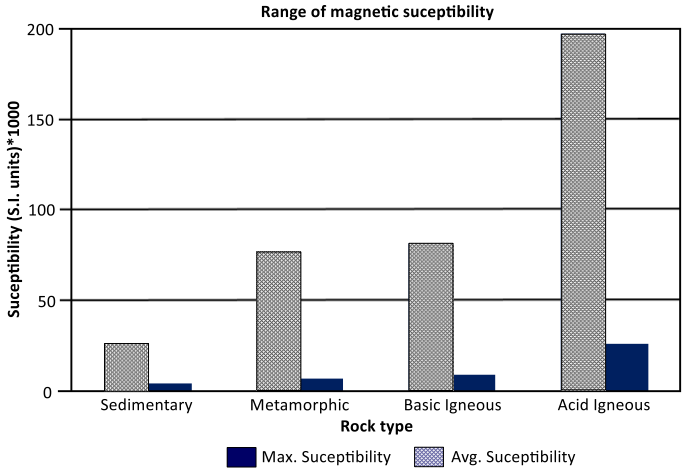


Fig. – 13 (a)

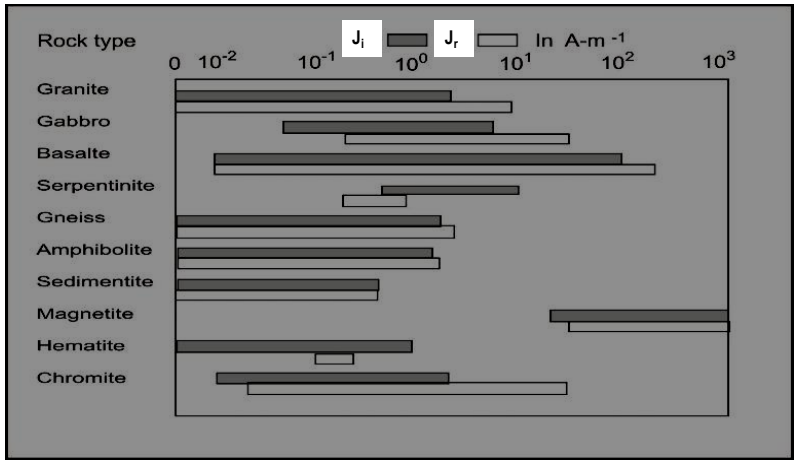


Fig. – 13 (b)

# Continued…

Dynamo action produced by the circulation of charged particles in couples convective cells within the outer fluid part of the Earth's core

(a)

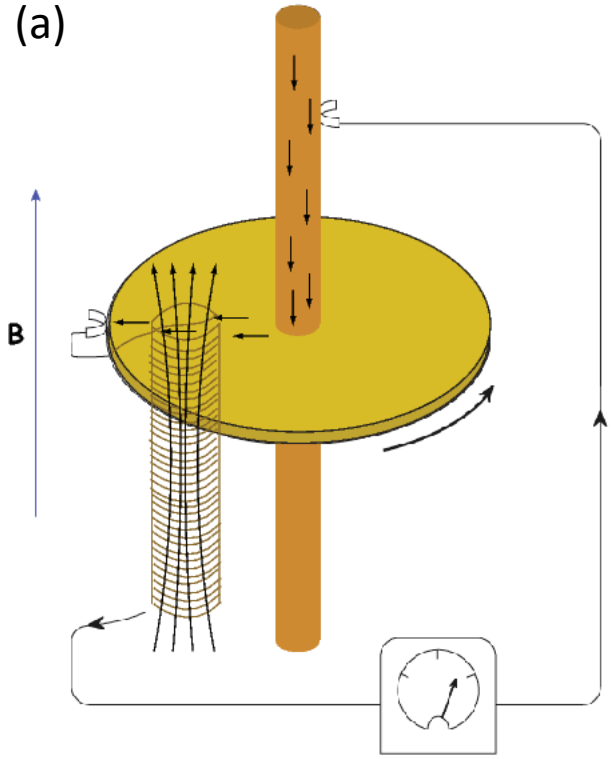


(b)

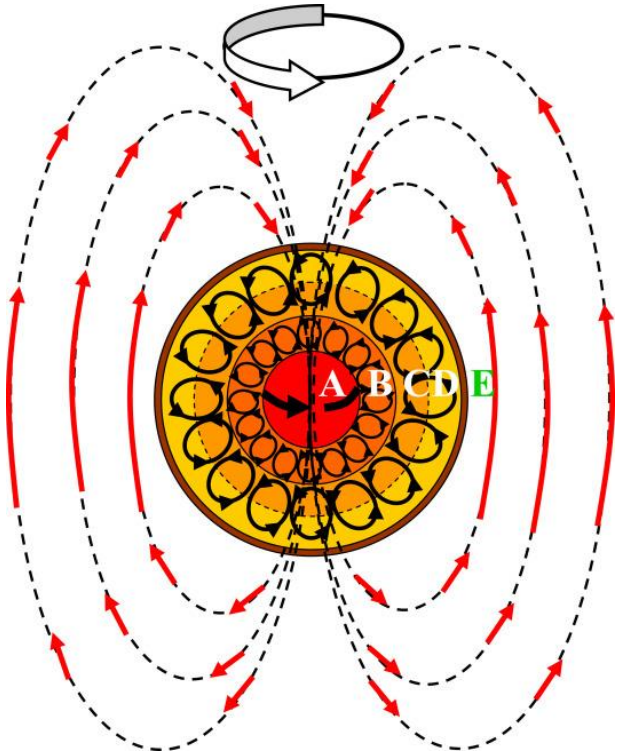


(c)

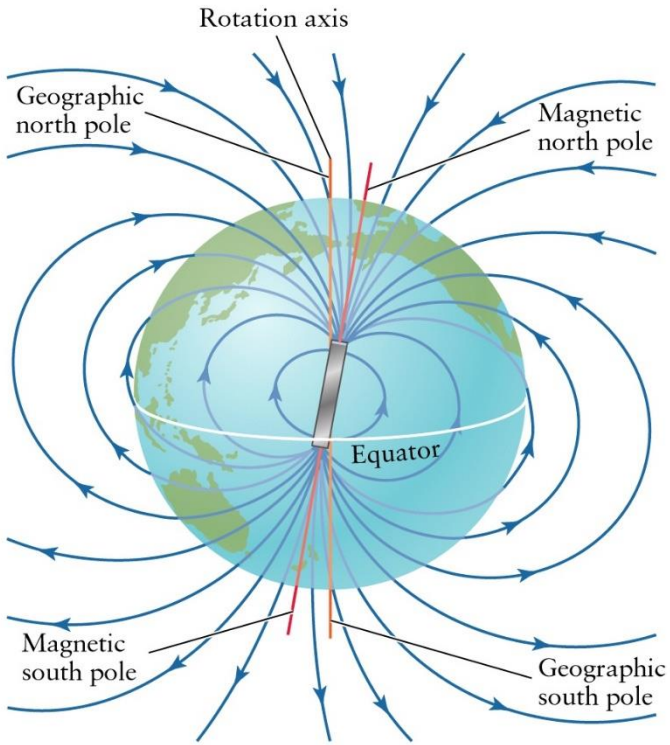


Fig. - 14

# Magnetometers, measurement and typical surveys

## Type of magnetometers:

Scaler magnetometer, measuring total field strength

- Proton Precession Magnetometer
- Optically Pumped

Vector magnetometer, measuring directional magnetic field

- Fluxgate magnetometer

## Magnetic survey:

- Ground Magnetic surveys: Relatively small areas on a previously defined target
- Airborne magnetic survey: Exploration of natural resources over a large area
- Marine Magnetic Surveys: Large-scale oceanographic surveying and petroleum search

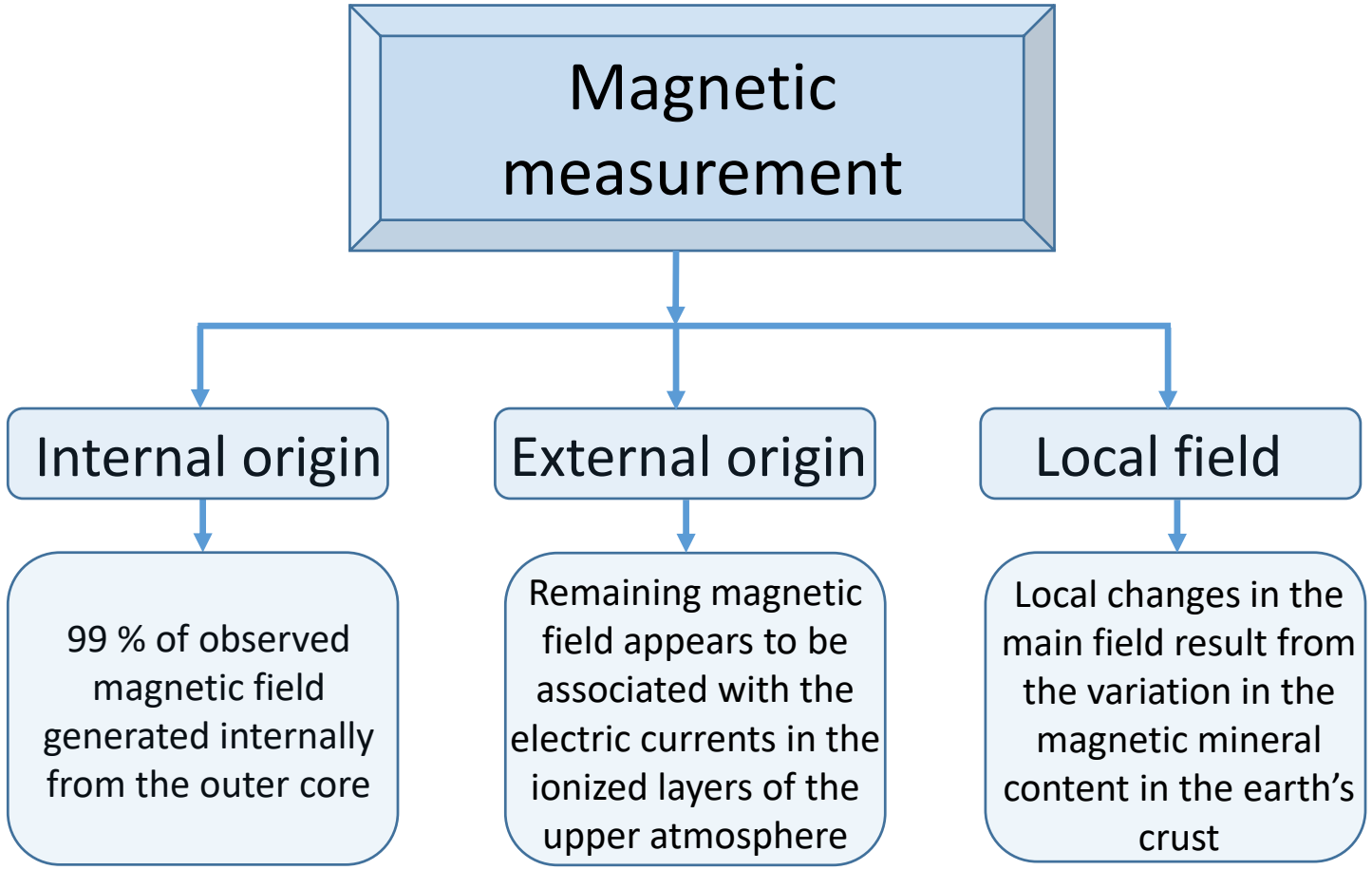


Fig. - 15

# Continued….

## PROTON PRECESSION MAGNETOMETER

- Two coils surrounding bottle of water or hydrogen rich fluid.
  - One to induce field in different direction then natural field,
  - One to measure voltage caused by precessing protons.

- Measurement process:
  - Protons originally aligned with natural field (A).
  - External coil is energized with a DC current resulting in a strong **B** field that aligns protons (B).
  - Current turned off; protons precess back to alignment with external field, generating AC current in receiver coil at Larmor Frequency (C). Larger fields → higher frequencies

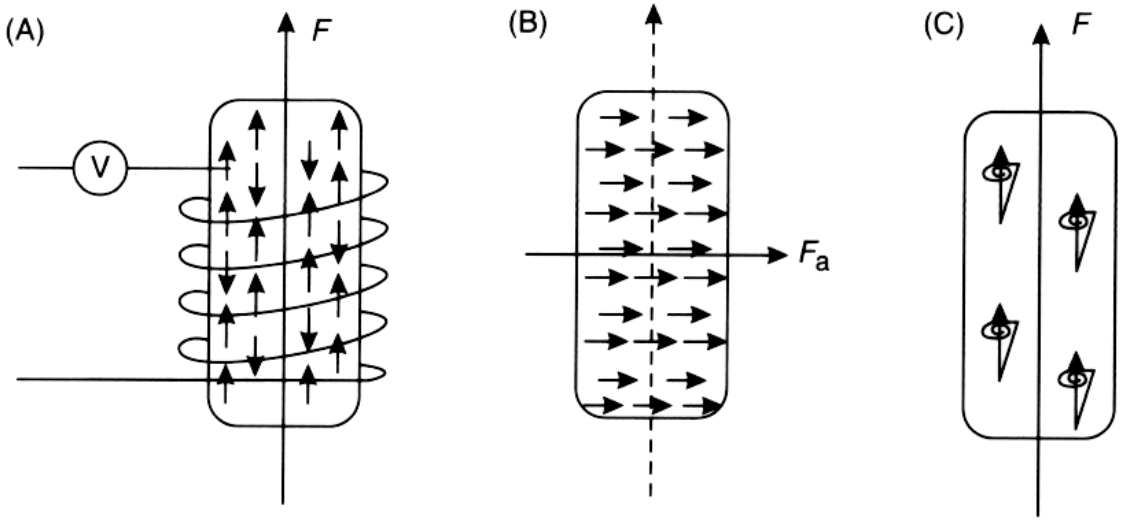


Fig. - 16

# Continued….

## ALKALI VAPOR MAGNETOMETER

- Basic Physics:
  - Uses precession frequency of alkali vapor,
  - Quantum mechanics.

- Magnetometer construction:
  - Bottle filled with cesium or rubidium vapor,
  - Polarized light source of same element,
  - Coil to generate radio frequency magnetic field,
  - Light detector.

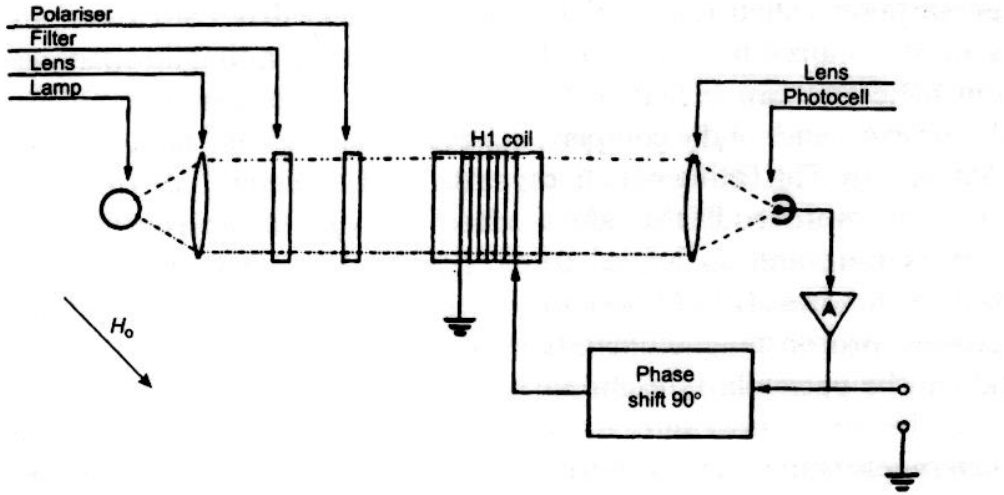


Fig. - 17

# Survey planning and typical survey

- Based on target dimension, line spacing and station intervals are designed. 500-1000 m, 50-100 m line spacing and 10 m station interval is maintained for a regional survey, detail survey and ultra detail survey, respectively. Survey lines are designed perpendicular to geological strike (maximum extent of the body).

- Similar design as ground-based surveys, except with larger line spacing. In sedimentary basins:
  - 4 km spacing
  - 1km flight height or greater.

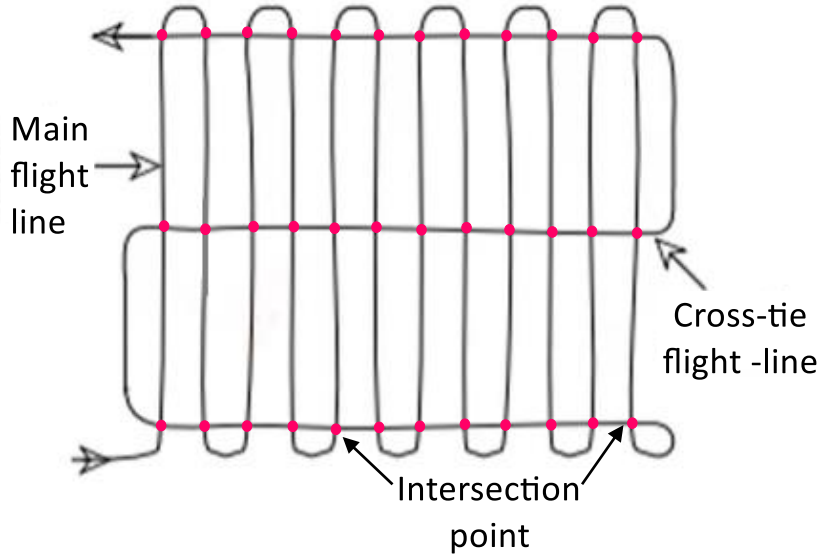

Fig. - 18

## Airborne Survey:

- To survey a region, flight lines are parallel and spacing from 100 m to a few km's (Fig. 18)
- Orientation of flight lines is set to be more or less normal to the trends of suspected subsurface features
- Cross-tie lines are flown at right angles to the main flight lines, and their separation is 5-6 time of the main flight line
- Measurements at the tie-line intersections provide check on the reliability of the survey, and if the large reading difference observed at the intersection point(s), area need to be resurveyed

# Magnetic Gradiometers

- The magnetic gradiometer consists of a pair of alkali-vapour magnetometer (sensitivity 0.01) maintained at a fixed distance from each other, generally 30 m distance maintain between two magnetometer

- The difference in outputs of the two instruments is recorded

- If no anomalous body is present, both magnetometers register the Earth's field equally and difference in the output is zero

- In-case of a magnetic contrast present in the subsurface rocks, the magnetometer closest to the structure will detect a stronger signal than the remote one

- As in gradiomerty survey we deal with the difference in the magnetic field from the individual magnetometers, thus final no need to apply the diurnal corrections to the final readings

- Vertical gradient measurement emphasizes shallow source magnetic anomaly and suppress the deep seated features.

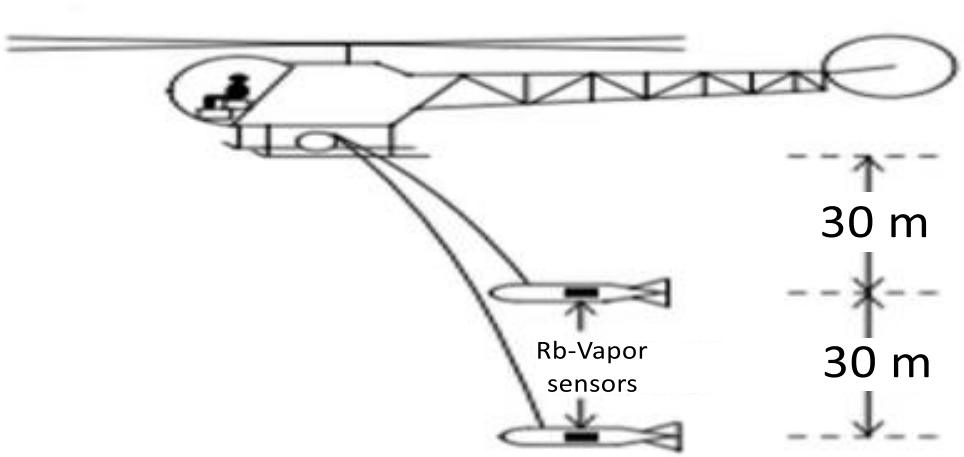


Fig. - 19

# Magnetic data correction

## Diurnal correction:

As the Earth rotates beneath the ionosphere, the observed intensity of the geomagnetic field fluctuates with a range of amplitude of about 10-30 nT at the earth's surface and a period of one day.

Diurnal variation of the magnetic field is removed by repeated observations made at the base during the day and interpolated the deviations and subtracted from the field readings.

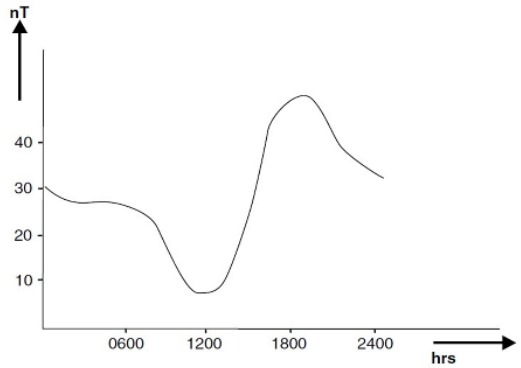


Fig. – 20 (a)

## IGRF correction:

The IGRF is an internationally agreed series of global sphere harmonic models of the earth's magnetic field whose sources are mainly in the Earth's core.

Core fields are described by the IGRF model. Once this field is subtracted from the data, results are generally residual magnetic anomalies solely due to the Geology

Crustal field (Fc) = Main field form outer Core (Fi)- IGRF (theoretical value)

Raw data must be visually inspected for spikes, gaps, instrument noise or any other irregularities in the data and (Mainly for Airborne Survey) there will be additional lag, heading corrections, etc.

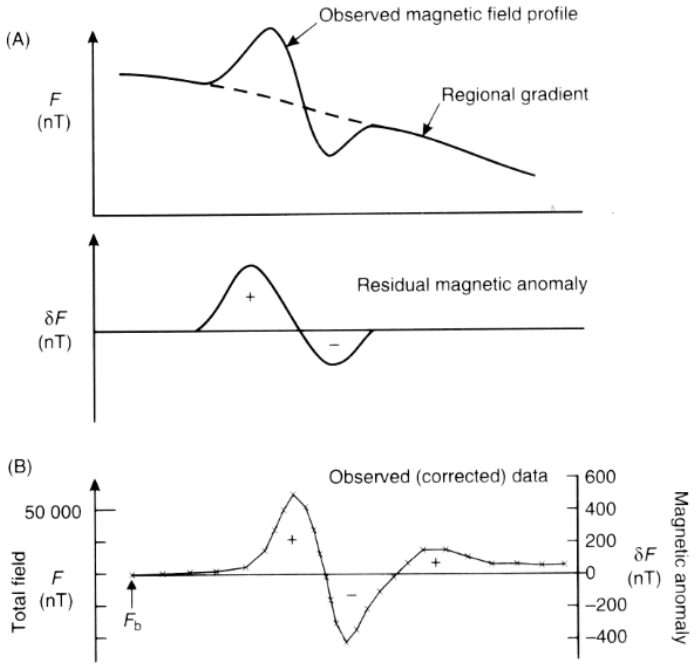


Fig. – 20 (b)

# Difficulty in magnetic anomaly interpretation

At different magnetic latitudes, the magnetic anomaly from the same magnetic body are noticeably different from each other.

Hence the concept of reduction to pole and reduction to equator have been introduced.

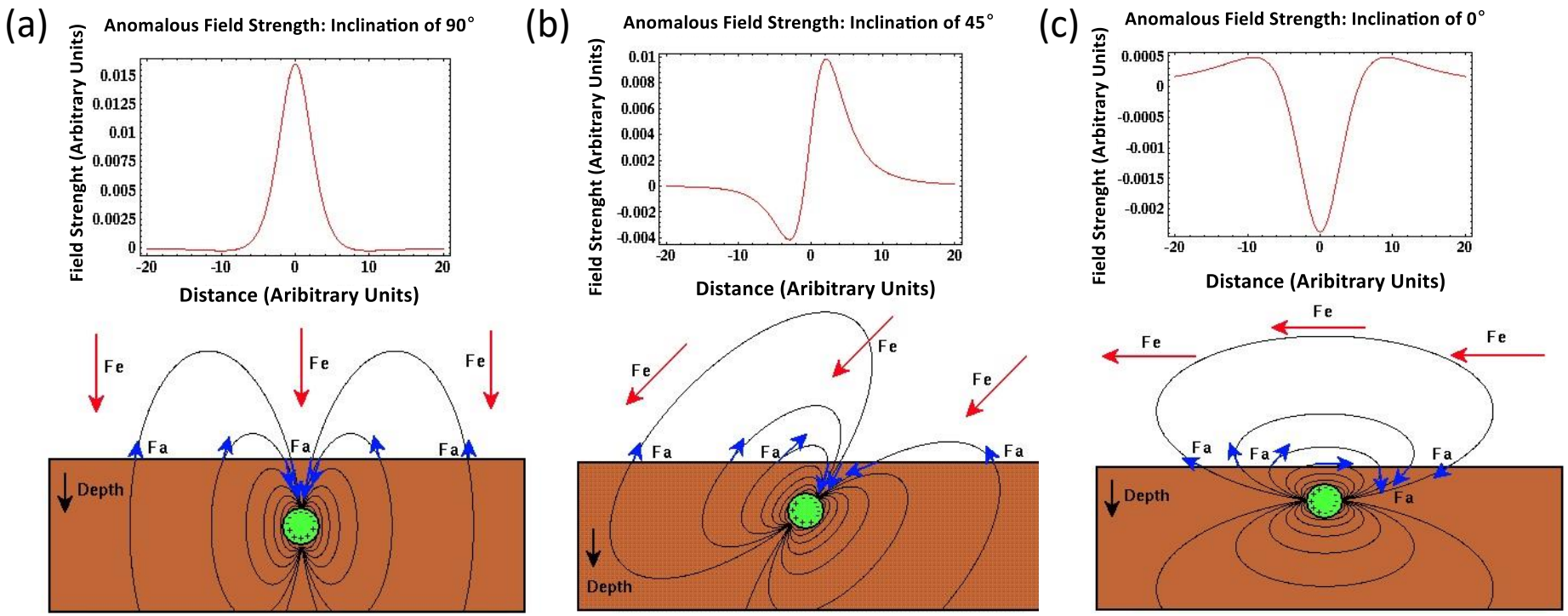


$F_e$ = Earth's Magnetic Field $F_a$= Induced Anomalous Magnetic Field

Fig. - 21

Additionally, interpretation of magnetic anomalies close to the magnetic equator is complicated by several reasons:

- Ambient field is horizontal
- Ambient field is weak (~35,000 nT compared to up to 70,000 nT in higher latitudes) and
- Structures striking N-S are difficult to identify

# Reduction to pole and equator of Magnetic data

## Reduction to the pole (RTP):

- To recalculate total magnetic intensity (TMI) data as if the inducing magnetic field had a 90° inclination, i.e. transform the dipolar magnetic anomalies to monopolar anomalies centered over their causative bodies
- To simplify the assumption that the rocks in survey area are all magnetised parallel to the earth's magnetic field
- RTP does not work well close to the magnetic equator (<10° inclination), as there is a large correction to be made for the amplitude of the anomalies

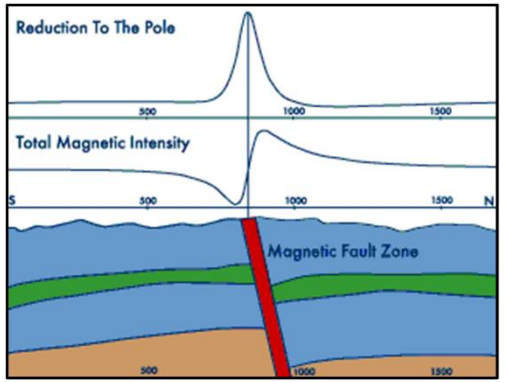


Fig. - 22

## Reduction to the equator:

- To correct the asymmetry and lateral shift of measured magnetic total field profiles, the transformations can be implemented in both space and frequency domains:
  - Space domain → Accuracy of transformation improves, as the length of the profile increases
  - Frequency domain → Applying a spectral window enables the transformation of short length profiles

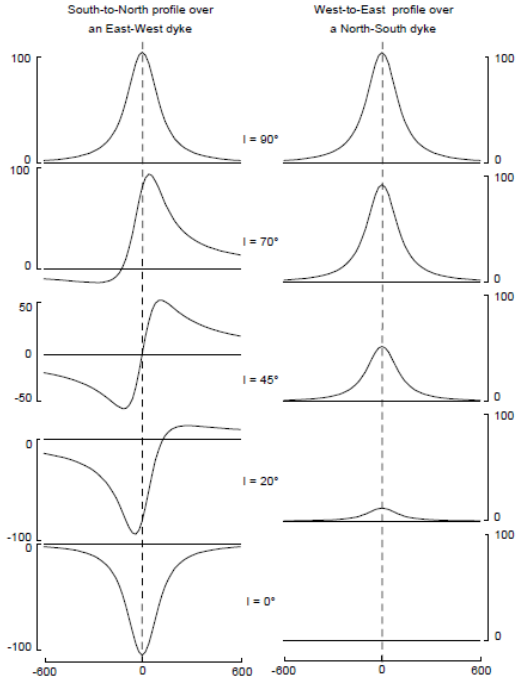


Fig. - 23

# Magnetic data interpretation

## Example-1:

General inferences can be made from magnetic anomaly shapes

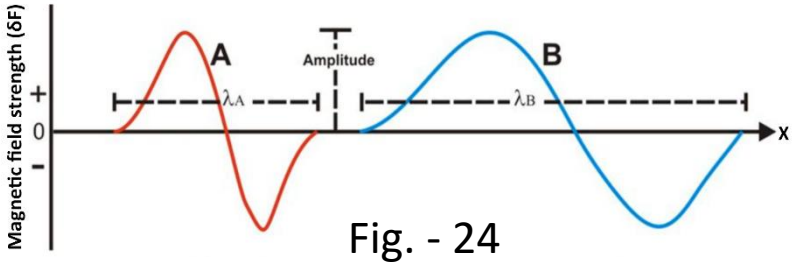


Fig. - 24

- Anomaly B is same form as A, but has longer wavelength, so must be deeper
- Amplitude of B greater than A, so B has greater magnetisation

## Example-2:

Magnetic anomalies caused by the same body at different depths

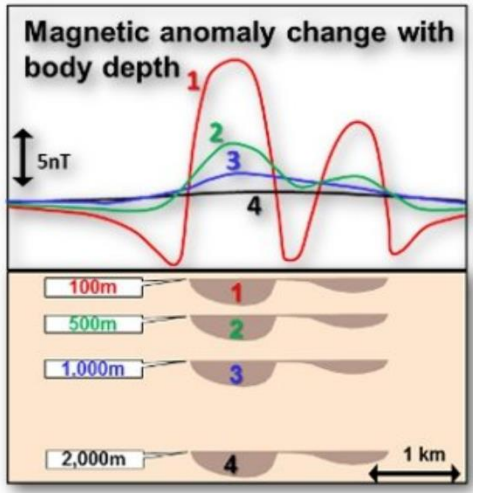


Fig. - 25

## Example-3:

A synthetic section with calculated magnetic anomalies for magnetic rocks typically found in sedimentary basins

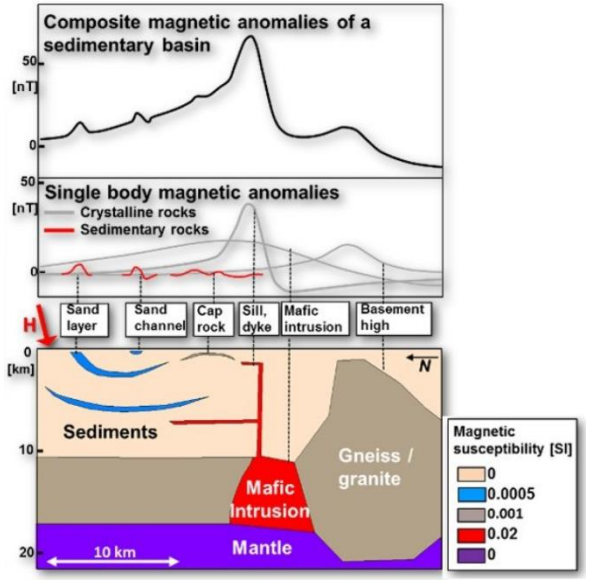


Fig. - 26

## Example-4:

Magnetic anomalies caused by the same body at different depths

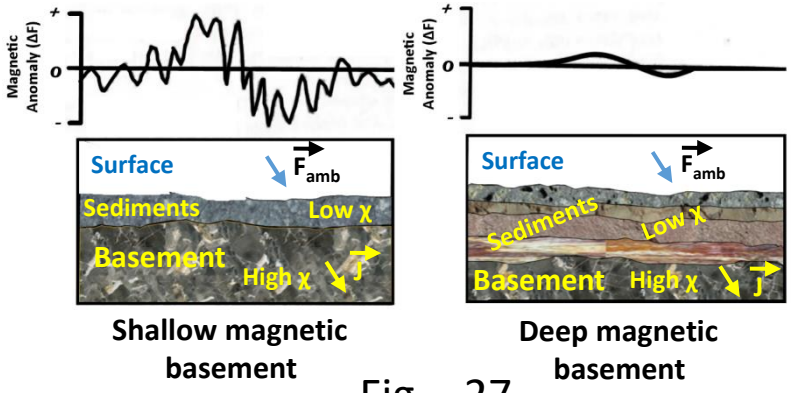


Fig. - 27

Crystalline basement rocks are commonly more mafic than overlying sedimentary deposites and are the main sources of magnetic anomalies

- Shallow basement (short wavelength), high amplitudes, steep gradients
- Deep Basement (long wavelength), small amplitudes gentle gradients

# Continued

Aeromagnetic 2D signatures associated with intra-sedimentary normal faults:

The anomalies for the truncated-layer and offset-layers models (a and b) are typical, whereas the contrasting-layers and thin-thick layers models (c and d).

- Bold blue lines- reduced-to-pole (RTP) magnetic anomaly
- dashed gray lines- HGM-potential
- Solid gray lines- gradient magnitude of the RTP anomaly and of its potential (HGM-RTP)

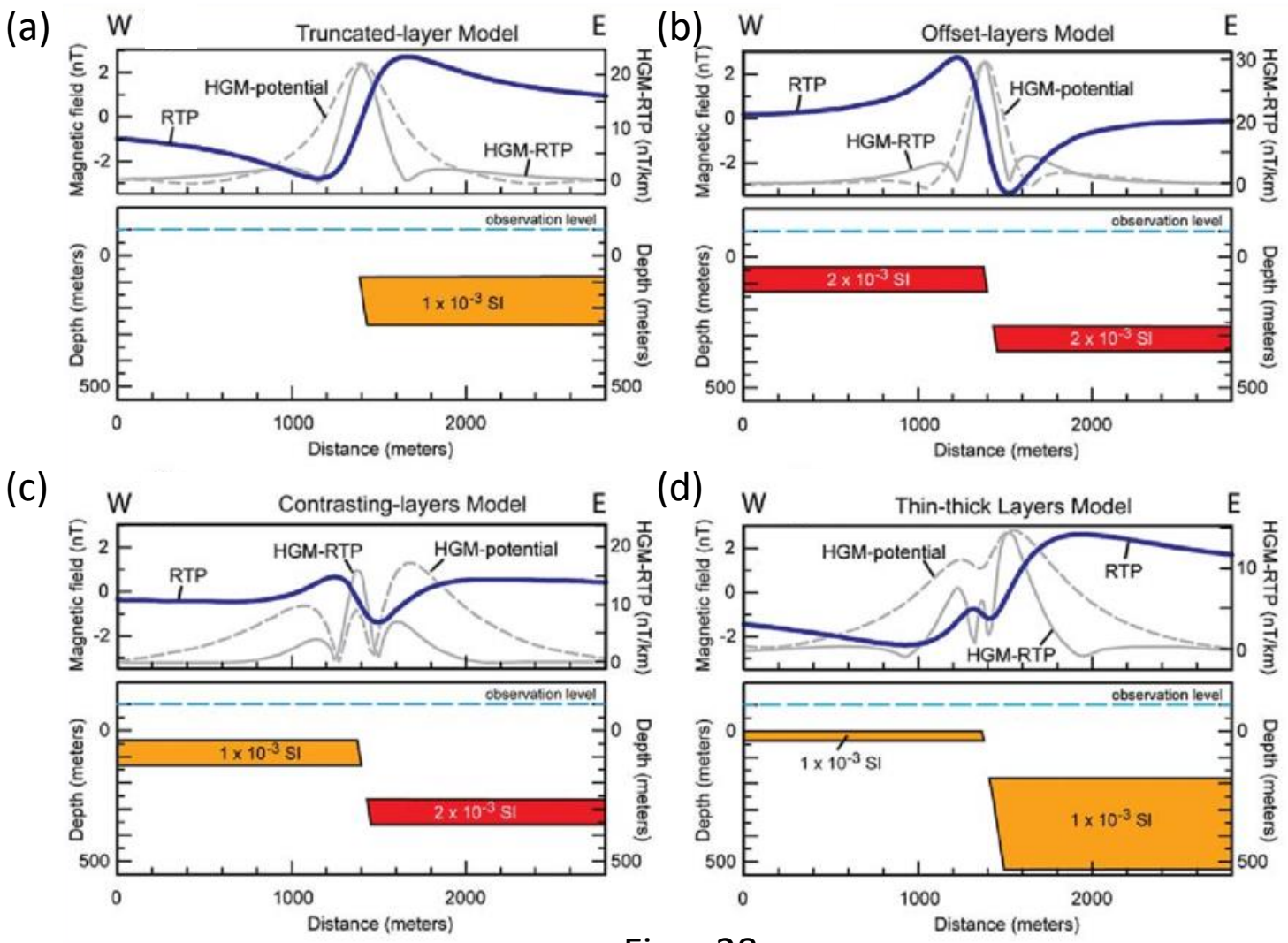


Fig. - 28

# A few successful stories

Fichler et al. (2005) correlated the depression on seismic section with a circular magnetic anomaly; interpreted as gas hydrates expulsion crater filled with magnetic glaciogenic sediments.

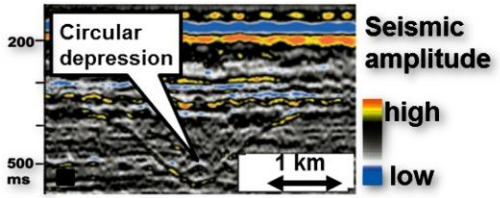


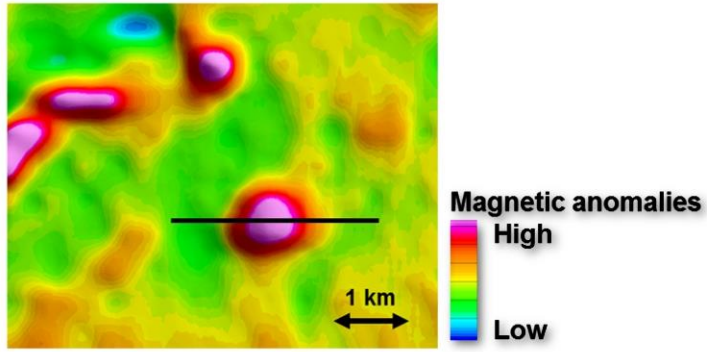


(After, Fichler et al. 2005)

Fig. – 29 (b)

Salem et al. (2010) used Tilt-Depth method applied to find out the sediment thicknesses in USA & Australia. The Tilt-Depth estimated sediments thickness were well corroborated (0.86% correlation) with the drilling data derived sediment thicknesses.

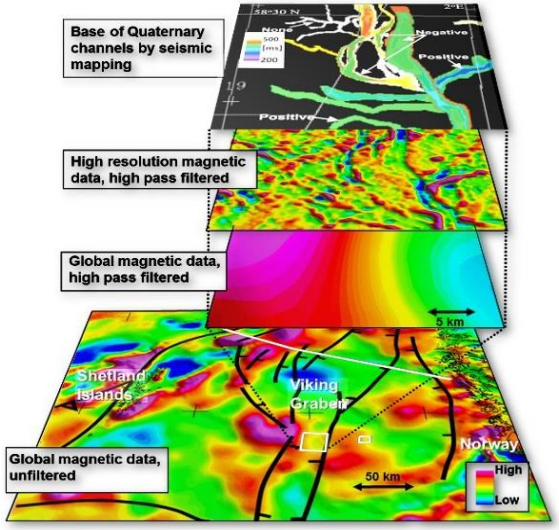


(After, Salem et al. 2010)

Fig. – 29 (a)

Badejo et al. (2021) used magnetic techniques to calibrate the hydrocarbon migration in petroleum systems in the Lower Tertiary, UK Central North Sea

Piggott and Pulham, (1993) developed a basement fault block pattern, sedimentation rate as the control on hydrocarbon sourcing, generation, and migration in the deep-water Gulf of Mexico: Proceedings, Gulf Coast Section

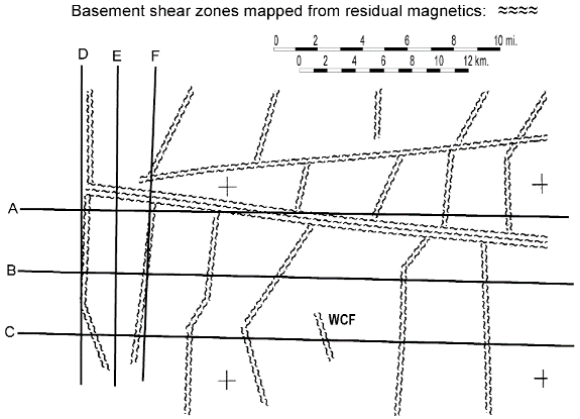


(After, Piggott and Pulham, 1993)

Fig. – 29 (c)

# Electromagnetic (EM) Method

# Basic concepts and application

- Faraday showed that a time-varying magnetic field leads to an induced electric field
- In 1865, Maxwell proposed that time varying electric field would produce a magnetic field

This two-way interaction between electric and magnetic filed are elegantly wrapped up in Maxwell's equations.

Maxwell's equations

$$\nabla . \vec{E} = \frac{\rho}{\varepsilon_0}$$

$$\nabla \times \vec{E} = \frac{\partial \vec{B}}{\partial t}$$

$$\nabla . \vec{B} = 0$$

$$\nabla \times \vec{B} = \mu_0 \vec{J} + \mu_0 \varepsilon_0 \frac{\partial \vec{E}}{\partial t}$$

A time- varying magnetic field creates a spatially varying electric field.

A time- varying electric field creates a spatially varying magnetic field.

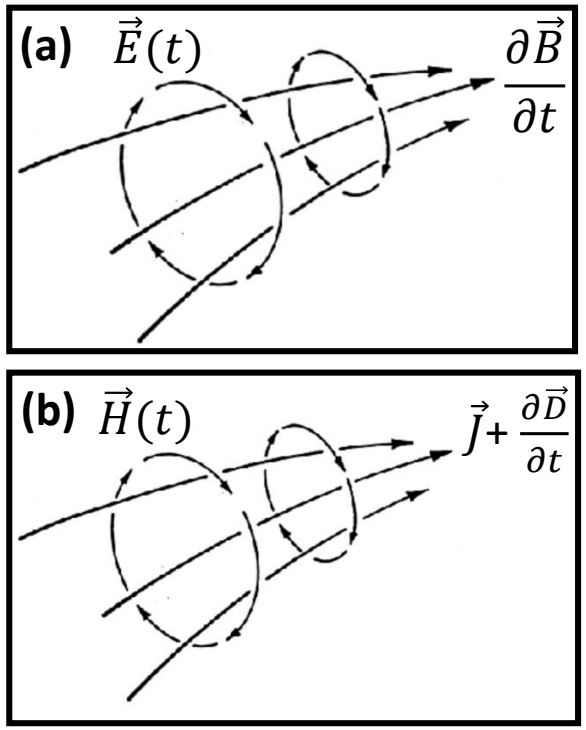


Fig. - 30

E = Electrical field (V/m)
D = Displacement current (Coulomb/m²)
H = Magnetic field (A/m)
B = Magnetic induction (Tesla)
$\mu_0$ = magnetic permeability
$\varepsilon_0$ = electrical permittivity

In Applied Geoscience, Electromagnetic (EM) methods make use of the response of the ground to the propagation of electromagnetic fields, which are composed of alternating electric intensity and magnetic force.

# EM method in geophysical prospecting

Electromagnetic technique measures the conductivity of the ground by inducing an electrical field through the use of time-varying electrical currents in transmitter coils located above the surface of the ground.

## Basic principles of EM tools:

- AC current is produced in a source coil
- Generates a magnetic primary field (Ampere's law)
- This generates a corresponding electric field (Faraday's law)
- Ohm's law changes this current due to encountered resistance
- These Eddy current produce a secondary magnetic field (Ampere's law) which are recorded together with the primary field in a receiver coil
- The measurement separates primary and secondary fields (Frequency-domain methods (FDEM), Time-domain methods (TDEM) )

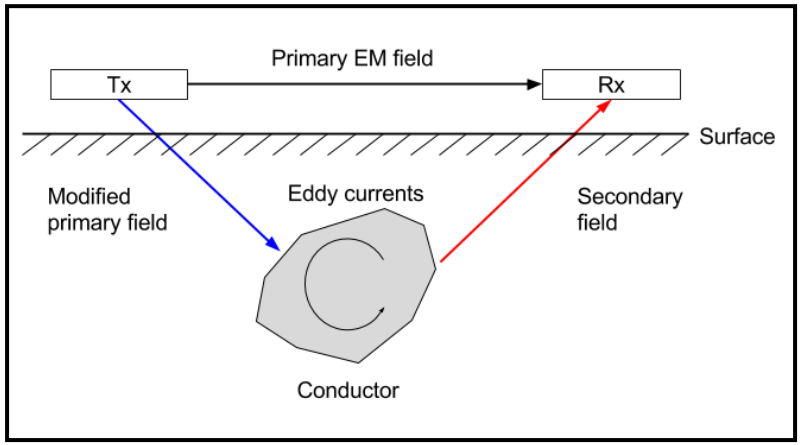


Fig. - 31

In FDEM, secondary fields are measured in the presence of primary field. This techniques used to provide rapid and generally shallow coverage.

In TDEM, secondary fields are measures in the absence of primary field. This techniques are commonly used to detect large deep targets.

## Electrical conductivity of rocks:

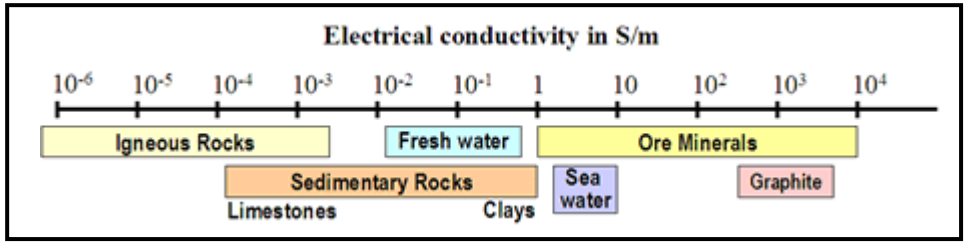


Fig. - 32

# Electromagnetic surveys

## Frequency Domain Data:

- The primary field is harmonic cos(ωt). At the receiver, the primary field can be written as $\overrightarrow{H_p}\cos(wt)$
- The currents induced in the conductor will also be harmonic with the same frequency ω. However, they will have a different phase. The resultant secondary field from these currents must also have the same frequency dependence. Hence, the secondary field can be written as $\overrightarrow{H_s}$cos(ωt+ψ), where ψ is a phase angle
- The secondary field it will lag the primary field by angles between 90° and 180°. The amount of phase difference is diagnostic of the conductivity of the body
- Induced voltage at the conductive body **E=** $\frac{\partial \emptyset_B}{\partial t}$ (*If the primary current varies as cos(ωt) then the flux ($\emptyset_B$) also varies as cos(ωt), while E varies with sin(ωt), i.e., the EMF lags the primary field by π/2*)
- The body in which the induction is occurring can be represented as a circuit element with self-inductance L and a resistance R. Through the laws of electromagnetic induction, the time varying currents that are set up in the conductor suffer a further lag

$$\varphi = \tan^{-1}\left(\frac{wL}{R}\right)$$

- As a result the secondary field lags the primary by a total amount

$$\psi = \frac{\pi}{2} + tan^{-1}\left(\frac{wL}{R}\right)$$

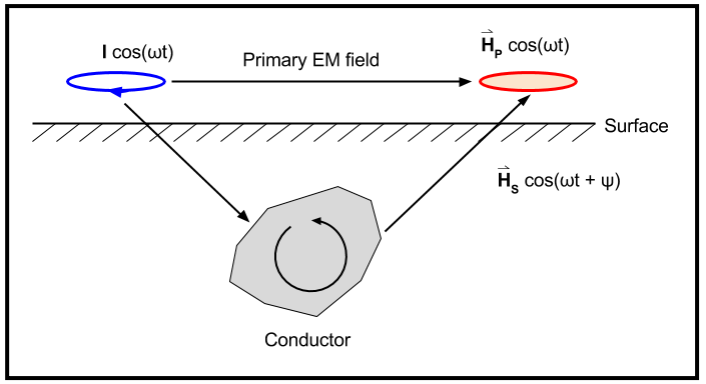


Fig. - 33

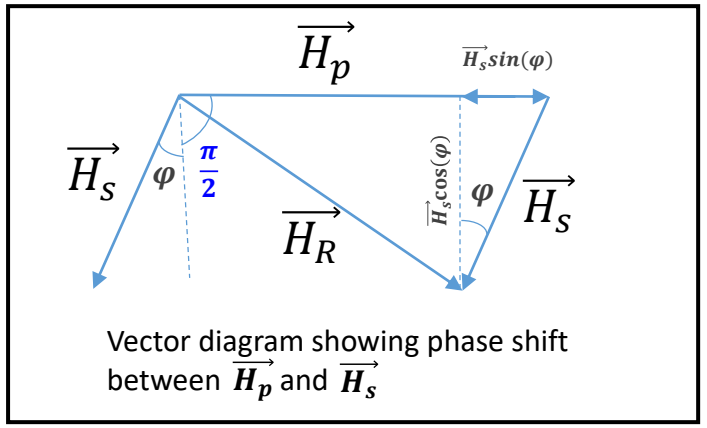


Vector diagram showing phase shift between $\overrightarrow{H_p}$ and $\overrightarrow{H_s}$

Fig. - 34

- Thus in case of good conductor $R \to 0; \varphi \to \frac{\pi}{2}$, i.e., the secondary field is 180° behind the primary field
- In case of very poor conductor $R \to \infty; \varphi \to 0$, i.e., the secondary field is 90° behind the primary field
- In case of moderate conductor, secondary field is somewhere between 90° to 180° out of phase of with primary field

# Continued……

## In-Phase and Quadrature Phase:

With the removal of the primary field the reading at the receiver pertains to the secondary field. What is generally presented as data is the ratio of the secondary field to primary field for a particular component of the field. (Remember that data could be magnetic fields measured with a magnetometer or voltages measured with a coil.) The data will be ratio of the secondary field to the primary field. Let the primary field be $\overrightarrow{H_p}\cos(wt)$. The secondary field is $\overrightarrow{H_s}\cos(wt+\psi)$, and can be written as

Insight regarding the expected value of the In-phase and Out-of-phase components can be obtained by examining the response of a single loop of wire (of resistance R and inductance L. The ratio $H_{secondary}/H_{primary}$ is given by

$$\frac{H_s}{H_p} = \text{(coupling coefficient).f}(\alpha) \quad \text{where} \quad f(\alpha) = \frac{\alpha^2 + i\alpha}{1+\alpha^2}$$

where α=ωL/R. A plot of f(α) provides considerable insight into electromagnetic data. Such a plot is probably one of the most important plots in electromagnetic induction. f(α) is a complex number and has real and imaginary parts.

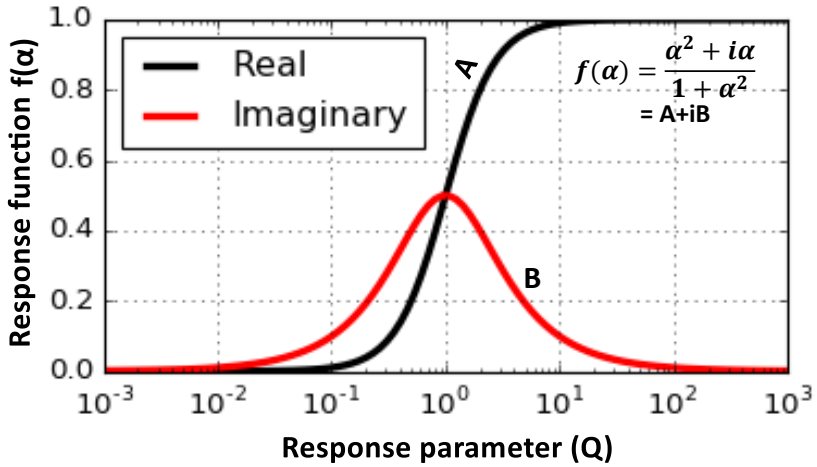


Fig. - 35

Therefore, if one measures only the imaginary components in an EM system, a very good conductor will give a very poor response

# TDEM

## What happen if conductor becomes deeper?

The secondary magnetic field becomes weaker. It can be difficult to detect a weak secondary field in the presence of stronger primary magnetic field.

Solution: Time-domain EM methods. Detects weaker secondary magnetic fields, by simply switching off the primary field, and observing the decay of the secondary magnetic fields.

## TDEM acquisition principle:

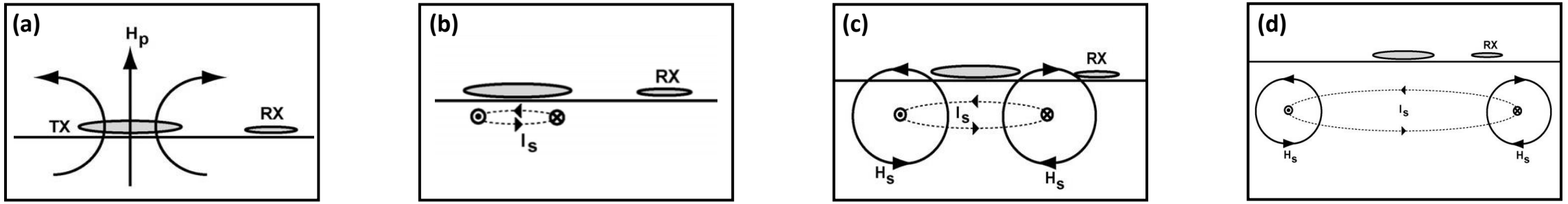


Fig. - 36

- Electric current flows through the transmitter loop
- generates a **static** primary magnetic field ($H_P$)

- Transmitter current is then **switched off**
- Then the primary magnetic field immediately falls to zero
- This change in magnetic field induces a secondary electric current in the Earth
- Secondary current acts to oppose the decrease in the primary magnetic field (Lenz's Law)

- Secondary electric current distribution can be approximated as a horizontal **loop of current** and generates a secondary magnetic field, $H_S$ ($t$)
- Over time the secondary electric currents spread out in diffuse pattern alike a smoke ring

- Secondary currents move deeper as time increases, and progressively gives information about deeper structure. Initially the magnetic field is oriented downwards at the RX
- As the current ring passes beneath the RX, the **sign** of $H_S$ changes

# TDEM: Field setup & measurements

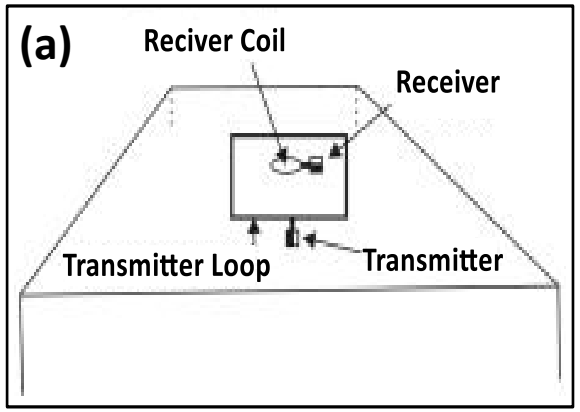


Sounding configuration

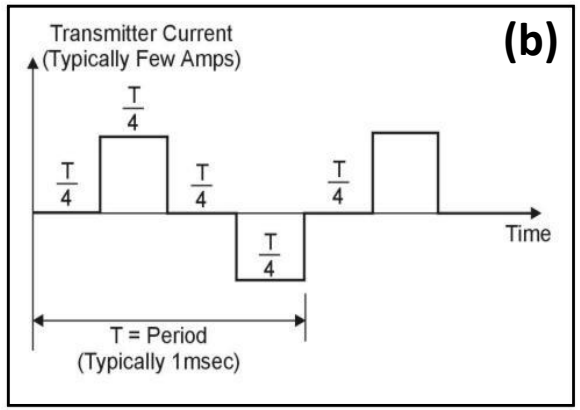


Transmitter current wave form

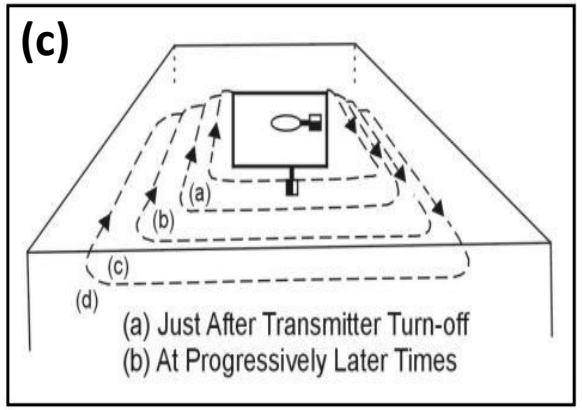


Transient current flow in ground

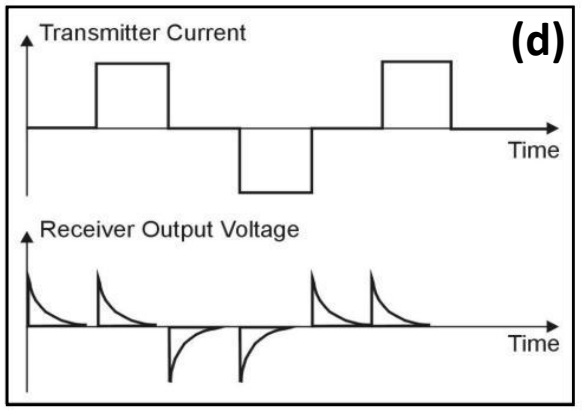


Receiver output wave form

Fig. - 37

Let the earth is homogeneous, the receiver output voltage vs. time curve divided into three part, such as early stage, intermediate stage, late stage. During late stage output voltage $e(t)$ linearly varies with time (t), given below

$$e\,(t) = \frac{k_1 M \sigma^{3/2}}{t^{5/2}}$$

where k1 = constant, M = product of Tx current & area (a-m$^2$), σ = conductivity

According to Wenner array configuration: $\rho_a(a) = 2\pi a \frac{V(a)}{I}$

Hence, the resistivity varies with time, can be expressed as:

$$\rho_a(a) = 2\pi a \frac{(k_2 M^{2/3})}{e(t)^{2/3} t^{5/3}}$$

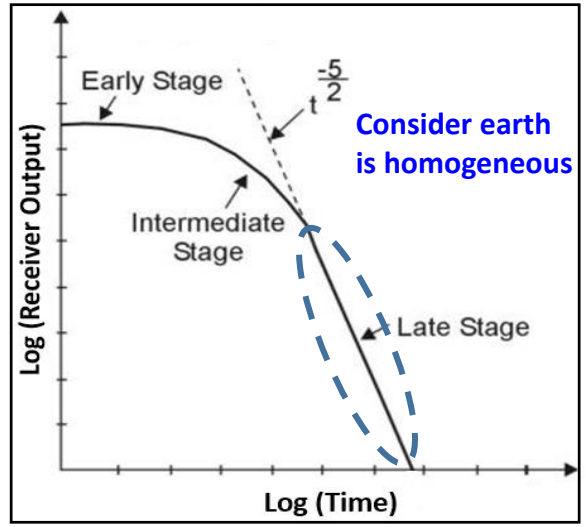


Fig. - 38

# TDEM: example for a two layer problem

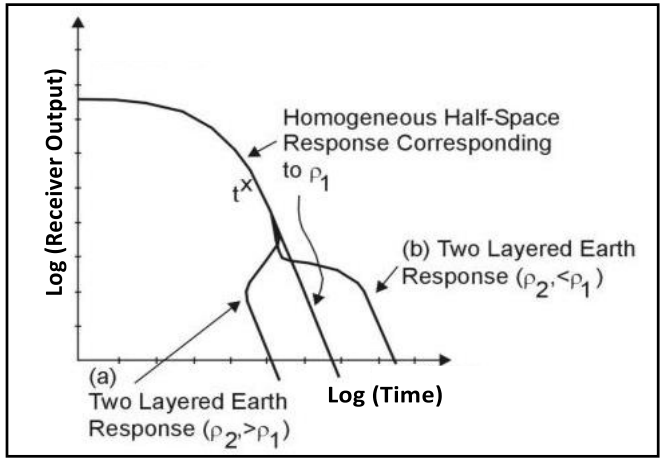


**Receiver output voltage, two layer earth.**

Fig. - 39

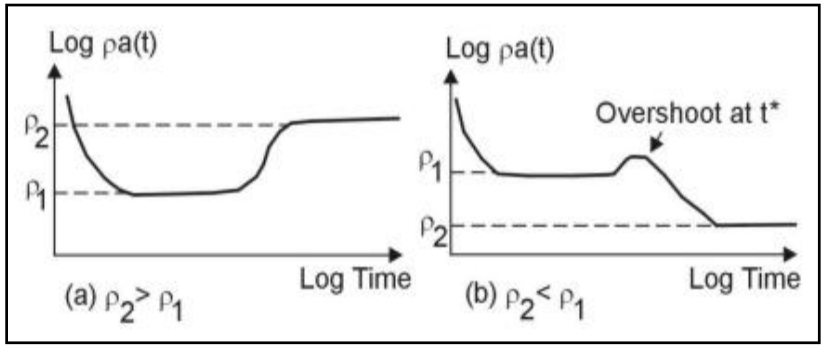


**Apparent resistivity, two layered earth.**

Fig. - 40

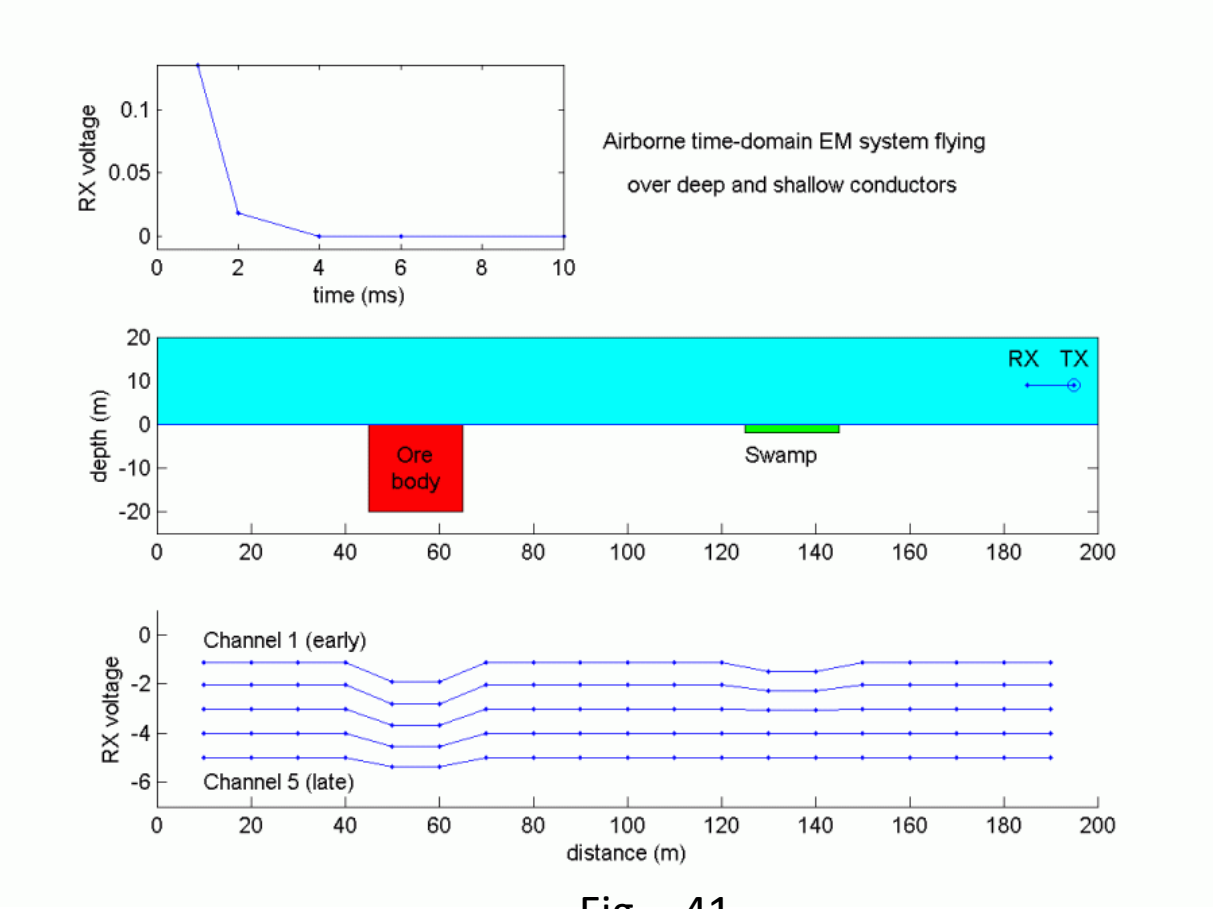


Fig. - 41

The information about the behavior of the apparent resistivity curve at early time and in the transition region is generally sufficient to allow the interpreter to determine relatively accurate resistivity of the subsurface.

# Depth of penetration of EM fields & typical surveys

The depth of penetration of an electromagnetic field depends upon its FREQUENCY and the ELECTRICAL CONDUCTIVITY of the medium.

The amplitude of EM fields decreases ($A_d$) exponentially with depth. The amplitude of EM radiation as a function of depth relative to its original amplitude $A_0$ is given by: $\mathbf{A_d=A_0e^{-1}}$

**Skin Depth:** This is the depth by which the amplitude has decayed to 1/e of its surface value. Penetration depth d is given by:

$$\mathbf{d \approx 503\sqrt{\frac{\rho}{f}}}$$ **where σ is the conductivity, ρ=1/σ is resistivity, f= ω/(2π) is frequency**

## Typical EM survey:

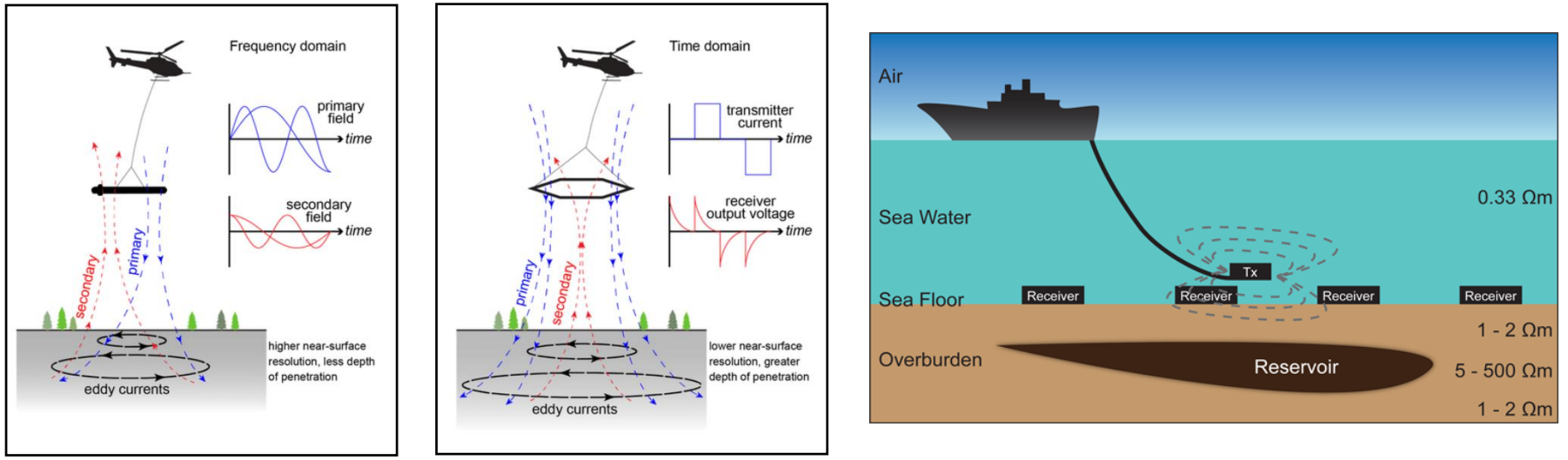


Fig. - 42

# Sea Bed Logging & hydrocarbon exploration

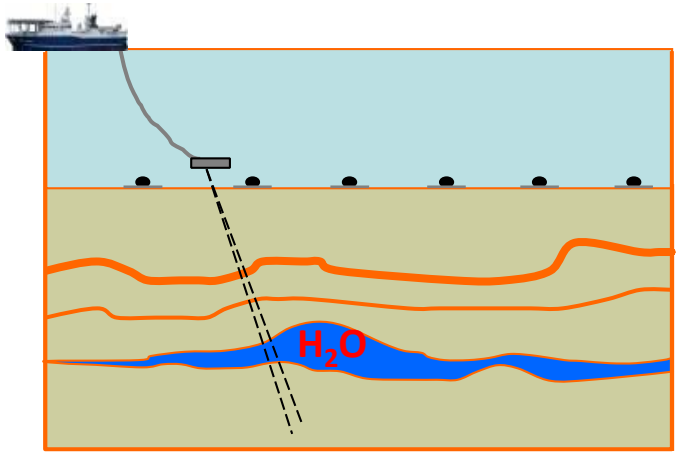


- Water-filled reservoir
- Low resistivity
- Less refraction of waves to receivers

Fig. - 43

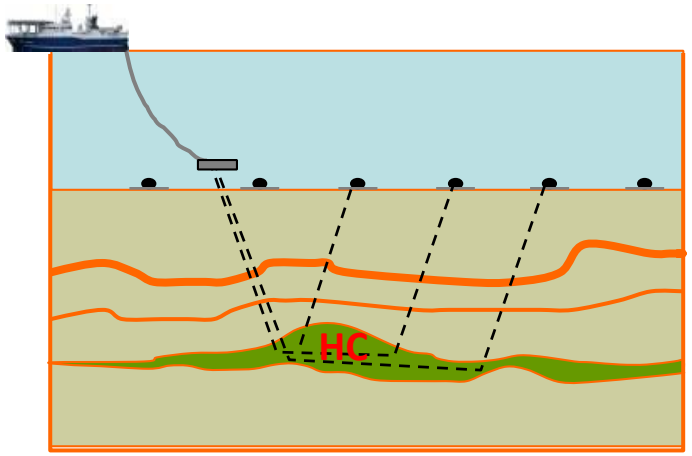


- Hydrocarbon filled reservoir
- High resistivity
- High Refraction of waves to receivers

Fig. - 44

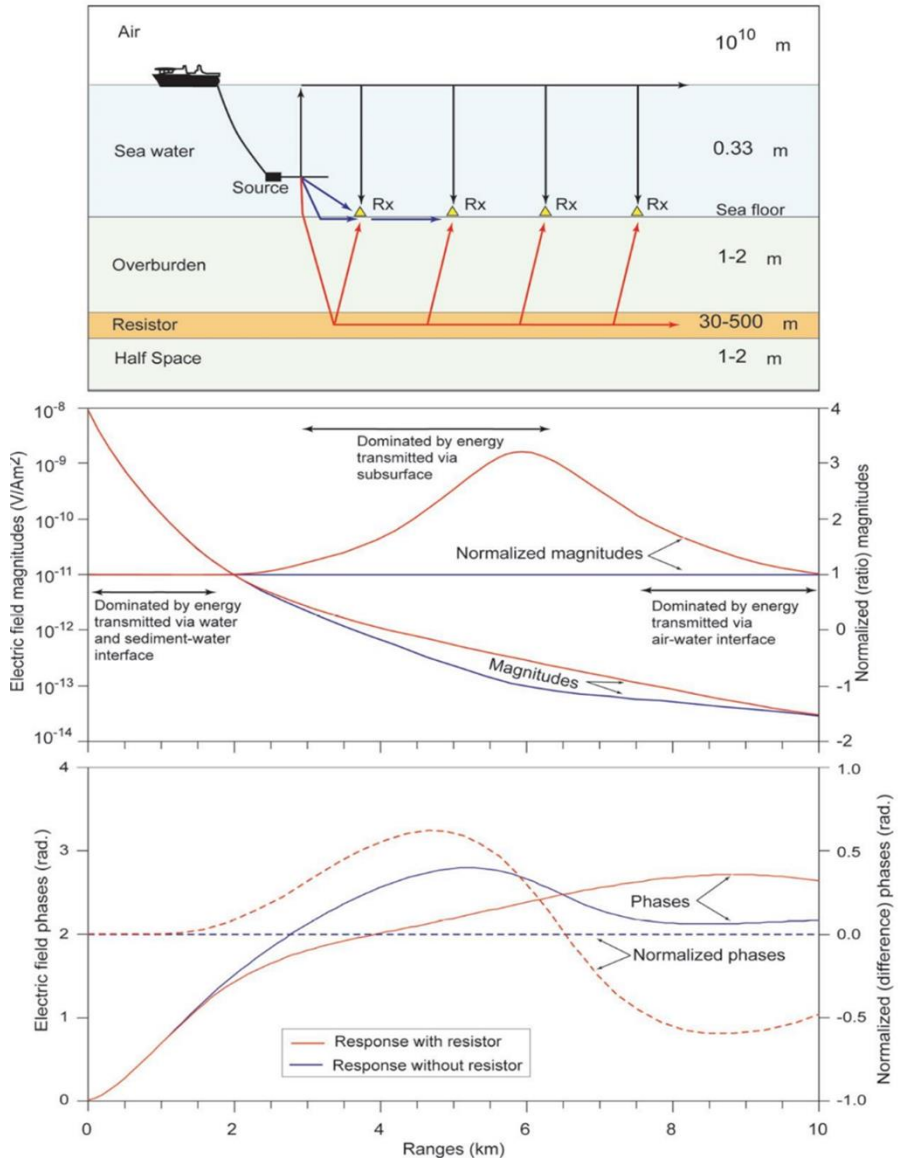


Fig. - 45

# A few case studies: Hydrocarbon exploration using EM

- Fanavoll et al. (2014) CSEM as a tool for better exploration decisions: Case studies from the Barents Sea, Norwegian Continental Shelf. They demonstrated how CSEM data can help industry make better decisions in various stages of exploration. CSEM data, being sensitive to hydrocarbon saturation and volume, have the potential to reduce the risk of exploration failures of a prospect by influencing the chance of success and expected size and volume

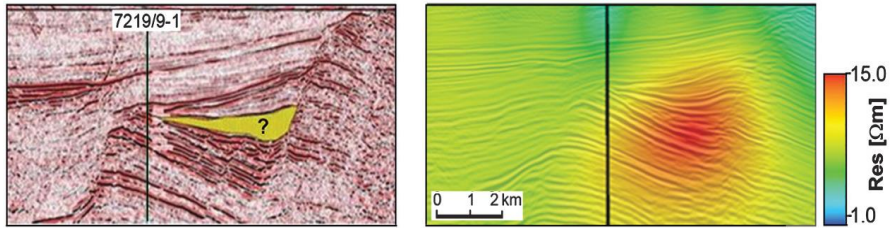


(After, Fanavoll et al., 2014)

Fig. - 46

- Schaller et al. (2017) carried out a land-based CSEM method for oil field exploration: An example from the Schoonebeek oil field
- Marine CSEM method is generally recognized to give additional information, and is especially applied for hydrocarbon exploration, primarily with the objective of de-risking the drilling activities (e.g., Darnet et al. 2007; Constable, 2010; Fanavoll et al. 2014)
- Schamper et al. (2009), 4D CSEM Feasibility Study: a Land Example. They argued that since resistivity is closely related to the nature of the fluids in the reservoir, one can also expect that changes in the fluid flow will induce resistivity changes that can be actually recorded when performing time-lapse measurements
- Buddo et al. (2015) documented the potential of electromagnetic methods in Oil & Gas Exploration in the Middle East

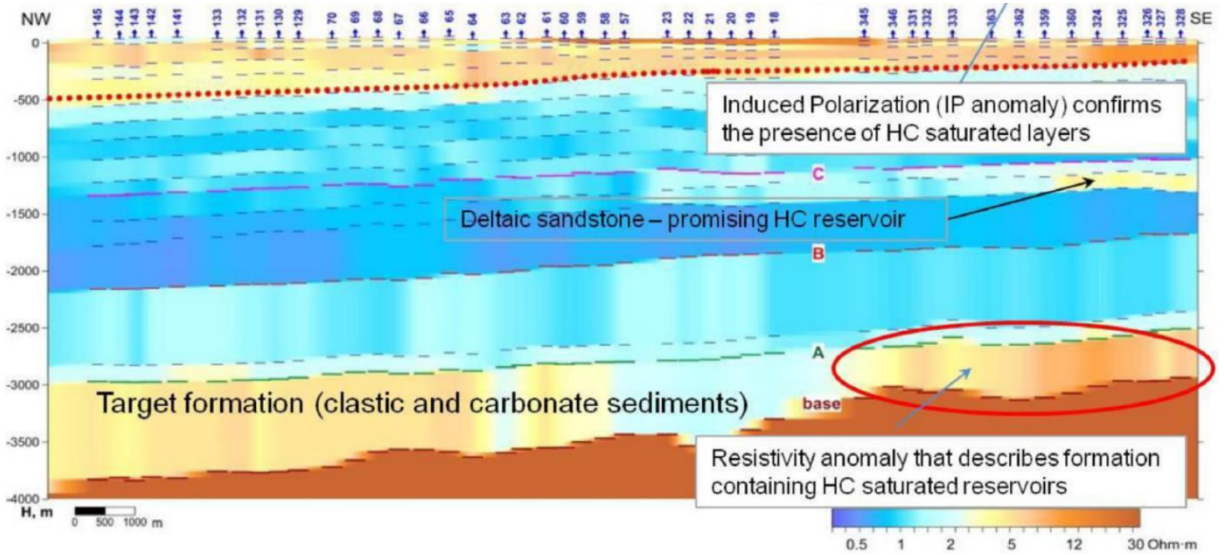


(After, Buddo et al., 2015)

Fig. - 47

# Magnetotelluric (MT)

# Basic Principles

- Magnetotellurics (MT) is a geophysical method that measures naturally occurring time-varying magnetic and electric fields
- Utilizing this natural resource, one can derive resistivity of the subsurface ranging from near surface to tens of thousands of feet
- The resistivity distribution of the sub surface is then interpreted in terms of rock type and geological structures

## Source of the natural time-varying electromagnetic waves:

- In the lower frequencies (generally less than 1 Hertz), the source of the signal is A result of interaction of the solar wind with the earth's magnetic field. As solar storms emit streams of ions, this energy disturbs the earth's magnetic field and causes low-frequency energy to penetrate the earth's surface (Fig. 48)
- The higher frequency signal (greater than 1 Hertz) is created by world-wide thunderstorms, usually near the equator. The energy created by these electrical storms travels around the earth (guided between the earth's surface and the ionosphere) with some of the energy penetrating into the earth (Fig. 49)

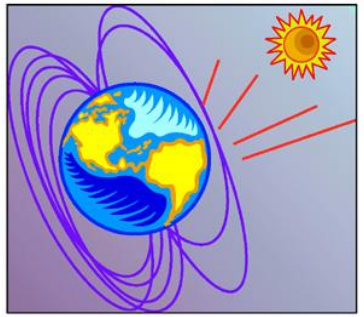

Fig. 48

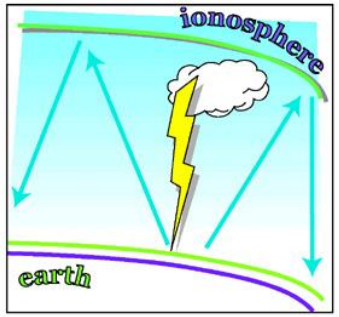


Fig. 49

## Measurements:

- These natural electric and magnetic fields are small, but measurable and signals strength varies over hours, days, weeks and even over the sunspot cycle (which is about 11 years and creates an increase the number of solar storms)
- To get enough signal to ensure high-quality data, geophysicists have to measure MT signals for an hour at each station
- In case of low frequencies (0.001 Hertz), we need to record for 16 minutes to get one sample of data
- To get a decent statistical average of good data we have to record for several hours

# What can MT tell us about the subsurface?

- The main parameter that is derived from MT is resistivity
- The main factor affecting resistivity is lithology and associated pore fluid, pressure, and temperature
- Based on resistivity contrast of the subsurface rock units and associated thickness, one can map out the subsurface resistivity variation
- Able to find out the geological features like fold belts, volcanics
- Depth of investigation near to > 20 km
- In hydrocarbon exploration, Magnetotelluric (MT) method has been used especially in reconnaissance stage and also in difficult areas due to topographic and structural complexity

NB: The deeper the target, the thicker it
has to be in order to be mappable by MT

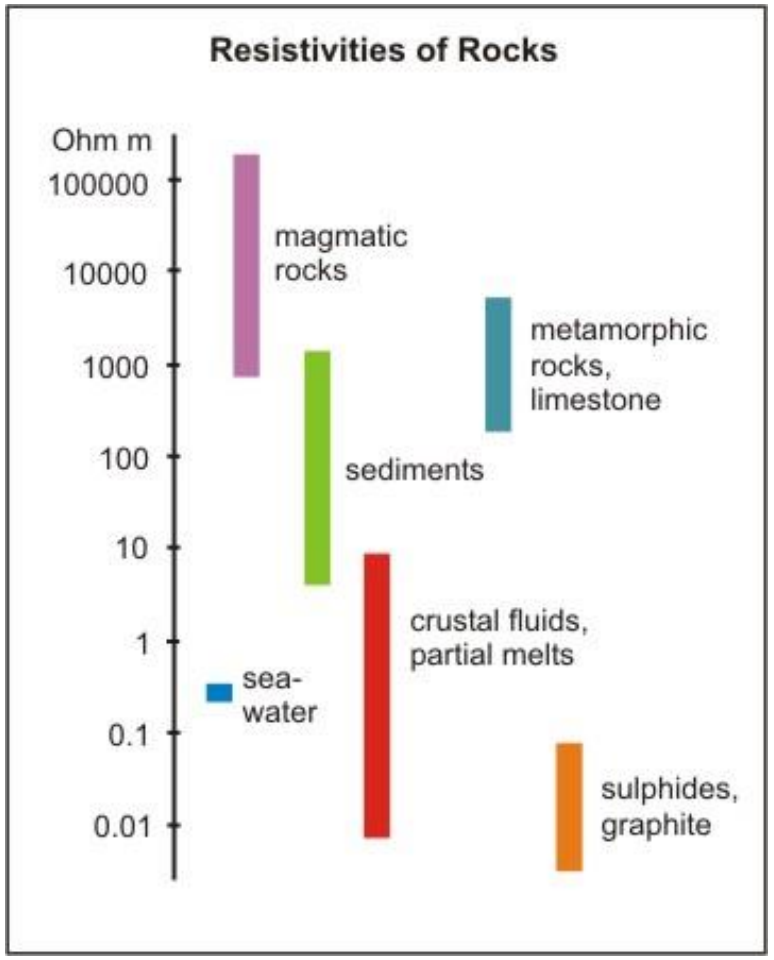


Fig. 50

# Data acquisition

- Two dipoles (4 Electrodes) & Three magnetometers (Fig. 51)
- Five channel data at each station: $E_X$ $E_Y$ $H_X$ $H_Y$ $H_Z$ (graphical representation in Fig. 52)
- $H_Z$ is recorded only to give us some information about the geologic strike, whereas $E_X$, $H_Y$, and $E_Y$, $H_X$ tell us about subsurface resistivity
- Magnetic fields are measured in two horizontal directions and in a vertical direction. Electric fields were measured in two horizontal directions (Fig. 51 )
- Each station is independent of the others, 24-hour recording
- Stations are synchronized with GPS signals (remote referencing)
- The stations are separated by 1/4 mile to tens of miles, depending on type of survey and targets
- In-field processing and editing

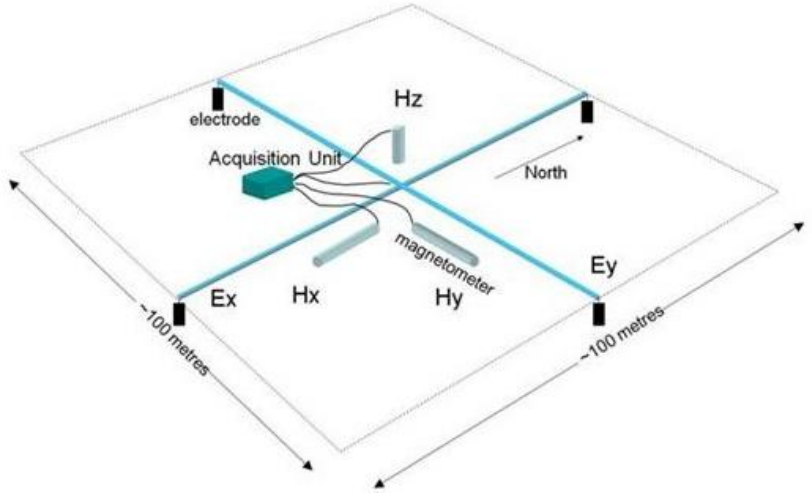


Fig. 51

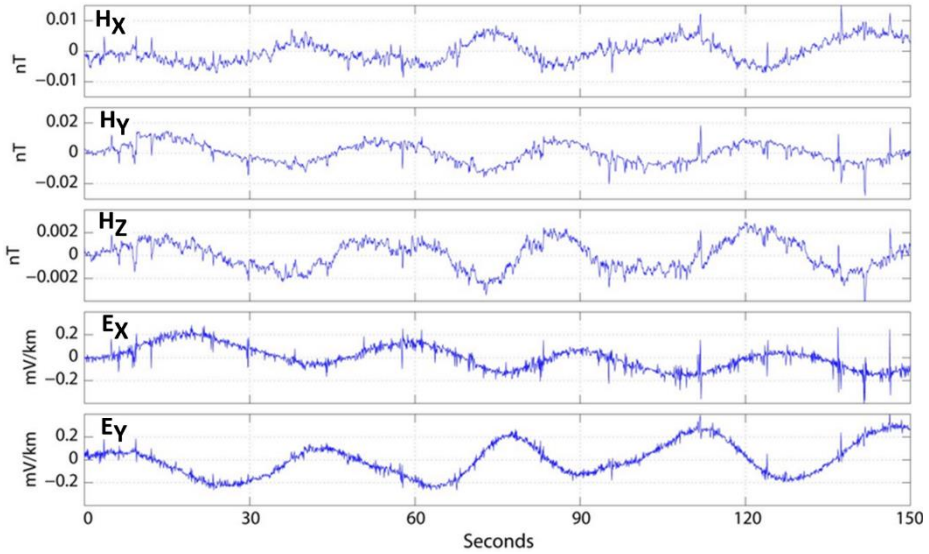


Fig. 52

# How to measure resistivity and phase of the Earth with MT

## How much energy is transmitted in to the Earth?

**Magnetotelluric response of a half-space, at normal incidence**

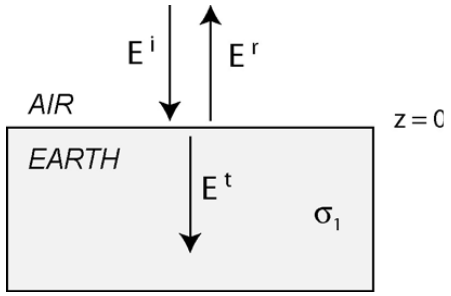


Fig. 53

- Amplitude of incident wave $E^i$, reflected wave $E^R$, transmitted wave $E^t$
- Consider some typical numbers for MT survey:
  Consider some typical numbers for a magnetotelluric survey:
  $\omega$ = 1 rad / s, $\sigma_1$ = 0.01 S/m, $\mu_0 = 4\pi\ 10^{-7}$ H/m, $\varepsilon_0 = 8.85*10^{-12}$ F/m, $k_0 = 3.33*10^{-8}\ m^{-1}$ and $k_1 = (1-i)*\ 7.93\ *10^{-5}\ m^{-1}$

$$\left|\frac{E^t}{E^i}\right| = 0.00006$$

*A small fraction of energy is transmitted into the Earth-Air boundary mostly reflected back into the air

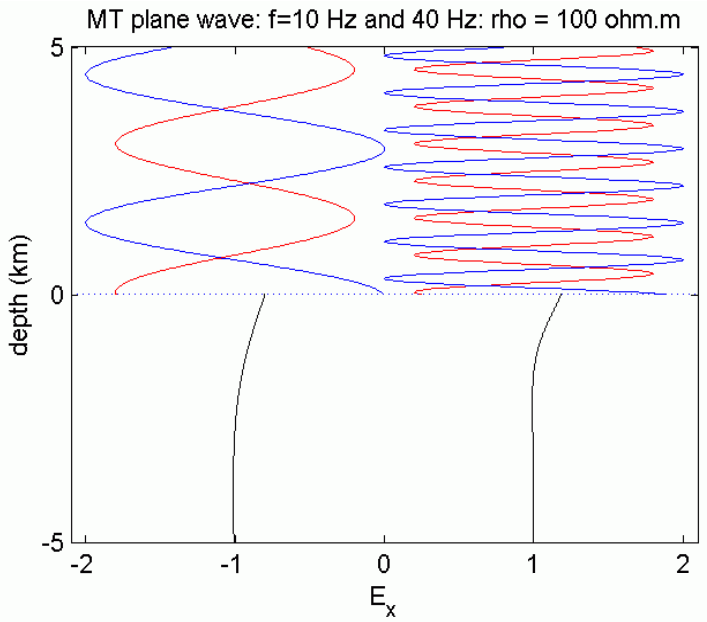


Fig. 54

$f$ : frequency (Hz)
$\sigma$ : conductivity (S/m)
$\mu$ : magnetic permeability
$\delta$: depth of penetration (m)

$$\delta = \frac{500}{\sqrt{\sigma f}}$$

$E_X$ : electric field
$H_Y$ : magnetic field
Z : impedance $\left(\frac{E_X}{H_Y}\right)$
$\rho_a$: apparent resistivity
$\Phi$ : phase (***function of frequency/ period***)

## Advantages of MT

- Natural source signal
- Plan waves- simple data analysis
- Powerful signals for deep exploration

$$\rho_a = \frac{1}{2\pi f \mu}\left|\frac{E_X}{H_Y}\right|^2$$

$$\Phi = \tan^{-1}\left(\frac{E_X}{H_Y}\right)$$

# MT Forward Problem in 1D

**Forward problem**

**Resistivity model of Earth** → **Predicted MT data**

**1) at f = 10 Hz, δ = 500** m in upper layer

- At high frequency, the skin depth is much less than the thickness of the 1st layer
- Average resistivity over a hemisphere, radius = δ is the resistivity of the upper layer.

**2) at f = 1 Hz, δ = 1580** m in upper layer

- EM signals are now just sampling the lower layer
- Average resistivity begins to increase as the 100 Ωm layer is being sampled

**3) at f = 0.1 Hz, δ = 5000** m in upper layer

- Hemisphere dominated by lower layer, so apparent resistivity close to 100 Ωm

**4) at f = 0.01 Hz, δ = 15800** m in upper layer

- Apparent resistivity close to 100 Ωm asymptotically

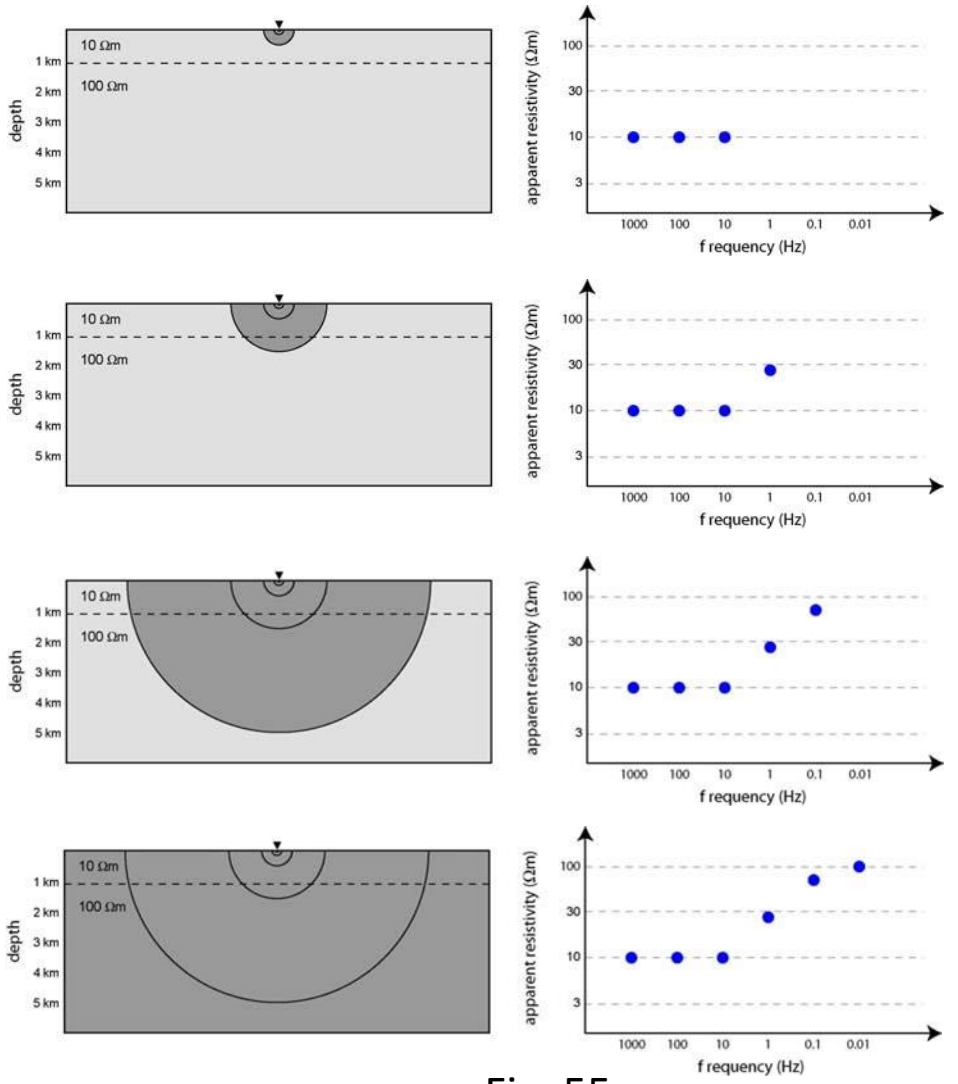


Fig. 55

# Impedance tensor and anisotropy

For station MT1 $Z_{xy} = \left|\frac{E_X}{H_Y}\right|$ For station MT2 $Z_{yx} = \left|\frac{E_Y}{H_X}\right|$

We can define the MT impedance tensor, **Z**, as:

$$\begin{bmatrix} E_X \\ E_Y \end{bmatrix} = \begin{bmatrix} Z_{XX} & Z_{XY} \\ Z_{YX} & Z_{YY} \end{bmatrix} \begin{bmatrix} H_X \\ H_Y \end{bmatrix}$$

For a 1-D Earth, wherein conductivity varies only with depth, diagonal elements of the impedance tensor, Zxx and Zyy (which couple parallel electric and magnetic field components) are zero, whilst the off-diagonal components (which couple orthogonal electric and magnetic field components) are equal in magnitude but have opposite signs, i.e.,:

$$\left.\begin{aligned} Z_{XX} &= Z_{YY} = 0 \\ Z_{XY} &= -Z_{YX} = Z \end{aligned}\right\} \text{ 1D Earth}$$

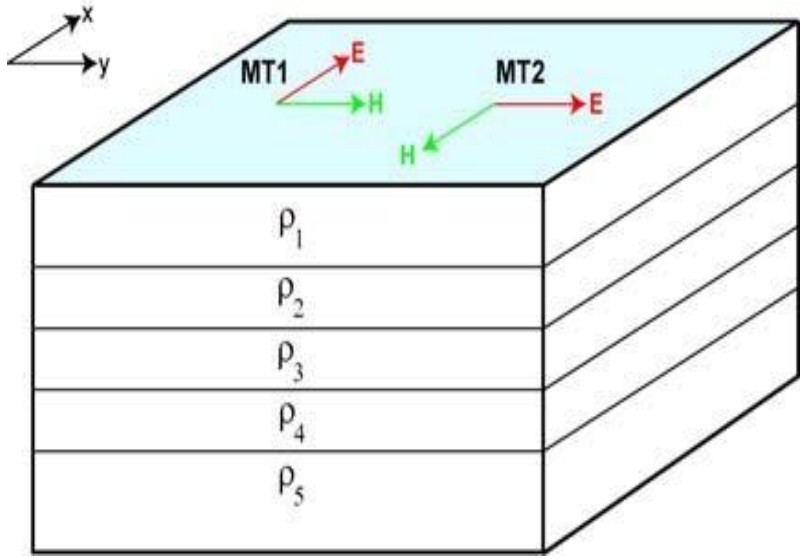


Fig. 56

For a 2-D Earth, in which conductivity varies along one horizontal direction as well as with depth, $Z_{XX}$ and $Z_{YY}$ are equal in magnitude, but have opposite sign, whilst $Z_{XY}$ and $Z_{YX}$ differ, i.e.,:

$$\left.\begin{aligned} Z_{XX} &= -Z_{YY} \\ Z_{XY} &\neq -Z_{YX} \end{aligned}\right\} \text{ 2D Earth}$$

For a 2-D Earth with the x- or y-direction aligned along electromagnetic strike, $Z_{XX}$ and $Z_{YY}$ are again zero. Mathematically, a 1-D anisotropic Earth is equivalent to a 2-D Earth.

# 1D MT sounding curves

1. Two layer, lower layer is conductive than the upper one

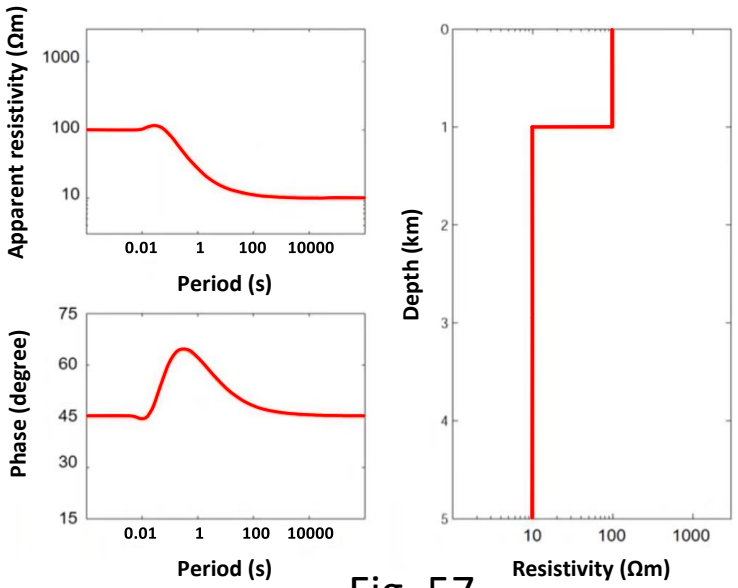


Fig. 57

2. Layer varying with depth

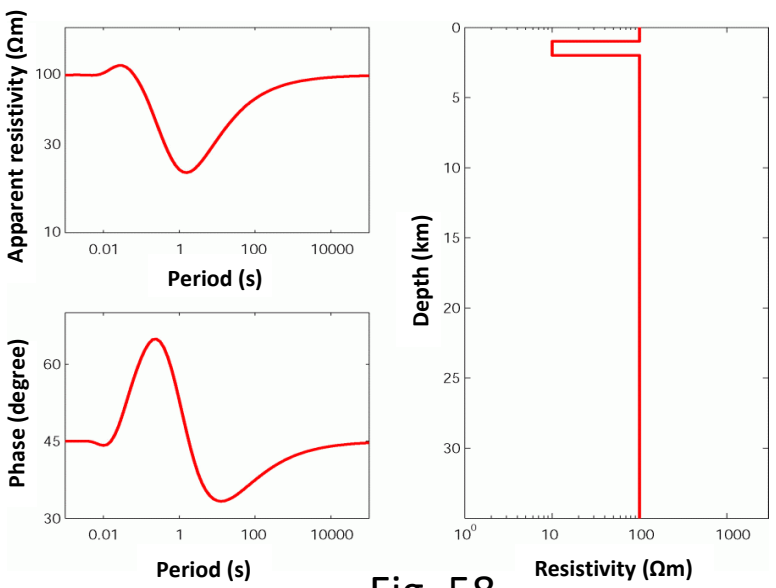


Fig. 58

3. MT responses several layers, each having an equivalent conductivity-thickness product for the conductive layer

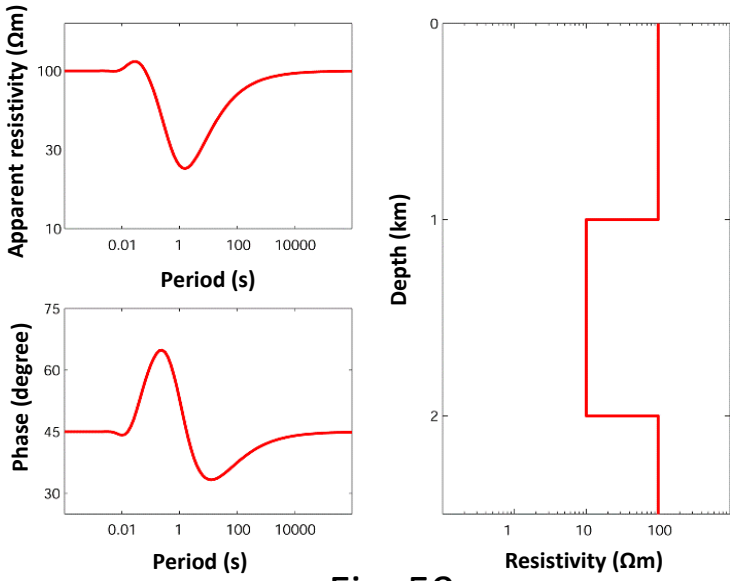


Fig. 59

4. Two layers: varying the conductance of the lower conductor

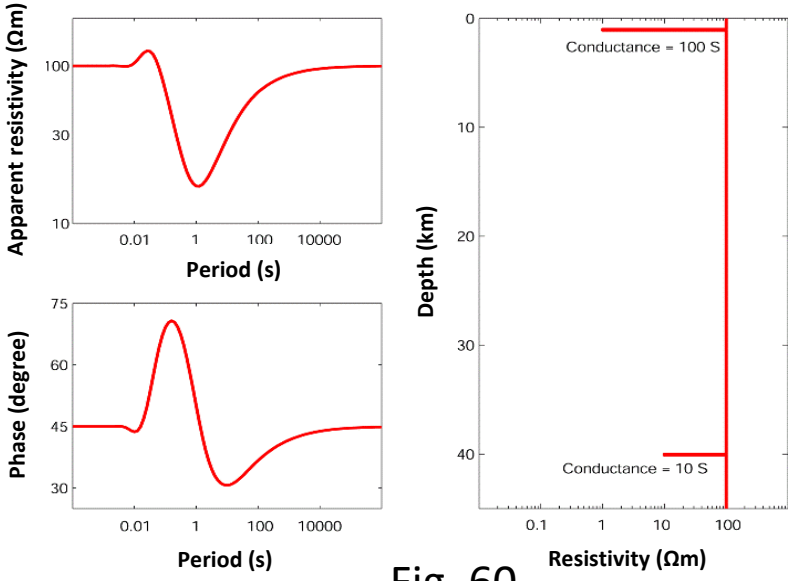


Fig. 60

# Transverse Electric (TE) and Transverse Magnetic (TM) mode

- According to the physical principle, current must conserved across the discontinuity, that means $j_y$ discontinuous, which demands that the electric field, $E_y$, must also be discontinuous ($j_y = \sigma E_y$), and all other components of the electromagnetic field are continuous across the boundary

- E-polarization/ TE mode, electric fields (currents) parallel to strike, it never tries to be discontinuous. Hence, it is less distracted and less sensitive to the discontinuity

- B-polarization/ TM mode, magnetic fields parallel to strike, and currents flowing perpendicular to strike. Since, $E_y$ is discontinuous across a vertical contact

- Therefore, B-polarisation resistivity's tend to resolve lateral conductivity variations, whereas, E-polarisation to resolve vertical conductivity variations

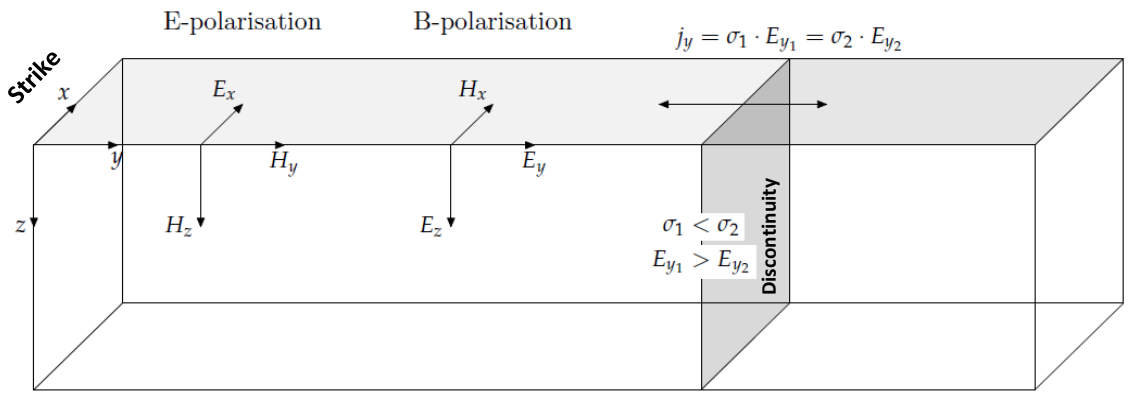


Fig. 61

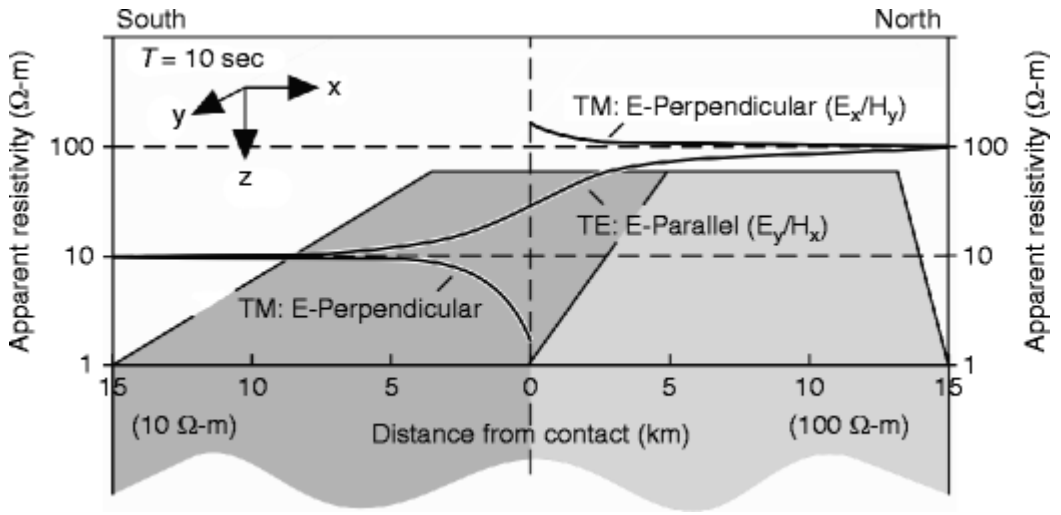


Fig. 62

# TE and TM mode response for a synthetic model

Resistivity model

Pseudo-section

Pseudo-section

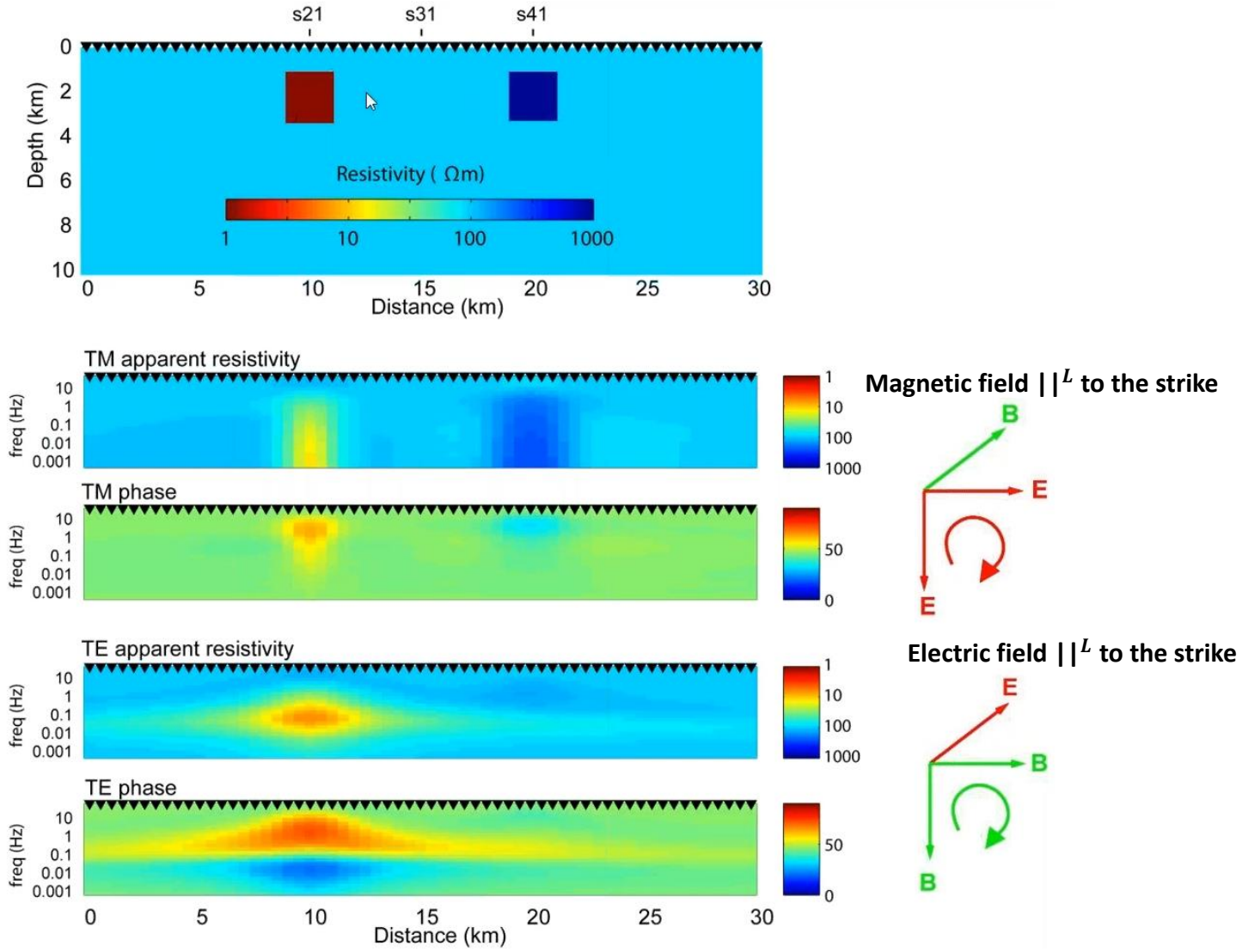


**Magnetic field $||^L$ to the strike**




**Electric field $||^L$ to the strike**




Fig. 63

# Adjustment length

- So far, we have stressed that MT measurements yield a volume sounding
- However, the field scenario depicted in the Fig.64 having the conductivity structure of the Earth varying laterally as well as with depth
- Lateral conductivity variations distort the sounding volume
- It is well known that EM fields of a given sounding period penetrate less deeply into high-conductivity heterogeneities
- Therefore, we need to consider horizontal adjustment length along with the vertical penetration depth

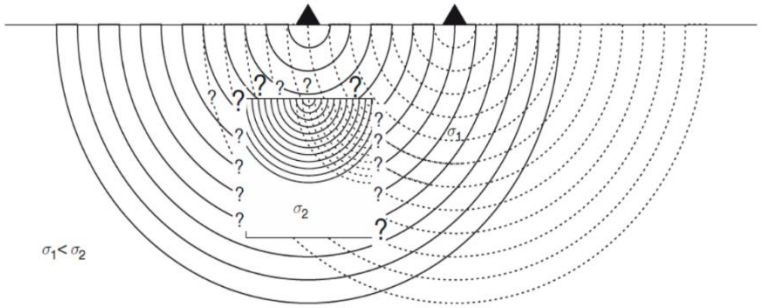


Fig. 64

Example:

Depth of penetration is = $503\sqrt{\rho T}$

= 15.906 m

The impedance phases diverge from the response expected for a 100 Ωm half-space (directly underlying site A) at periods of ~10 s. For example, at ~8 s, the phase splitting (Δφ) is ~2°. Therefore the horizontal adjustment length at ~ 10 s is approximately twice the penetration depth (p ~ 14 km.

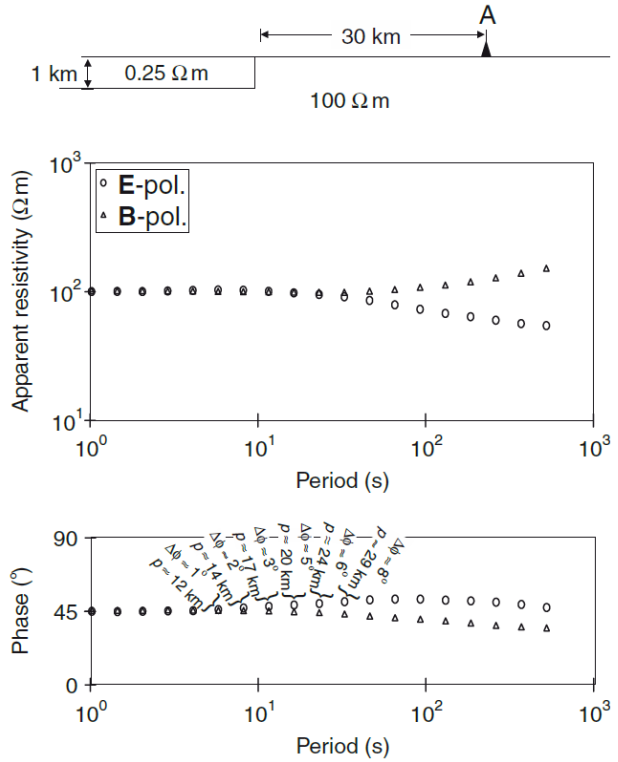


Fig. 65

# MT studies in India

- **2700 stations**
- **Time frame: 1980-2008**

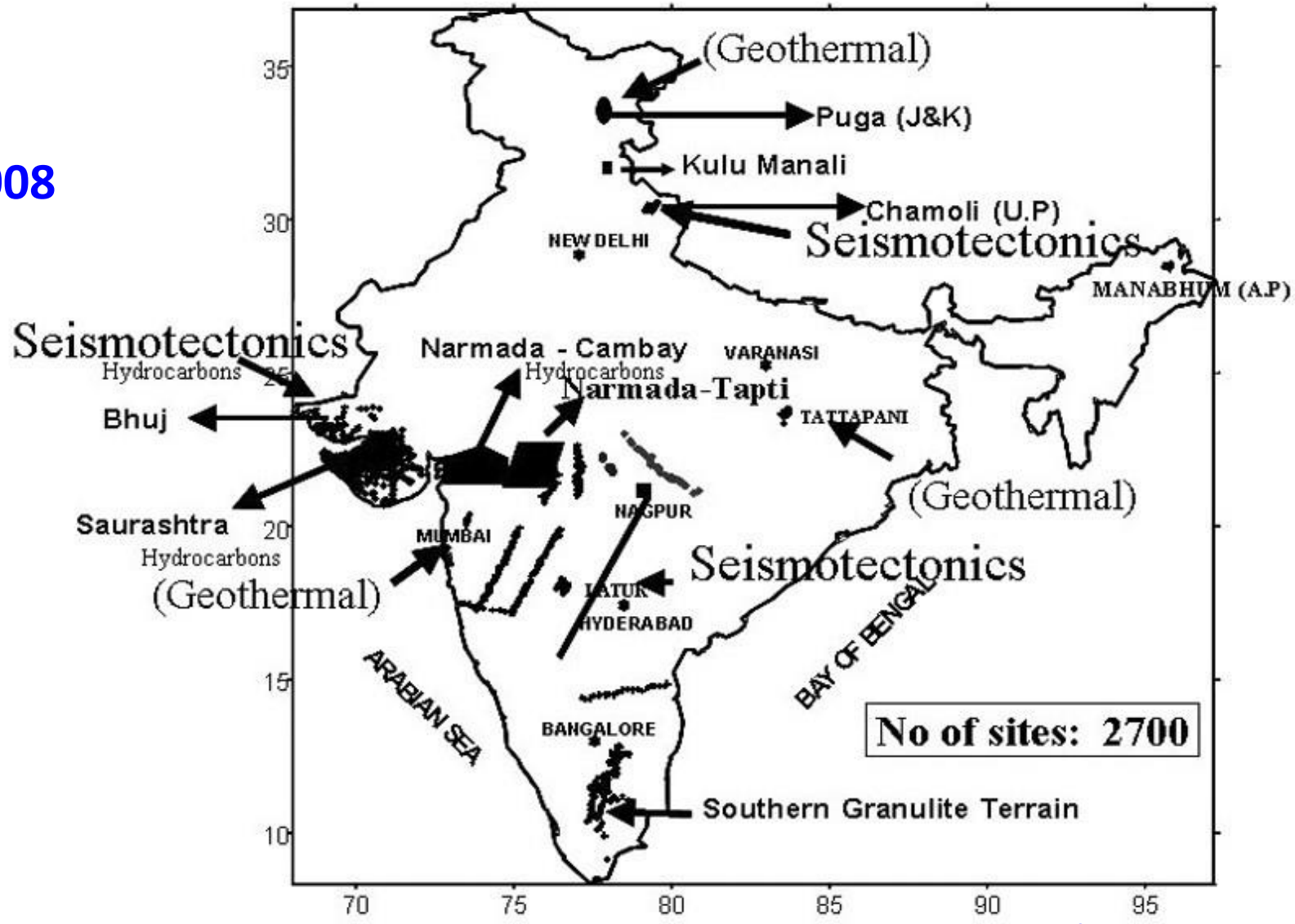


Fig. 66

(After, Harinarayana, 2008)

# Continued…..

Status report of MT study in India during 2016-19

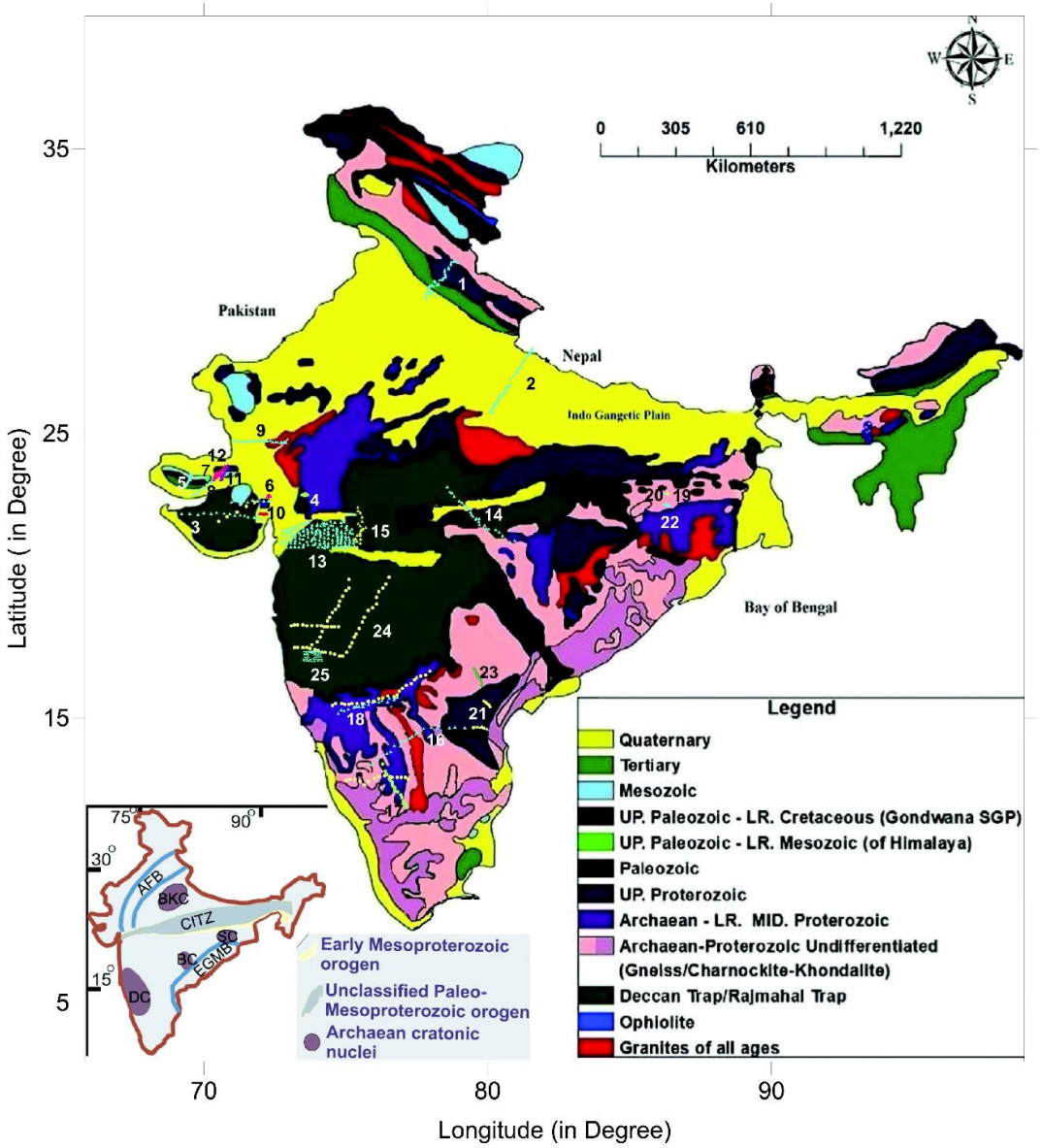


Fig. 67

(After, Israil et al. 2020)

# A few case studies: hydrocarbon exploration using MT

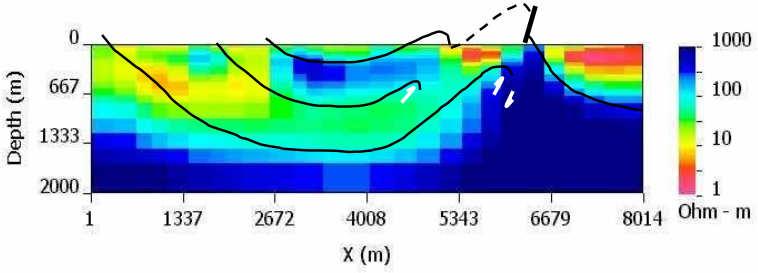


Fig. 68

Grandis et al. (2004) mapped the subsurface overthrust structures (interpreted geological boundaries) of Tanjungkerta, Sumedang, West Java.

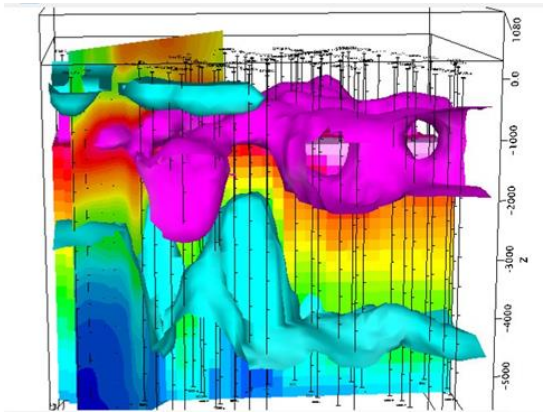

Fig. 69

Lugão et al. (2017) represents 3D resistivity model in depth for the onshore Sergipe-Alagoas (SEAL) Basin, Brazil, showing structure of the basement (cyan), sediment sequence (purple) and top carbonate layer (cyan)

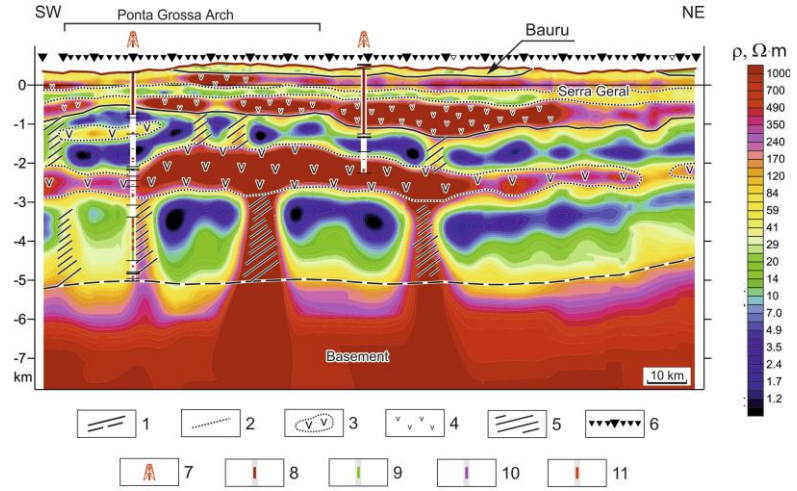


Fig. 70

Palshin et al. (2017) addressed the Litho-stratigraphic layers of Parana sedimentary basin of Brazil, using MT data and validated the results with resistivity log data

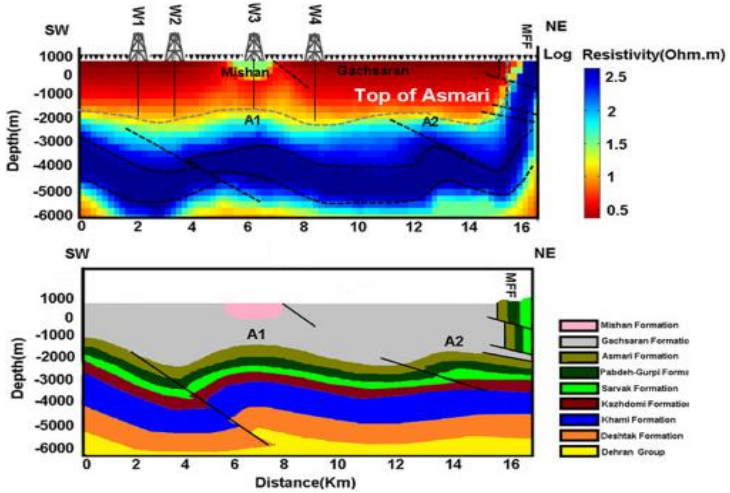


Fig. 71

Sarvandani et al. (2017) Interpreted sub-surface sedimentary layers and established a rock strata model of Gachsaran oil field using magnetotelluric data.

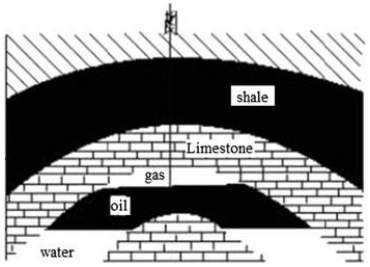


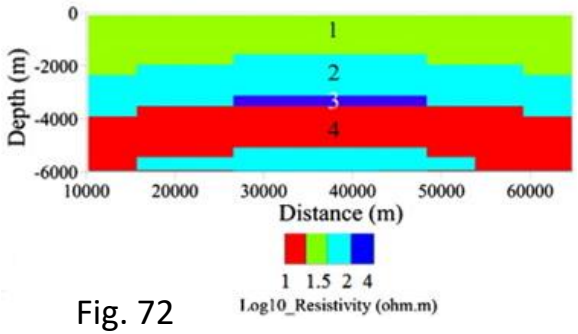


Fig. 72

Zhang et al. (2014) documented a theoretical assessment of magnetotelluric method for oil and gas exploration with synthetic examples

# Remote Sensing (RS)

# Basic concept

## Remote sensing is…

The practice of deriving information about the Earth's land and water surfaces using images **acquired from an overhead perspective**, by employing **electromagnetic radiation** in one or more regions of the electromagnetic spectrum, **reflected or emitted** from the Earth's surface.

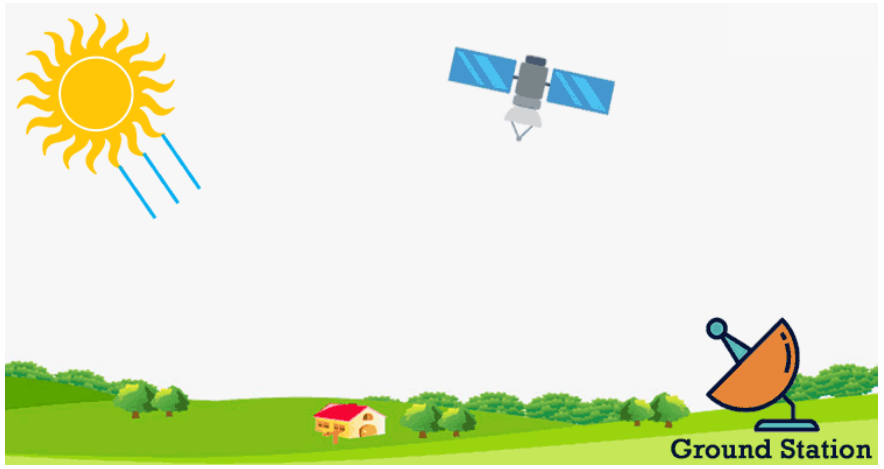


Fig. 72

**Major objective** is to Analyze and Understand the Environmental and natural resources information

**Sensors**

A device that gathers energy and converts it into a signal and presents it as suitable for obtaining information about the target under investigation

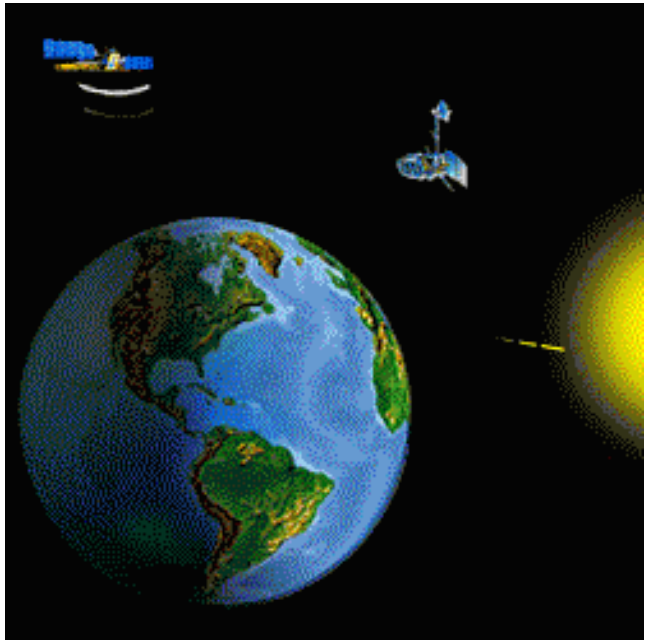

Fig. 73

# Physics of RS

- Energy propagates in the form of Electromagnetic Radiation, propagate through the space at speed of light travels about 1 ft/ nanosecond ($10^{-9}$ s)
- Light can either be reflected, absorbed or transmitted on a surface, and the proportion of these three will vary at each wavelength for a particular object
- Reflection is emission of photons caused by excitation of the surface, due to incident radiation
- Reflected energy $E_r$= incident $E_i$ – absorbed and transmitted energy $E_t$ (this relation holds for each wavelength)
- Spectral reflectance $\rho = {E_r}/{E_i}$
- The power of emitted photons is each wavelength depends on the surface
- An RS sensor detect spectral responses from objects in various wavelength ranges
- Each class of object has different spectral responses across wavelength
- Spectral reflectance values are plotted against corresponding wavelength (known as spectral reflectance)

Electromagnetic spectrum

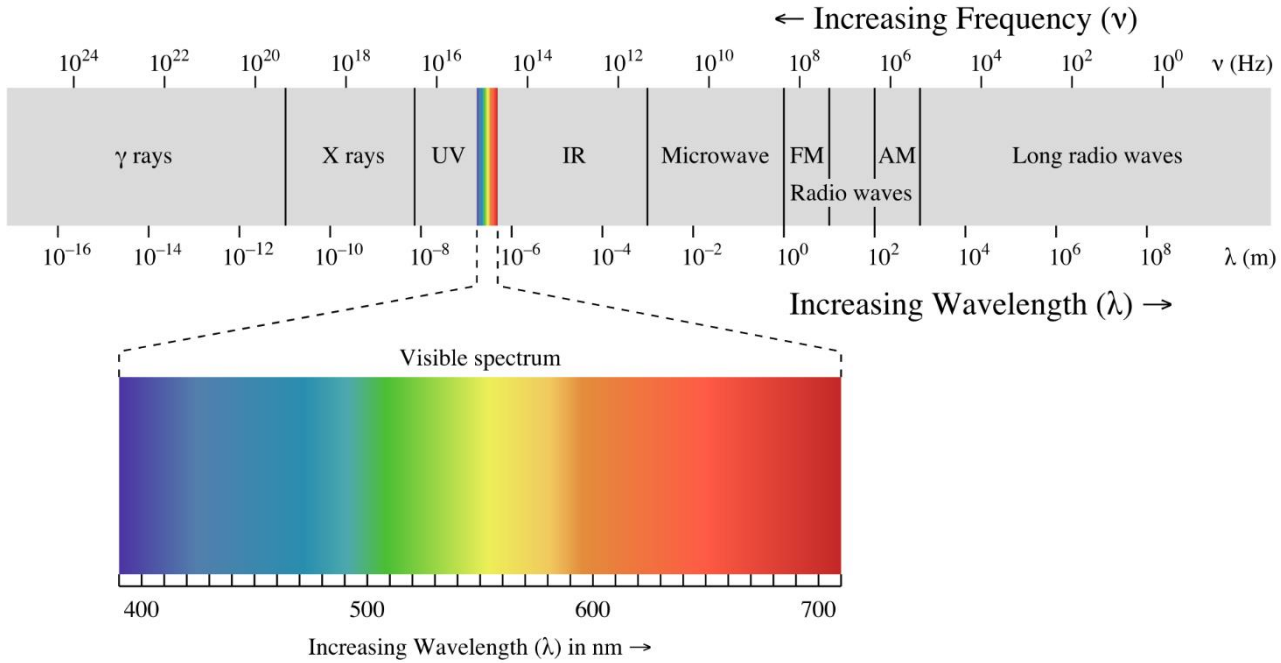


Fig. 74

# Particle model of Electromagnetic energy

The total emitted radiation ($M_\lambda$) from a blackbody is proportional to the 4th power of its absolute temperature. This is known as the Stefan-Boltzmann law and is expressed as:

$M = \sigma T^4$

In addition to computing the total amount of energy exiting from a theoretical blackbody such as the Sun, we can determine its dominant wavelength ($\lambda_{max}$) based on Wein's displacement law:

$\lambda_{max} = A/T$ (where $A = 2898 \mu m.K$)

According to wave theory and the quantum theory, the relationship between the energy and frequency ($\vartheta$) of radiation is expressed as:

$Q = h \times \vartheta$

(where h is Planck constant $6.626 \times 10^{-34}$)

Rayleigh Scattering: Particle diameter ≪wavelength (λ)

Rayleigh scattering cross−section $(I) \propto \frac{1}{\lambda^4}$

Mie Scattering: Particle diameter ≈ wavelength (λ)

Non selective Scattering: Particle diameter ≫ wavelength (λ)

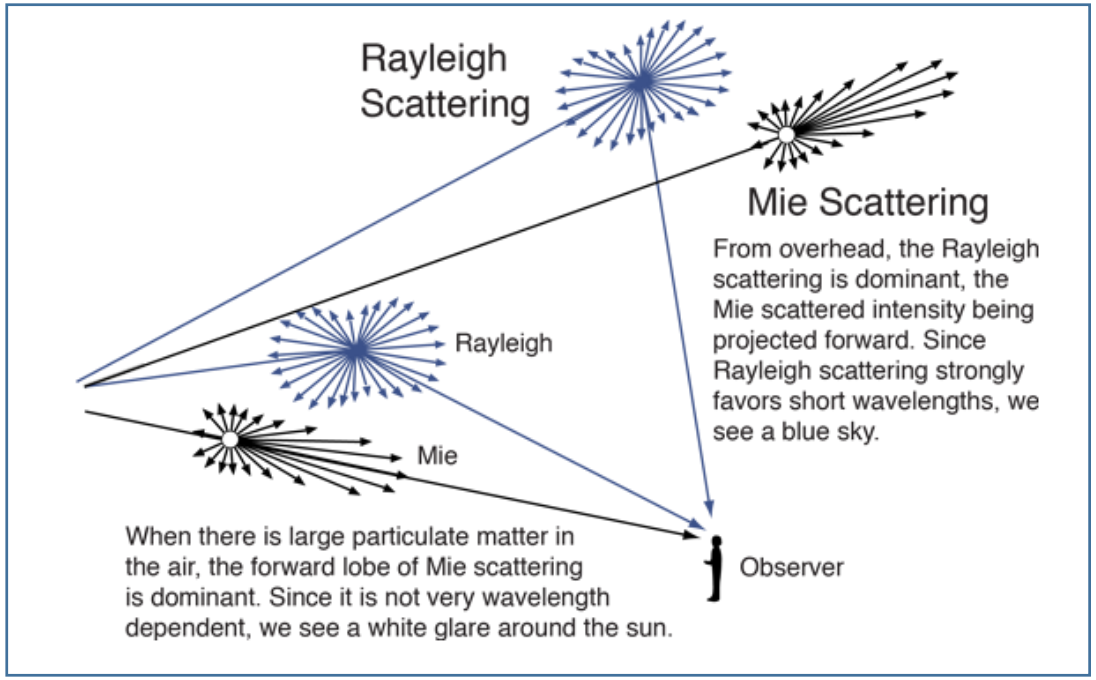


Fig. 75

# Surface scatter (Reflection) mechanism

## Rayleigh criterion:

- Widely used to estimate the degree of roughness
- The Rayleigh criterion states that a surface can be considered as smooth, if the surface irregularities are less than λ/8

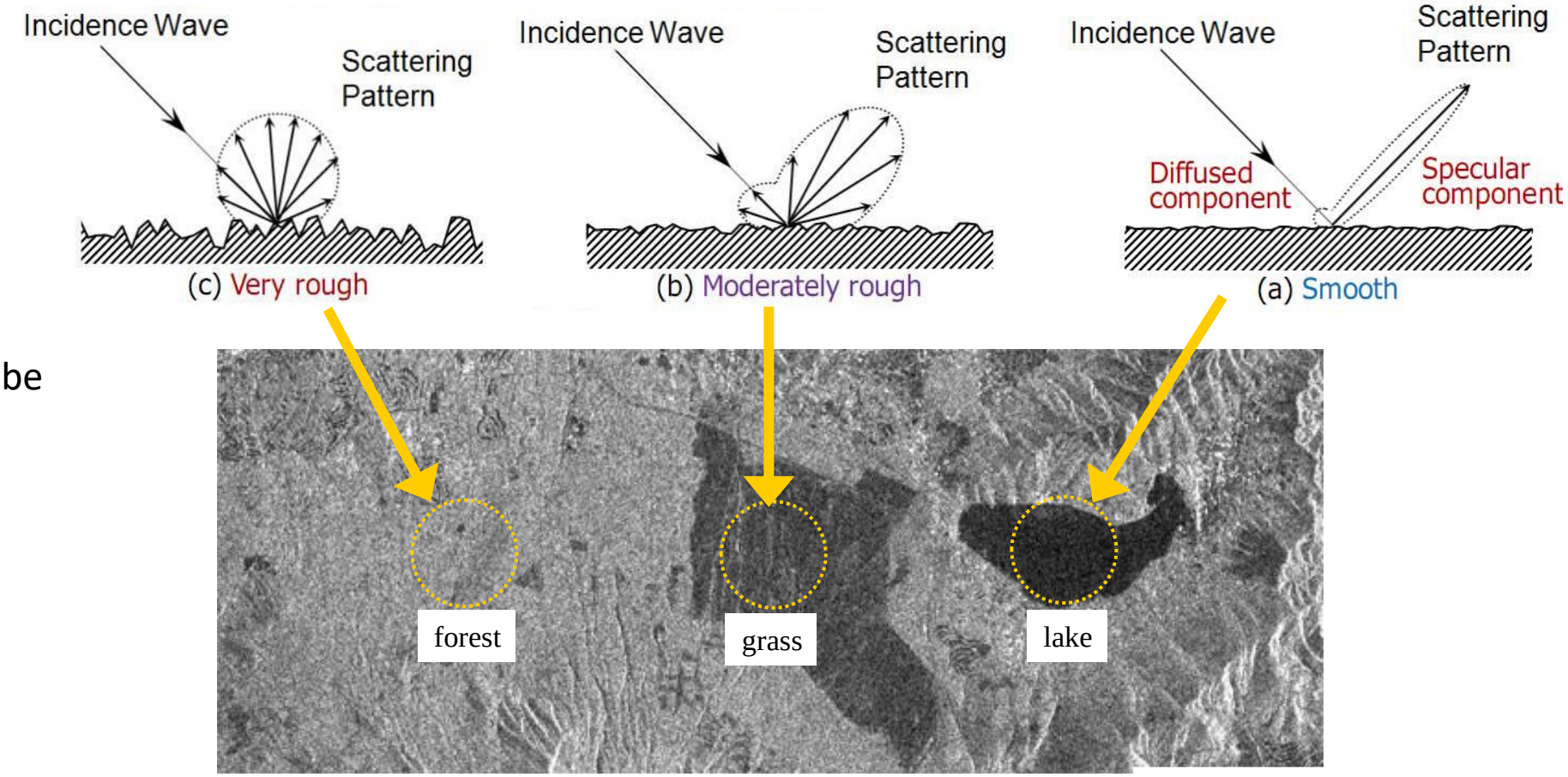


Fig. 76

# Atmospheric windows

- The spectral band for which the atmosphere is transparent are called the Atmospheric windows
- It is important for sensor design

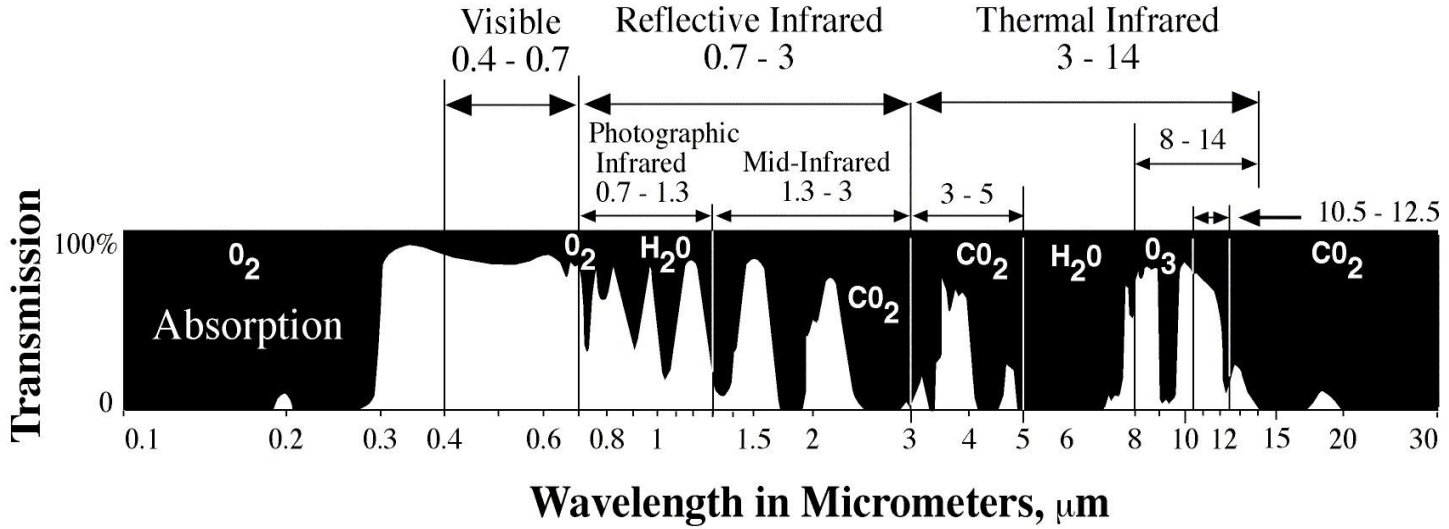


Fig. 77

- **The windows**
  - **UV & visible: 0.30-0.75 $\mu m$**
  - **Near infrared: 0.77-0.91 $\mu m$**
  - **Mid infrared: 1.55-1.75; 2.05-2.4 $\mu m$**
  - **Far infrared: 3.50-4.10; 8.00-9.20; 10.2.-12. $\mu m$**
  - **Microwave: 7.50-11.5 mm; 20.0+mm**
- **X-rays and UV are very strongly absorbed**
- **Gamma & IR are somewhat less strongly absorbed**

# Types of RS

## Optical Remote Sensing

- sensors detect solar radiation
- Wavelength extends from visible and near IR (300 nm) to short IR (3000 nm)
- Requires spectral reflectance signatures of various materials on the earth surface

## Thermal Infrared Remote Sensing

- sensors detect thermal infrared radiation emitted from the earth
- The middle wave infrared (3000 nm to 5000 nm) and long wave infrared (8000 nm to 14000 nm)are within the TIR region. These radiation are emitted from warm objects like Earth's surface, sea surface and forest fire

## Microwave Remote Sensing

- Satellites carry their own flashlight emitting microwaves to illuminate the targets, and sensor records the backscattered microwaves from earth
- Microwave wavelength range from 1 mm to 1 m EM spectrum
- Mostly active sensors, having own sources of energy, and thus images can be acquired both day and night

**(a) Visible & Reflected IR Remote Sensing**

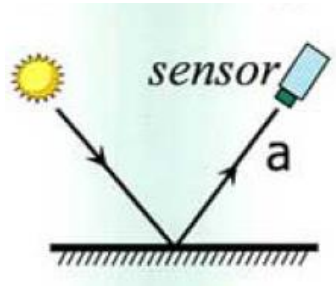


**(b) Microwave Remote Sensing**

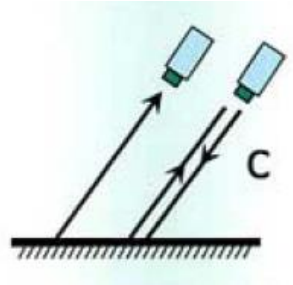


**(c) Thermal IR Remote Sensing**

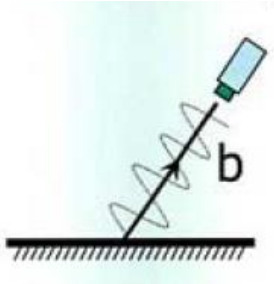


Fig. 78

# Types of Platforms

- Where the sensors are placed
- Depending upon the working environment they are classified as follows:

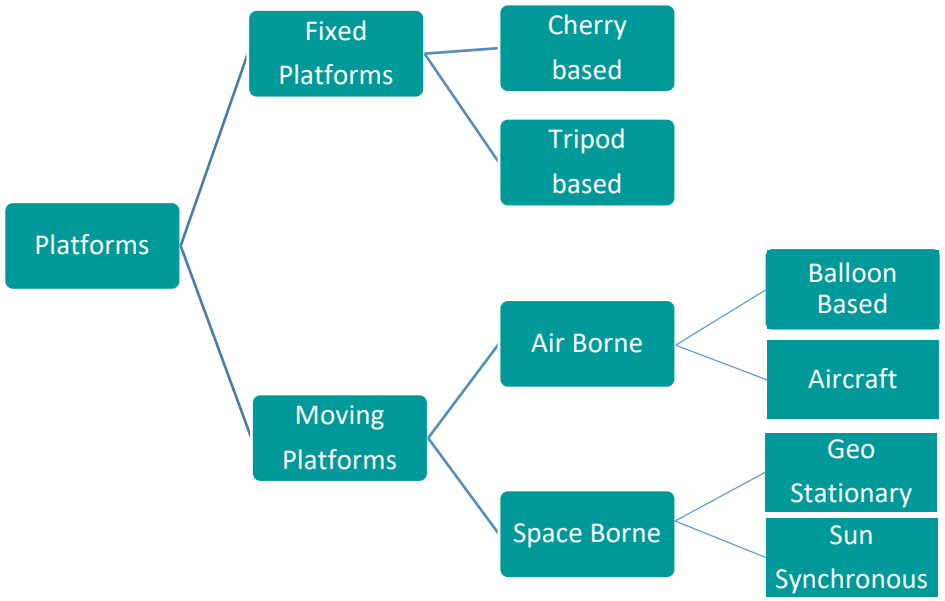


Fig. 79

## Sun Synchronous Platform

- Crosses particular places at same local time
- 600 – 900 km altitude
- North to South rotation
- Polar Orbit
- Inclination 80°/ 100° to Equator
- Orbital period 100 minute

## Geo Stationary Platform

- Faces towards particular portion of the earth
- 3600 km altitude
- West to East rotation
- Equatorial Orbit
- Angular coverage 120
- Orbital period 24 H

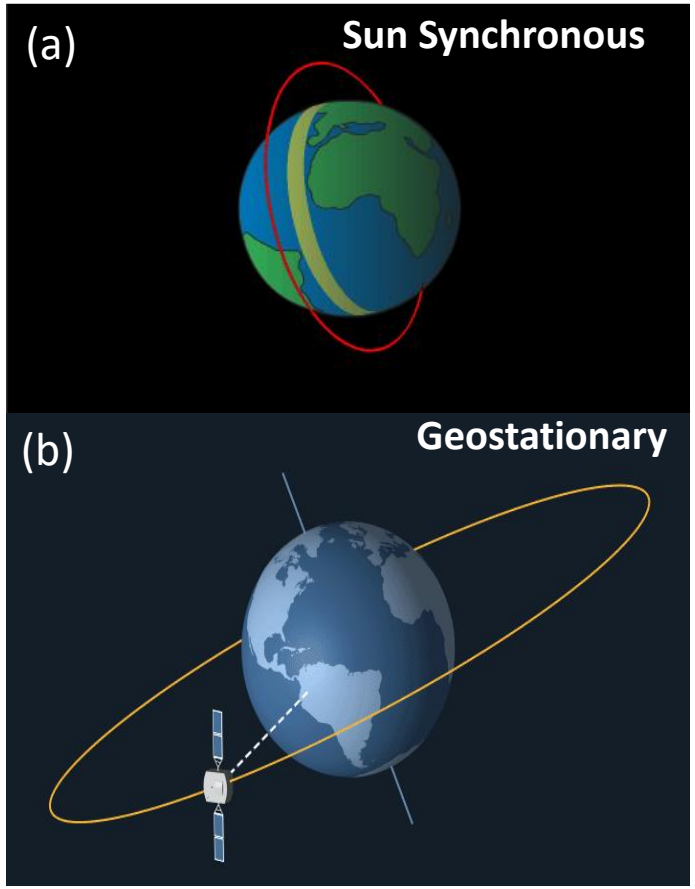


Fig. 80

# Resolution

- Resolution of an image refers to potential detail provided by the imagery

- In remote sensing, we refer to four types of resolution: **spatial, spectral, temporal & radiometric**

## Spatial resolution:

- The size of the smallest possible feature that can be detected (pixel size)

## Spectral resolution ($\Delta\lambda$):

- Ability of a sensor to define fine wavelength intervals
- The finer spectral resolution, narrower the wavelength

**Spectral resolution of different materials**

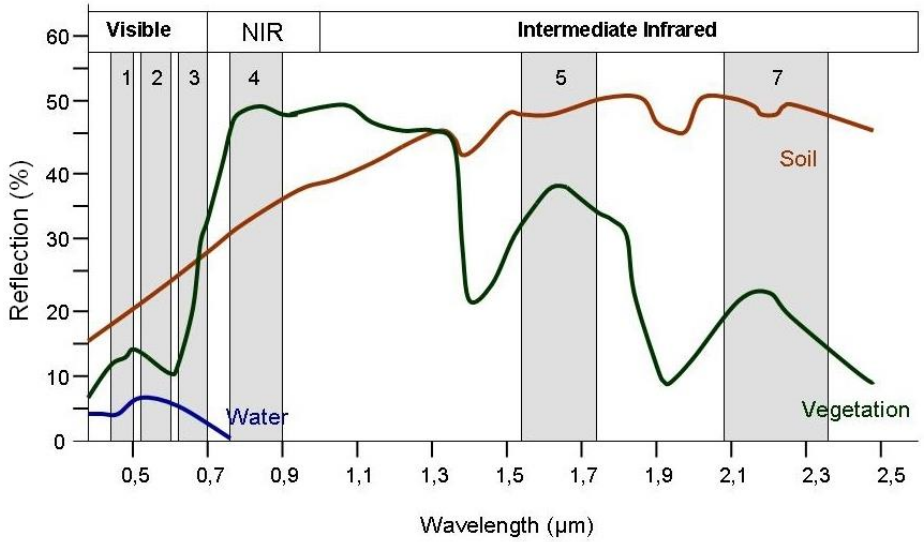


Fig. 81

## Temporal resolution:

- The revisit period and the length of time for a satellite to complete one entire orbit cycle, i.e., start and back the exact same area at same viewing angle
- The finer spectral resolution, narrower the wavelength

## Radiometric resolution:

- Ability to discriminate very slight differences in reflected and emitted energy
- The finer radiometric resolution of a sensor, the more sensitive it is to detecting small differences in energy

# Oil spill identification using satellite imagery

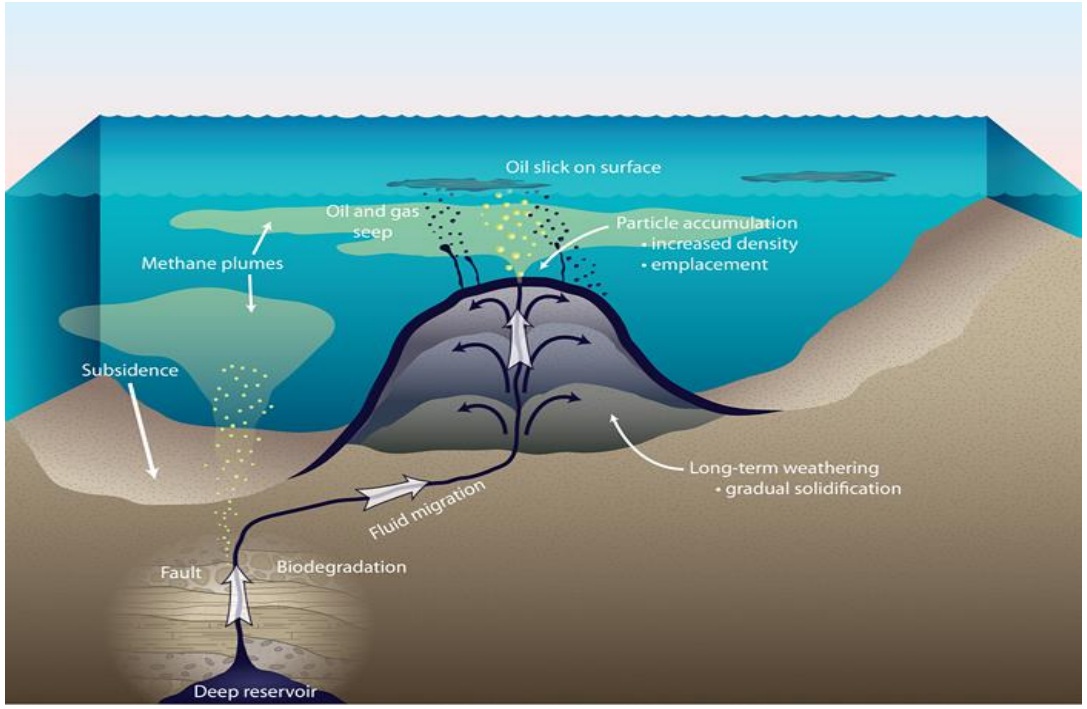


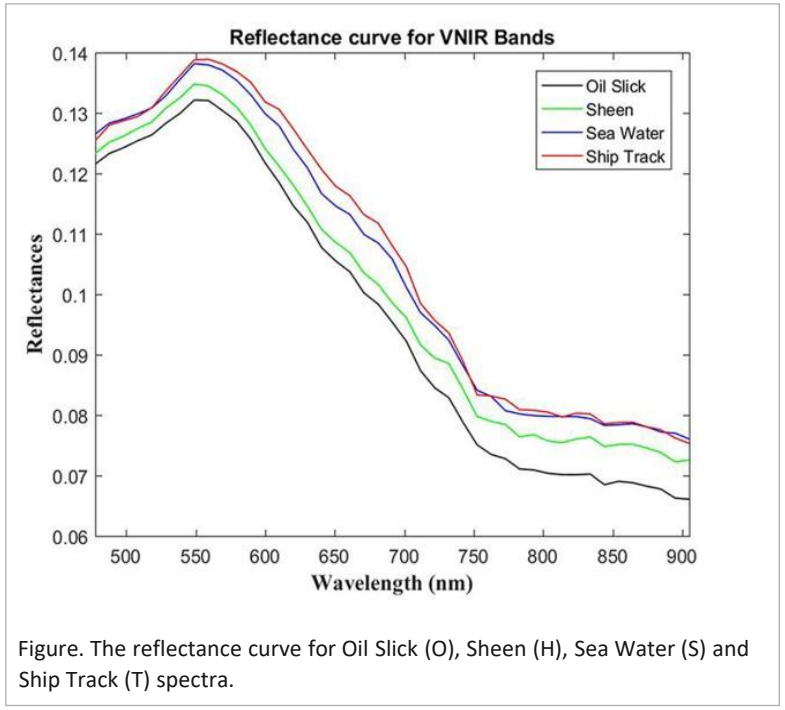


Figure. The reflectance curve for Oil Slick (O), Sheen (H), Sea Water (S) and Ship Track (T) spectra.

Fig. 82

The spectral reflectance of water in the Ship Track is higher than that of the background Sea Water, which in turn is higher than the spectral reflectance of the Sheen and Oil Slick. As the thickness of the oil spill changes, the reflectance varies within the visible and NIR spectral ranges

# Case study: Hydrocarbon detection using RS study

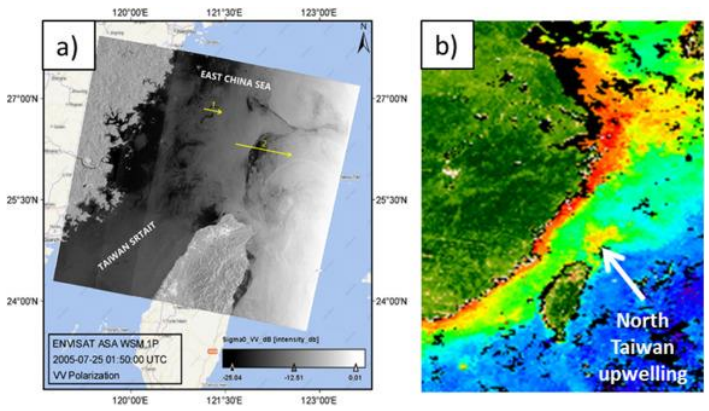


Fig. 83 **(After Alperset et al. 2017)**

Alperset et al. (2017) documented the challenges and pitfalls of radar imageries for oil spill detection

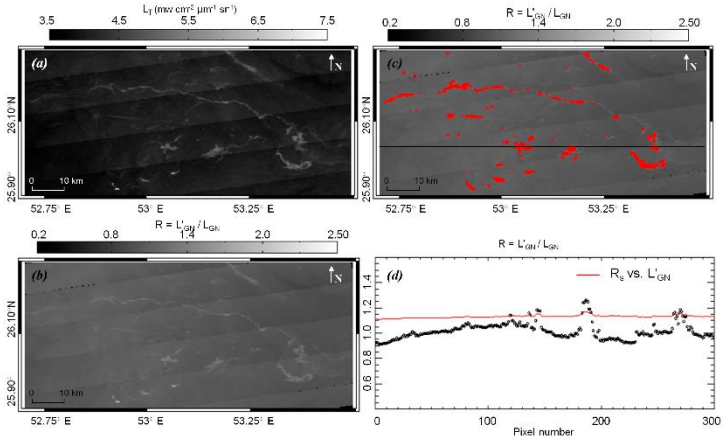


Fig. 84 **(After Pisano et al. 2015)**

Pisano et al. (2015) Detected oil spill in Arabian using Near-Infrared MODIS Imagery

**Prabaharan et al. (2013) identified** the Surface and subsurface lineament analyses for delineating hydrocarbon reservoirs in the Nagapattinam Sub-Basin of Cauvery Basin.

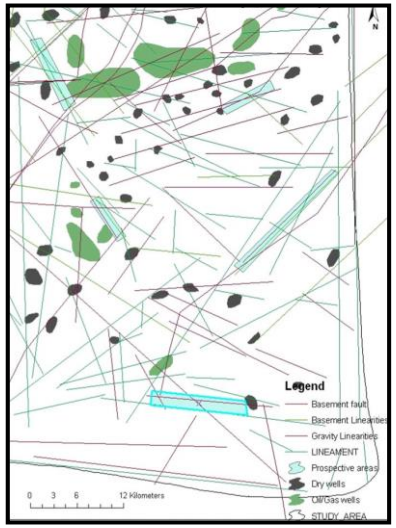


**(After Prabaharan et al. 2013)**

Fig. 85

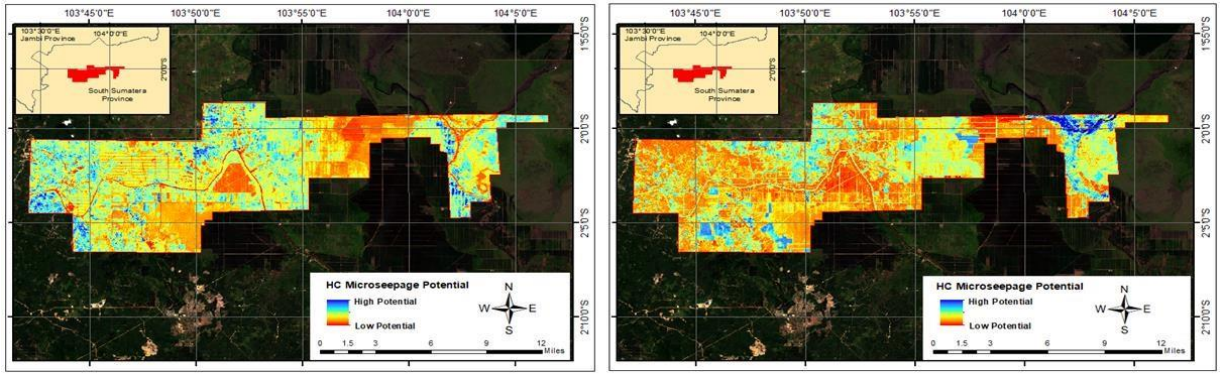


Fig. 86 **(After Putra et al. 2019)**

Putra et al. (2019) detected onshore oil and gas reservoir through mapping of hydrocarbon microseepage using remote sensing

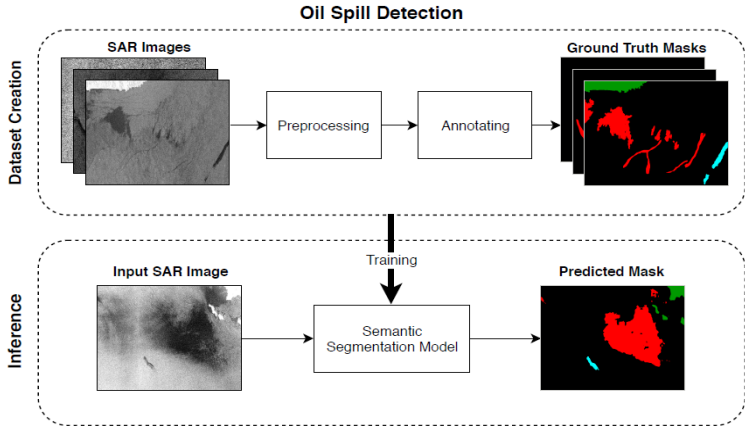


Fig. 87 **(After, Krestenitis et al. 2019)**

Krestenitis et al. (2019) Oil Spill Identification from Satellite Images using convolutional neural networks

# Well log analysis using AI/ ML & Mathematical tools

Rock layer identification using combined wavelet and Fourier transform of wireline log data

# Identification of Formation Interface

## Wireline log data (Well-7)

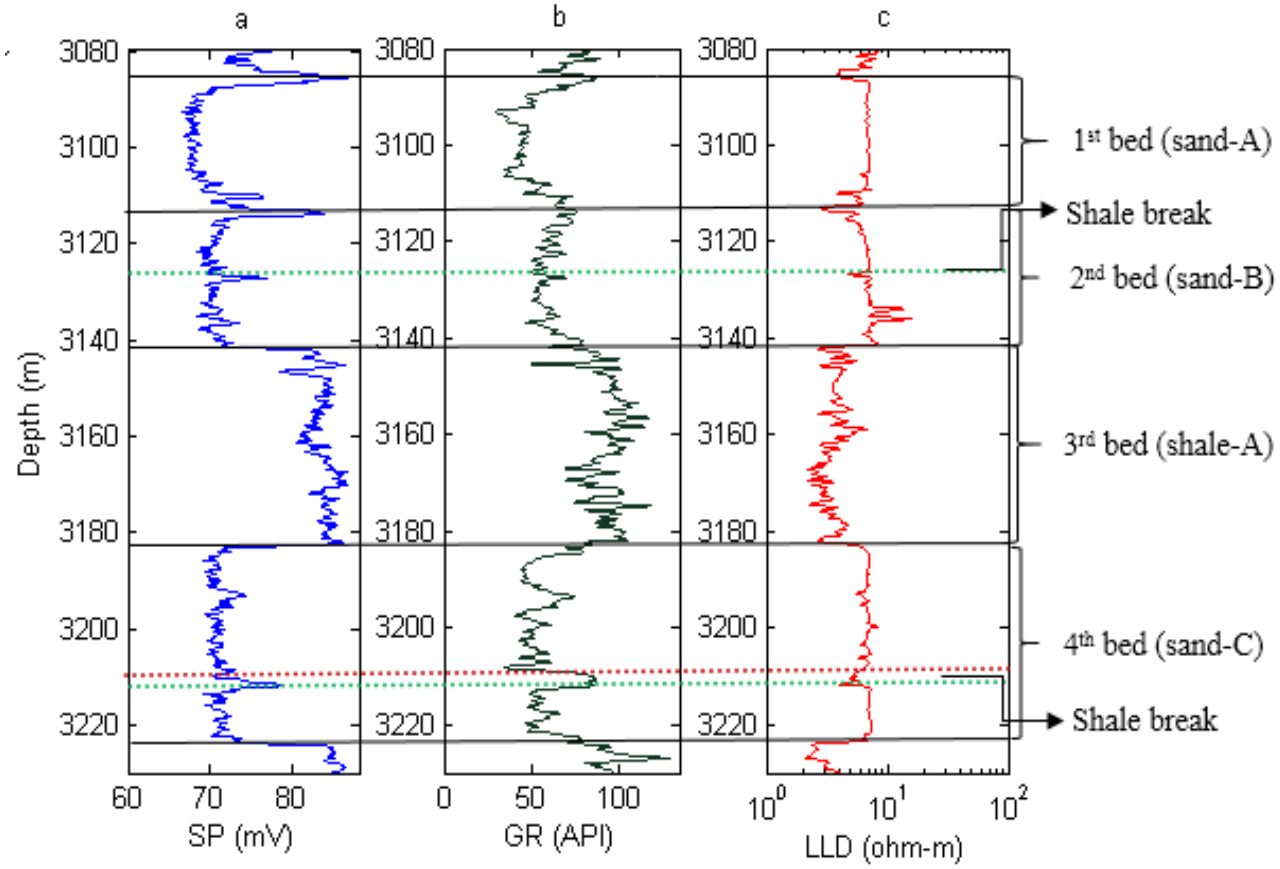


Fig. 88

## Flow chart

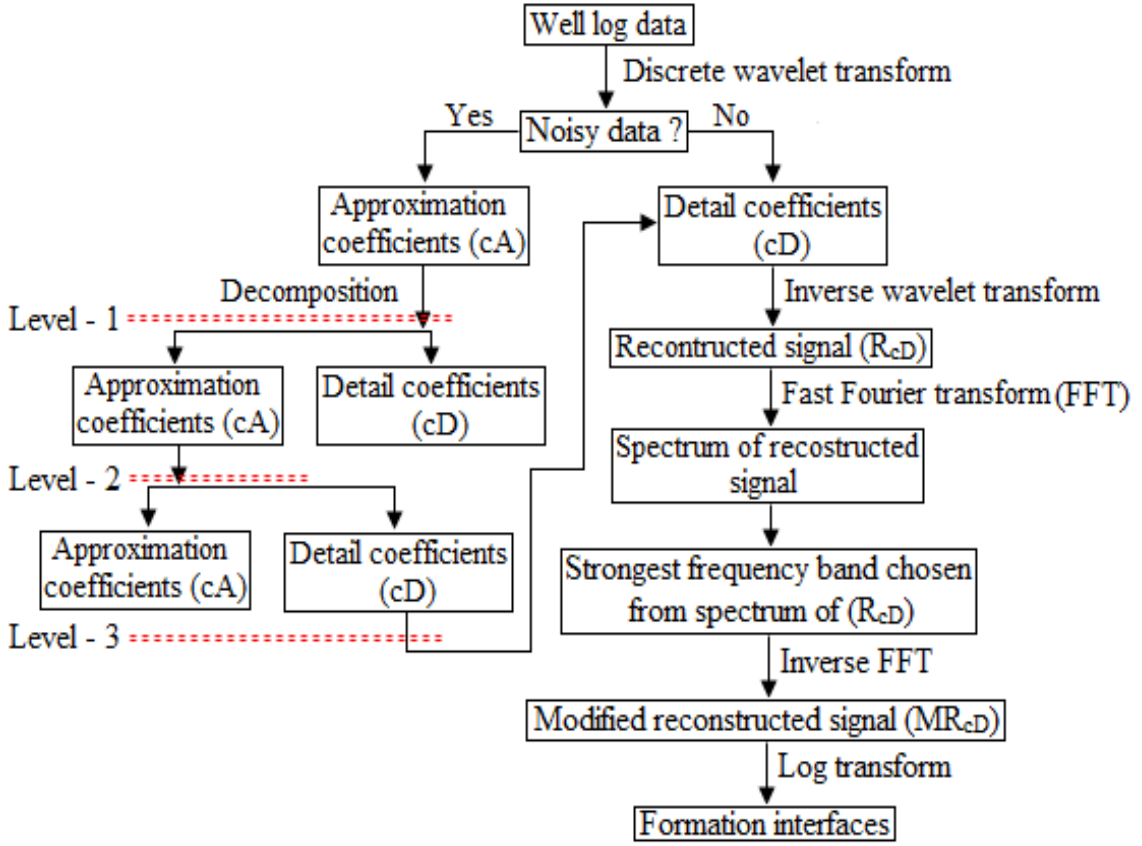


Fig. 89

- Spontaneous potential - SP,
- Gamma ray – GR and
- Latero-log deep resistivity - LLD

**(Mukherjee and Roy, 2016)**

# Continued…

**Detail wavelet coefficients (cD) from DWT**

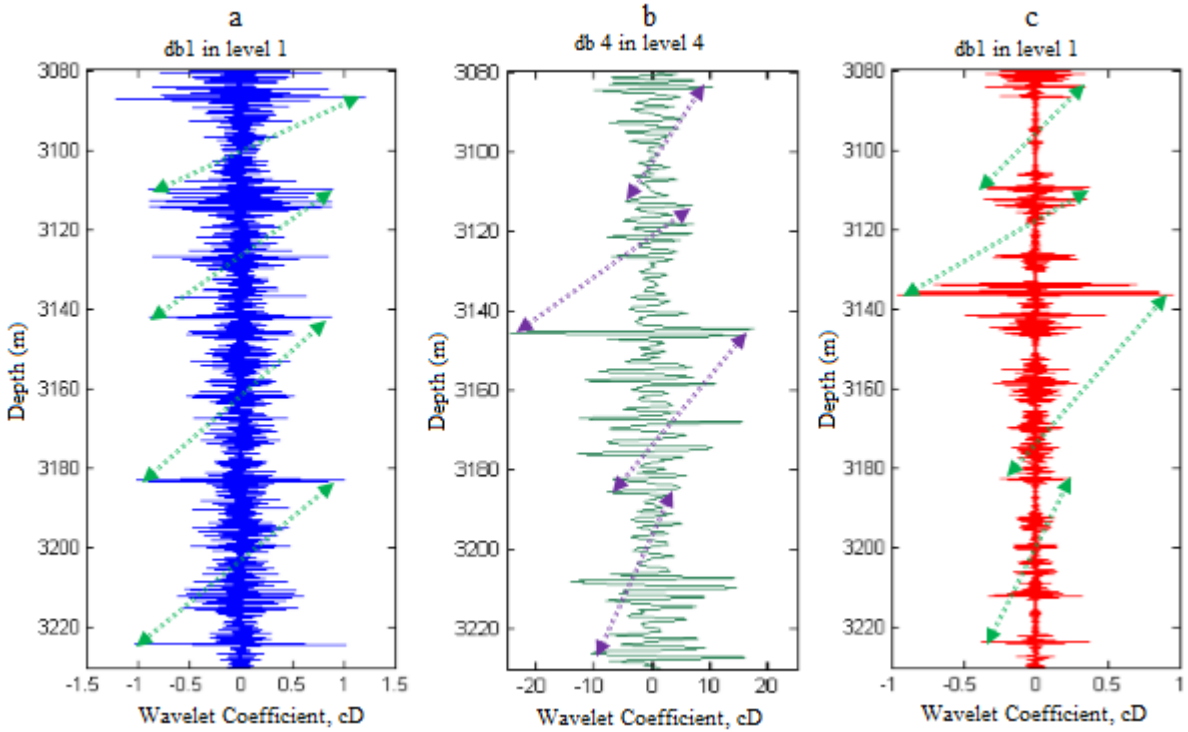


Fig. 90

**(Mukherjee and Roy, 2016)**

- Interpreter faces difficulties in finding the formation interfaces through mere visualization of the details coefficients.
- Discerning formation interfaces using combined DWT and FT analysis, which is much clearer on that aspect

# Continued…

## Reconstructed signal (RcD) of the logs from detail wavelet coefficients

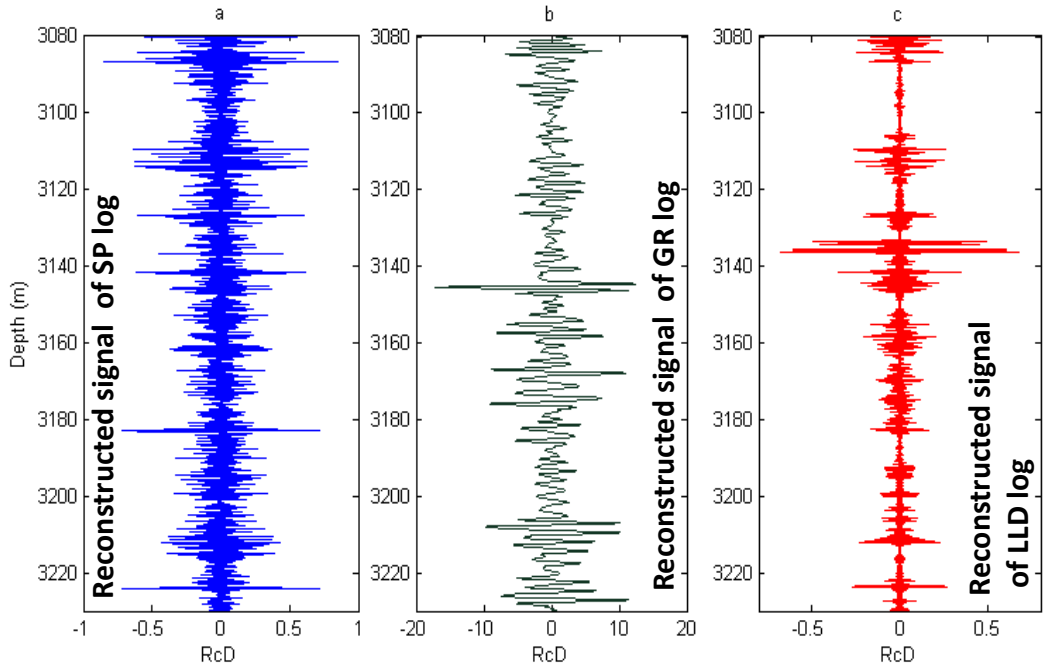


Fig. 91

- Reconstructed signals are basically contained the high frequency component of the raw log signal (log data).
- There are dissimilar frequency band has been observed in the amplitude spectrum of reconstructed signal.
- Inverse FT was applied to the chosen frequency band (s) and corresponding results provide a modified reconstructed data (MRcD)

**(Mukherjee and Roy, 2016)**

## Spectrum analysis of RcD (S) and selection of strongest band

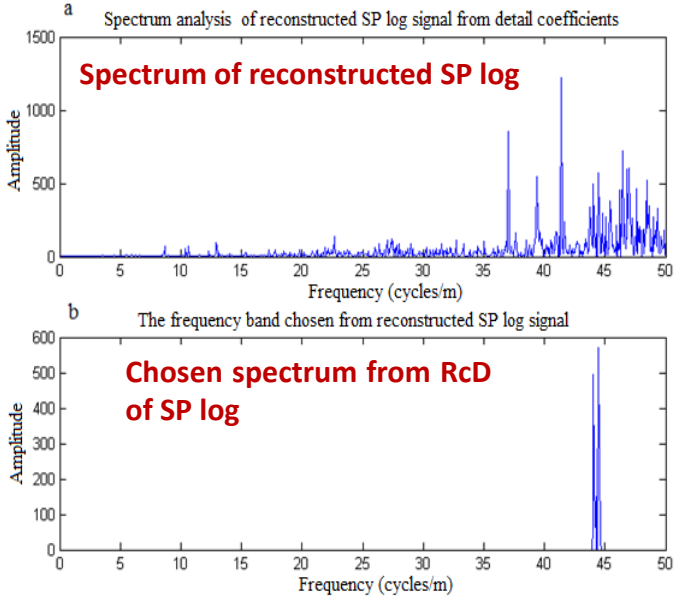


Fig. 92 (a)

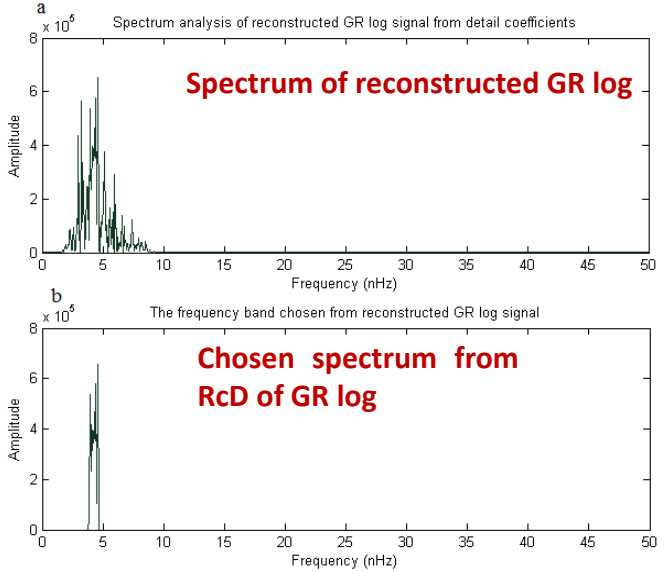


Fig. 93 (b)

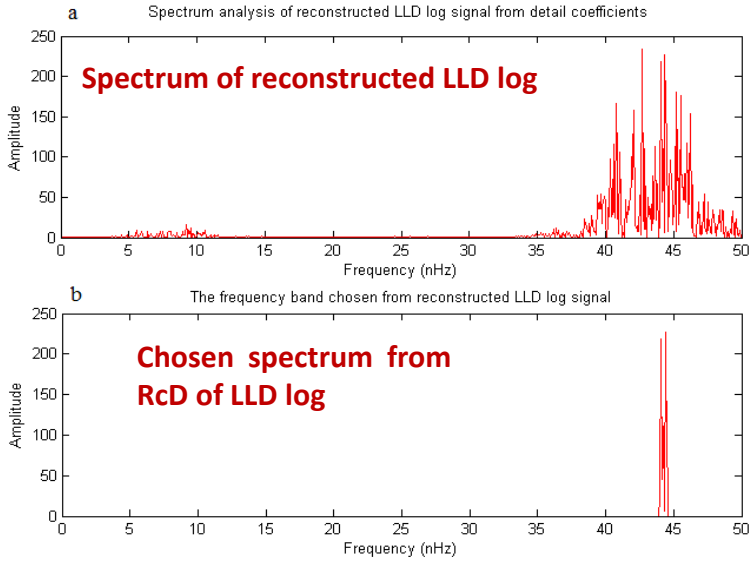


Fig. 94 (c)

# Continued…

**Logarithmic conversion of modified reconstructed log responses**

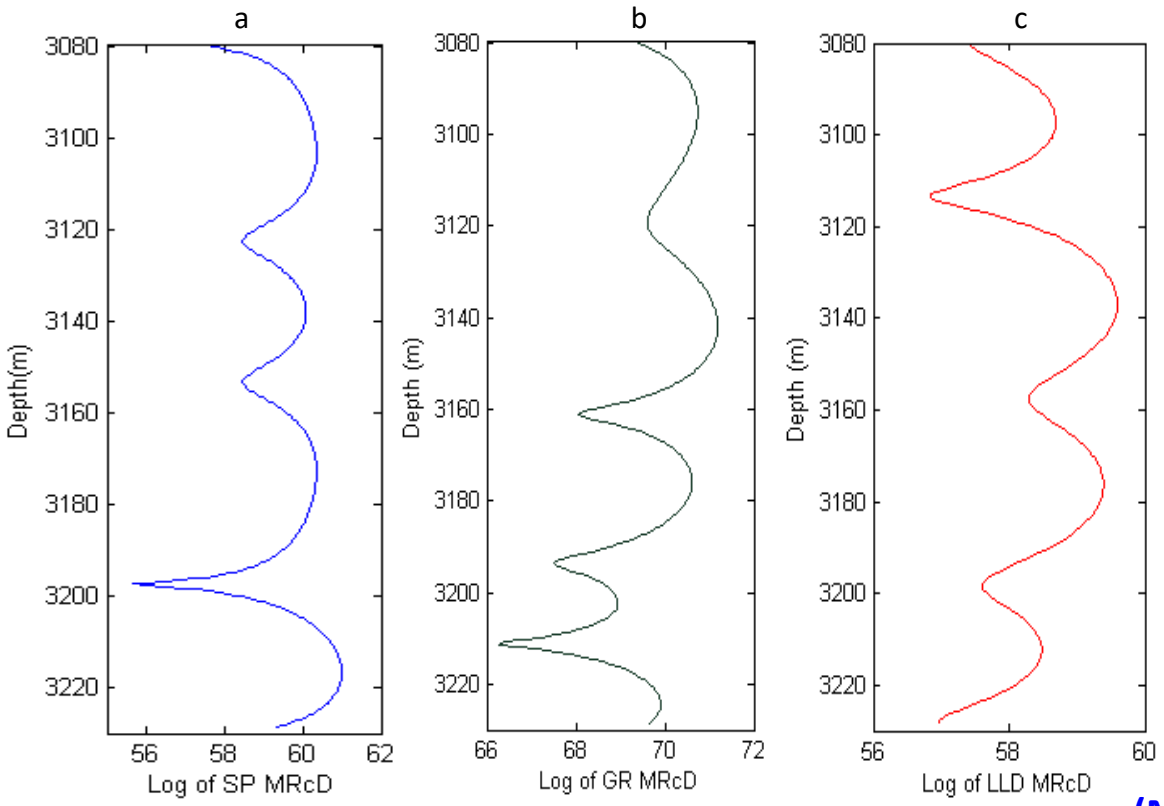


Fig. 95

- logarithmic transform of MRcD of studied log (s) was computed gives four waveforms within the studied interval.
- These four waveforms represents the actual four bed boundary within the formation.

**(Mukherjee and Roy, 2016)**

## Important findings:

- Represented analysis illustrates that formation interfaces can be easily detected and interpreted using the combined DWT and FT technique in semi automated way and its superior than tradition log interpretation.

# Thin bed identification using Walsh transform

# Identification of Thin Beds

**Wireline log responses at the hole NGHP-02-17-C**

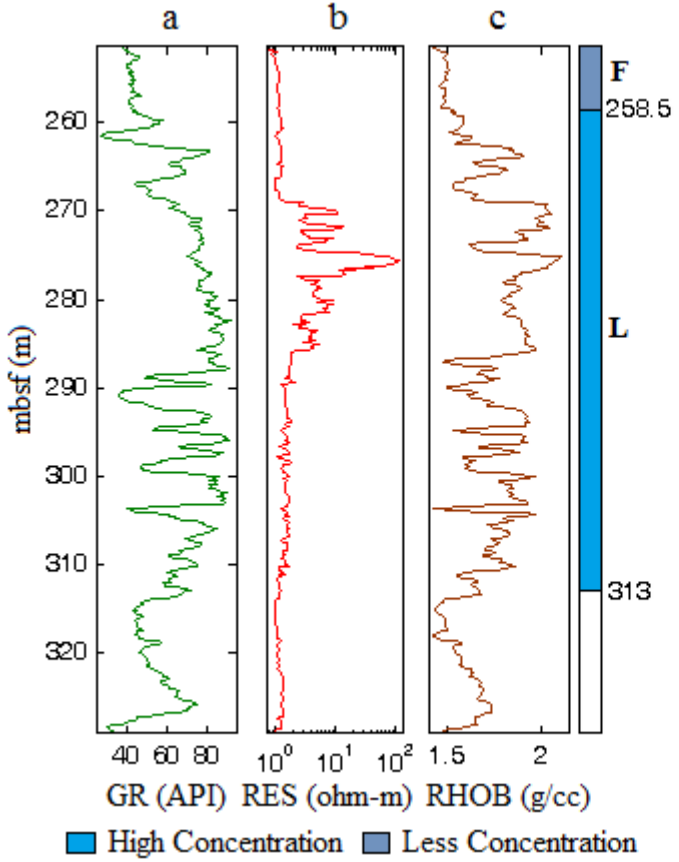


Fig. 96 (a)

**Normalized version of the wireline log response**

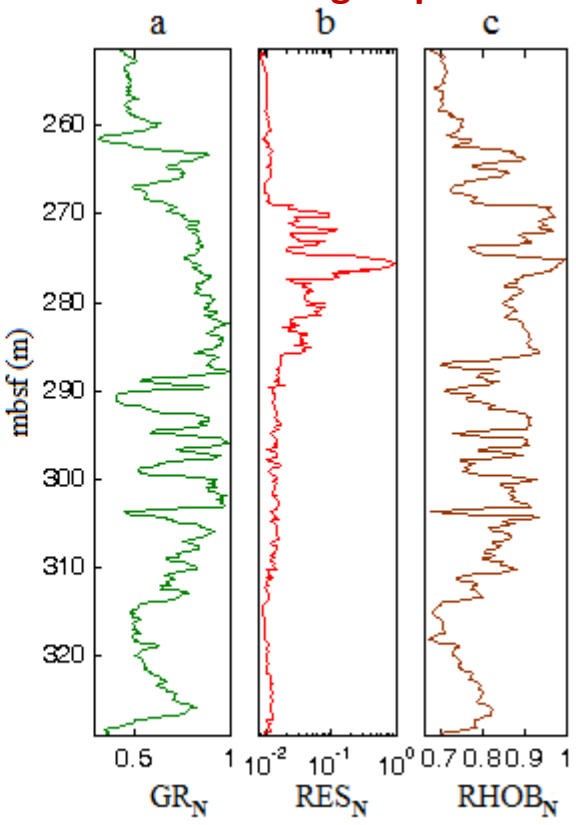


Fig. 96 (b)

**Walsh low pass version of the normalized log responses at the Hole NGHP-02-17-C**

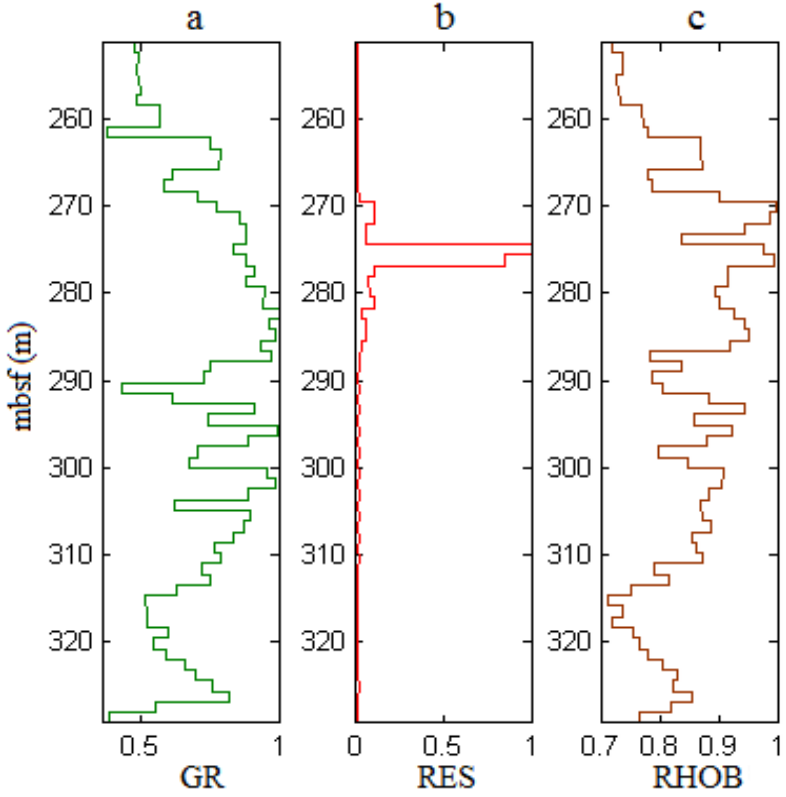


Fig. 97

- Gamma ray log – GR,
- Laterolog deep resistivity log – RES,
- Bulk density log – RHOB,
- F - Indicates fracture type gas hydrate zone and
- L - Indicates layered type gas hydrate zone

**(Mukherjee and Sain, 2019)**

# Continued…

**Walsh low pass picked boundaries over the low pass version of wire-line log data in Hole NGHP-02-17-C**

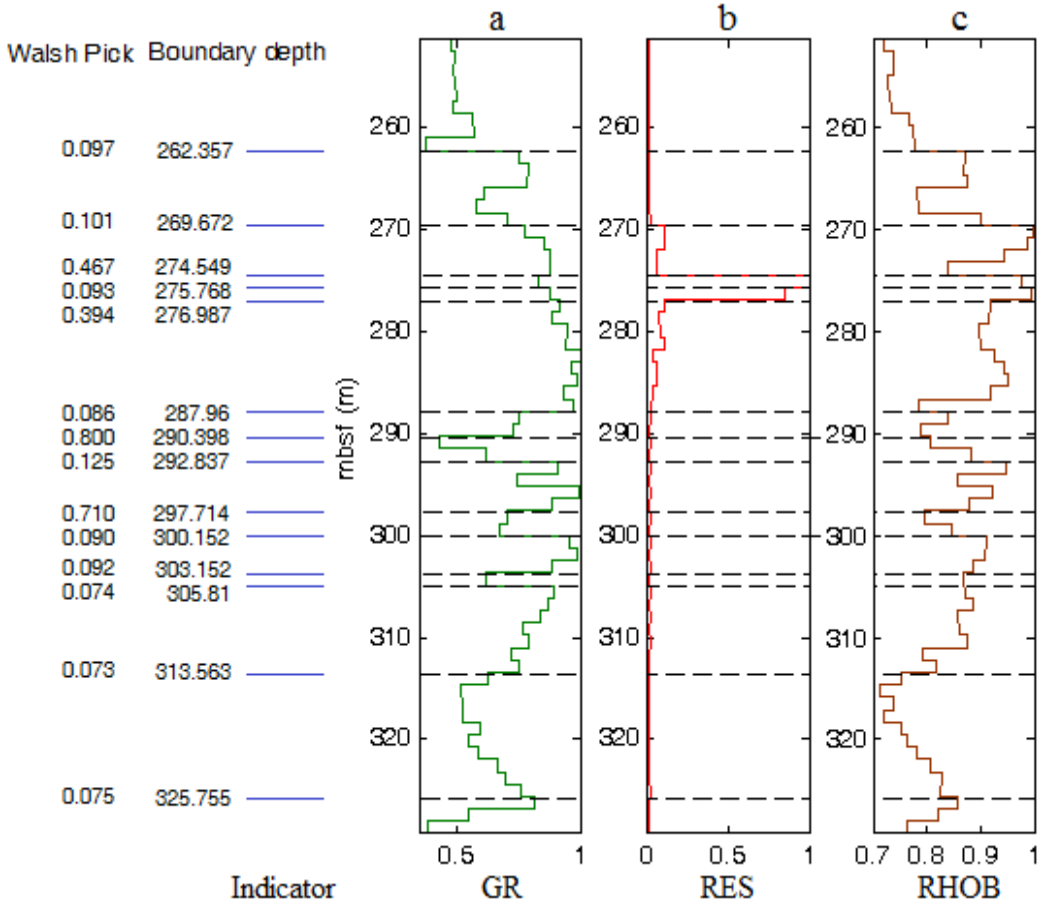


**Weight value for GR = 0.25; RES = 0.5; RHOB = 0.25**

**Walsh Check value = 0.07**

**Identified thin bed ~ 1.2 m**

Fig. 98

**Walsh low pass picked boundaries are plotted over the original log responses in Hole NGHP-02-17-C.**

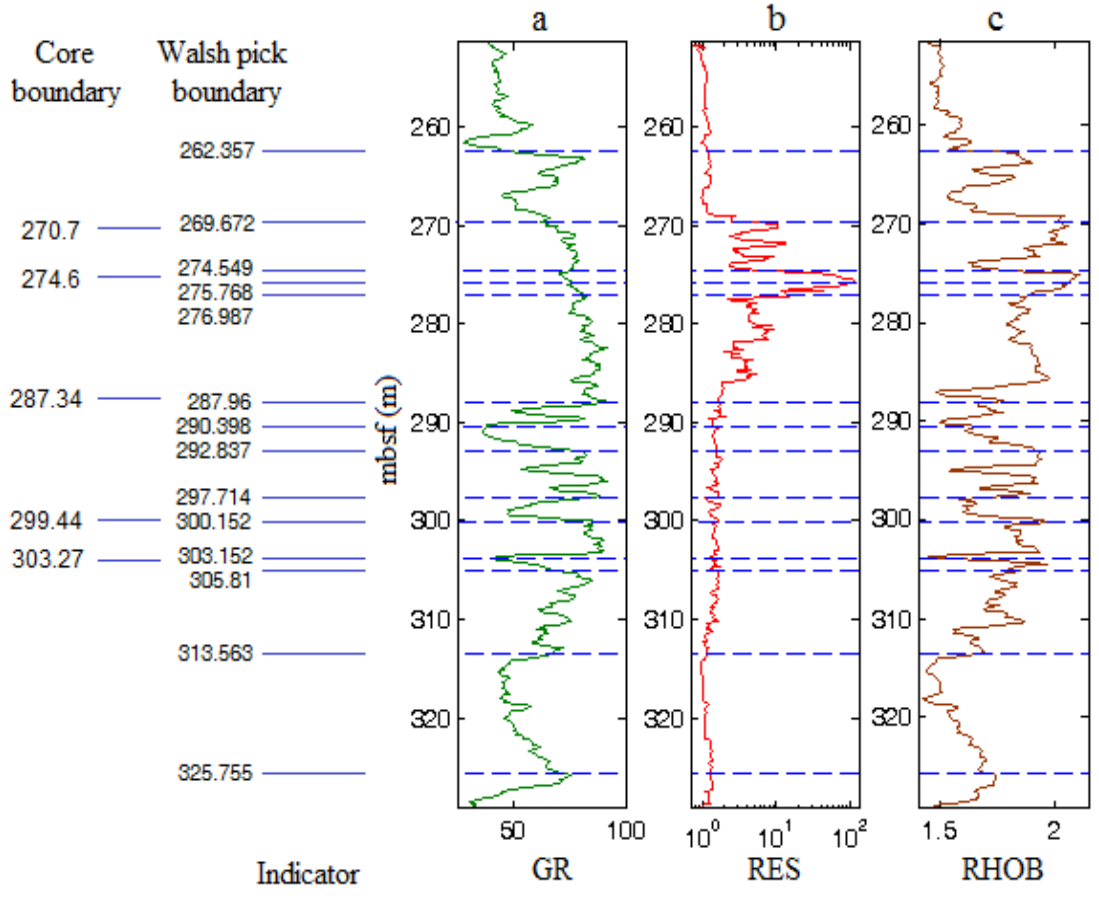


Fig. 99

**(Mukherjee and Sain, 2019)**

❖ **Similar analysis has been carried out on well log data of Assam-Arakan basin and maximum resolved thin bed of 5.7 m has been obtained (Mukherjee and Roy, 2016).**

**Translation of cluster analysis and artificial intelligence into lithology prediction**

# Wireline logs and core-derived lithology

**Wireline logs of well NGHP-02-17-C**

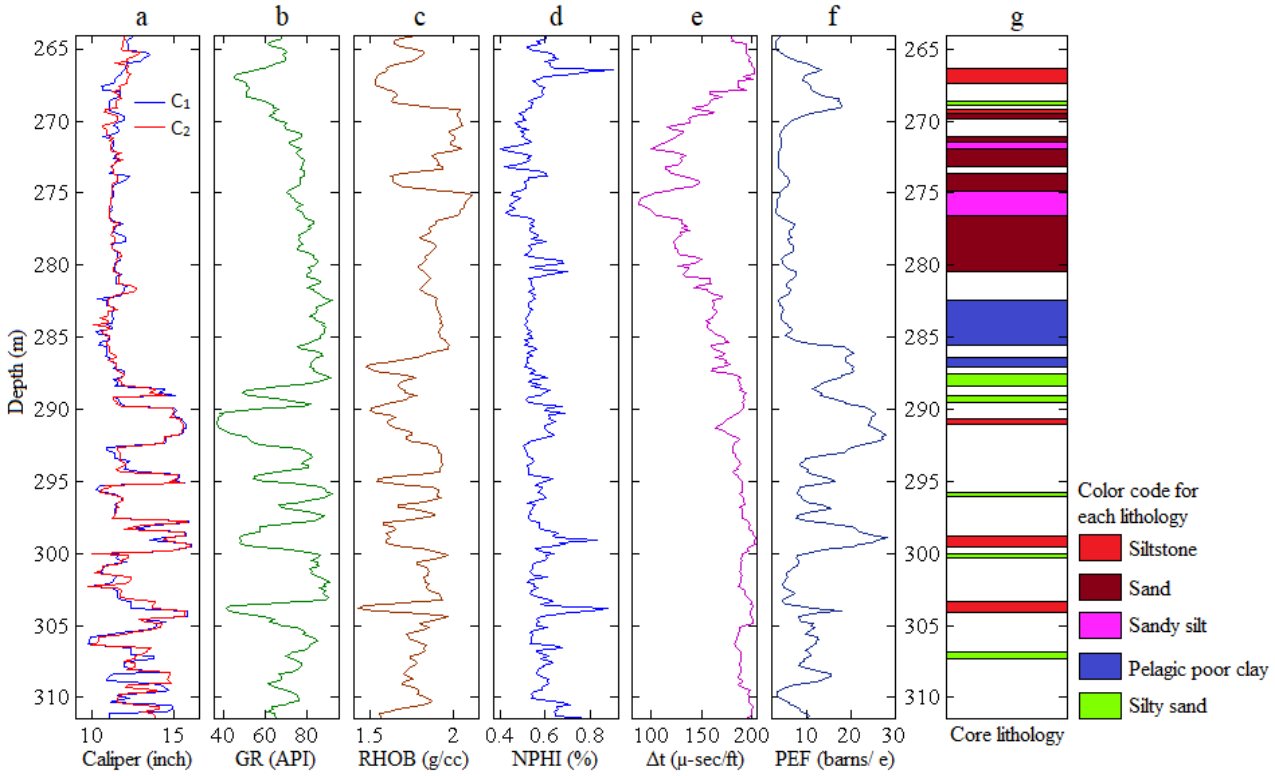


Fig. 100

**Wireline logs of well NGHP-02-23-C**

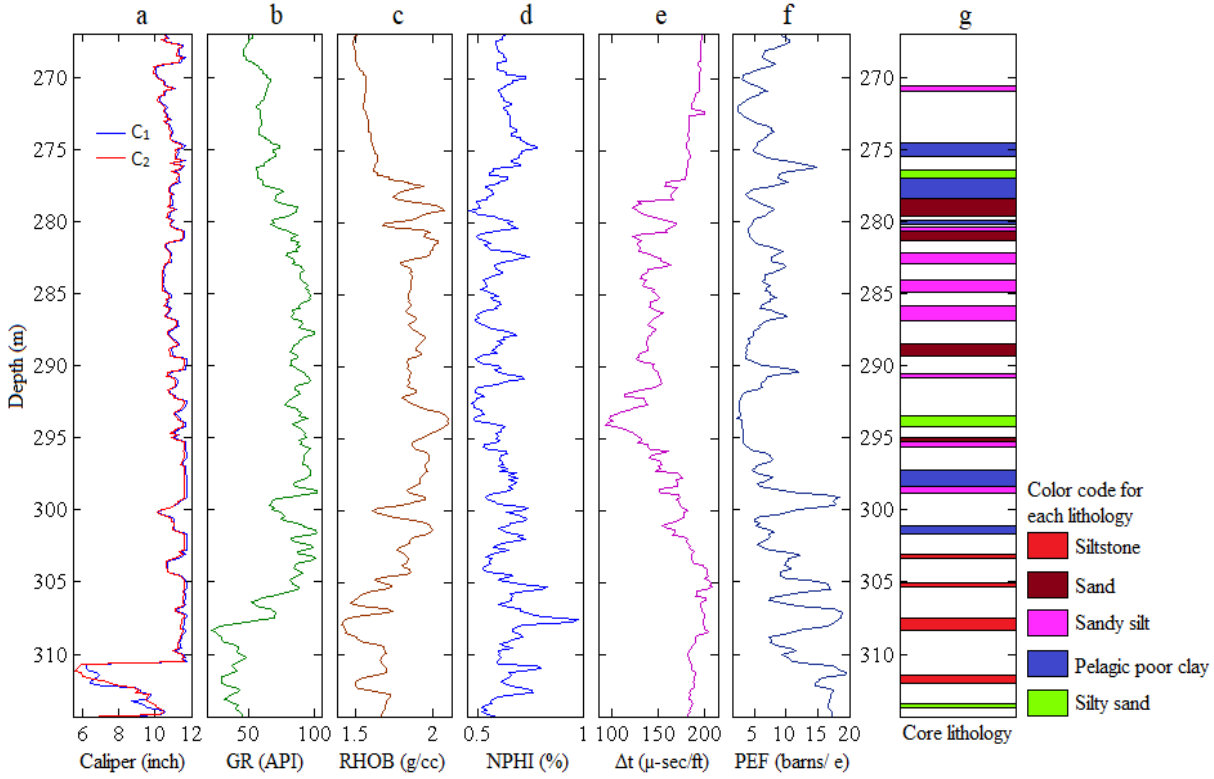


Fig. 101

**(Mukherjee and Sain, 2021)**

- Study area: KG basin
- Log data associated with gas hydrate sediments

- Caliper log – Caliper
- Gamma ray log – GR
- Bulk density – RHOB
- Neutron porosity – NPHI
- Sonic transit time log – Δt
- Photo electric factor log – PEF

# Crossplot technique: a traditional way of lithology discrimination

**Crossplot of available log values associated with core sample (a) for *GR, RHOB, NPHI*; (b) for *GR, RHOB, Δt*; (c) for *GR, RHOB, PEF*; (d) for *GR, NPHI, Δt*; (e) for *GR, NPHI, PEF*; (f) for *GR, Δt, PEF*; (g) for *RHOB, NPHI, Δt*; (h) for *RHOB, NPHI, PEF*; (i) for *RHOB, Δt, PEF*; (j) for *NPHI, Δt, PEF*.**

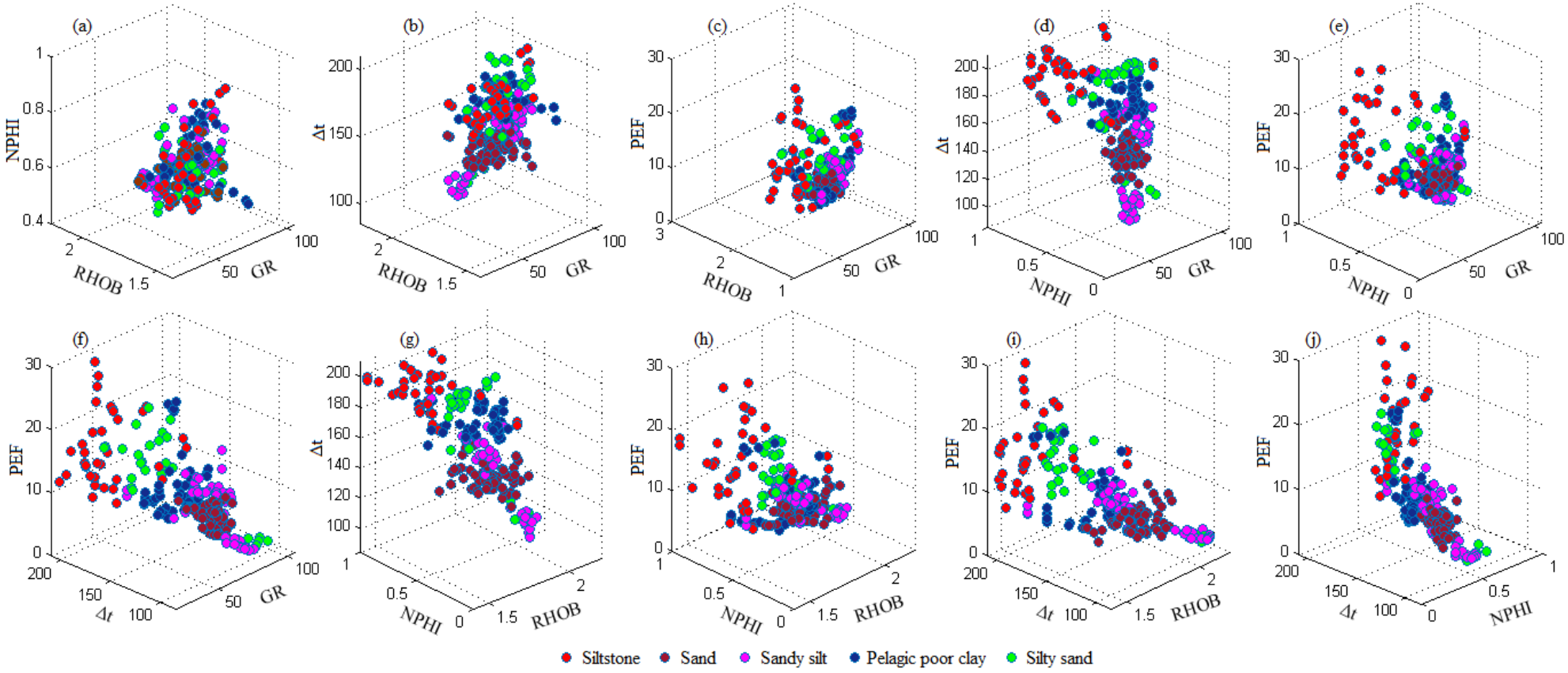


(Mukherjee and Sain, 2021)

Fig. 102

- It is to be noted that the log values associated with the core segments do not show any distinct characteristics for classifying the lithologies present in the depth range of study, and hence can't be used to classify lithologies using log character

# Lithology discrimination using HCA

**Hierarchical cluster analysis (HCA):**

The combination of "Minkowski" distance measurement scale (with "complete" linkage/ agglomeration approach (also called farthest neighbour having the largest distance between objects in two clusters) has been chosen for the delineation of cluster analysis.

**Dendrogram shows the separation of five clusters that represent five distinct lithology from the HCA analysis of 312 log samples at well (a) NGHP-02-17-C and (b) NGHP-02-23-C.**

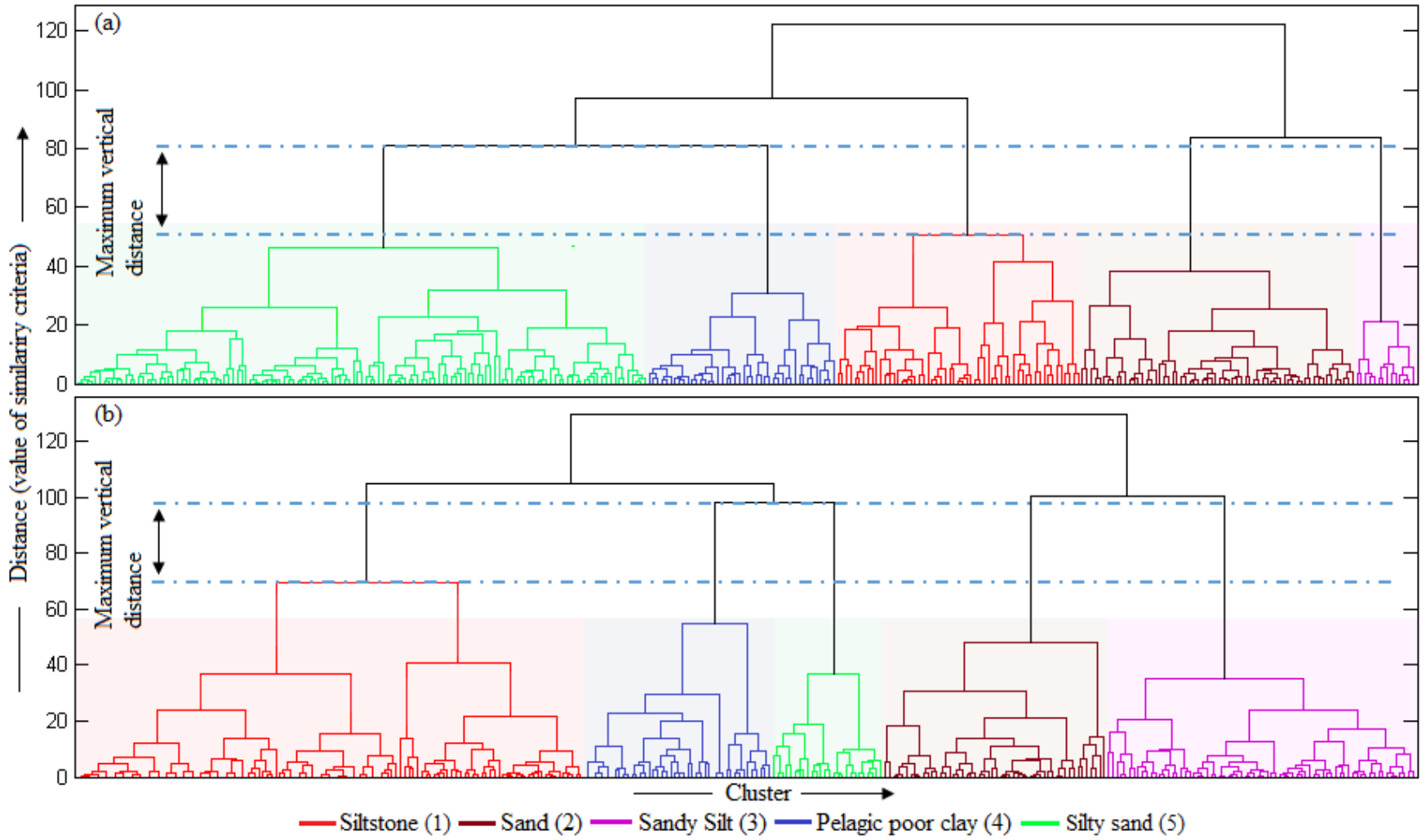


Fig. 103 **(Mukherjee and Sain, 2021)**

# Pattern extraction among the logs and associated lithology's using ANN

**Designed Network**

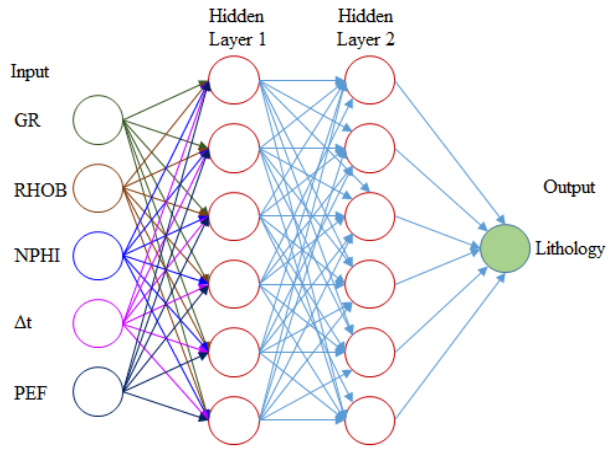


Fig. 104

**Performance of networks**

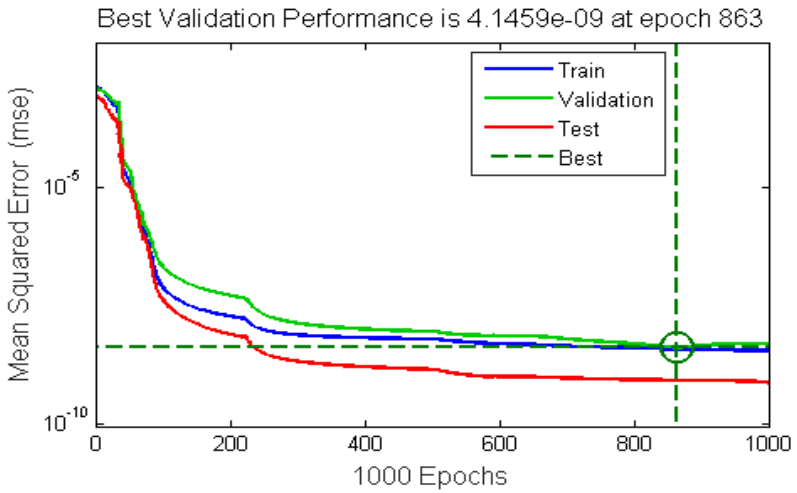


Fig. 105

**Network and learning logarithm:**

- The feed-forward BP network is exploited with the TRAINLM training function, LEARNGDM adaptation learning function and mean square error (MSE) performance function.

**Regression analysis for (a) training, (b) test, (c) validation and (d) all results for the lithology network.**

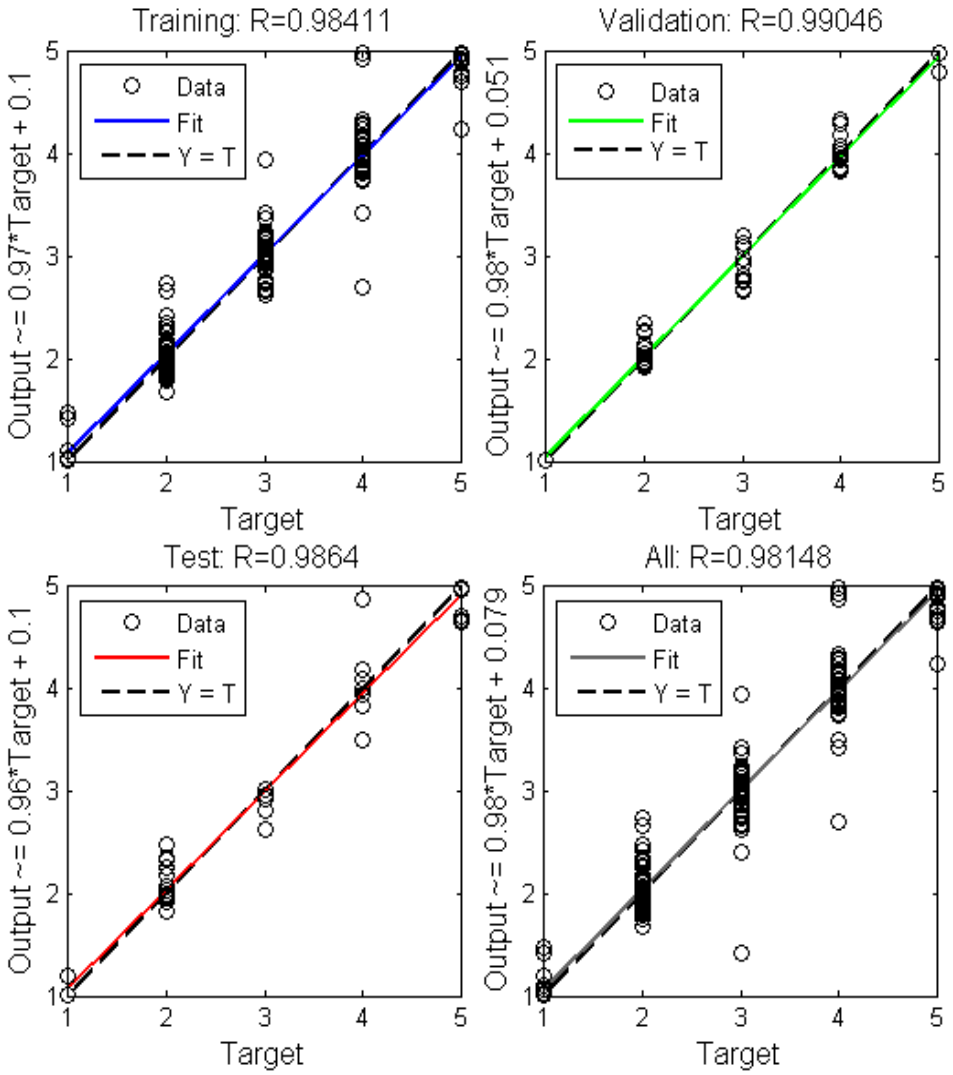


**(Mukherjee and Sain, 2021)** Fig. 106

# Comparison of HCA, ANN and Core derived lithology

**(a) core derived lithology, (b) lithology obtained using HCA and (c) ANN predicted lithology at well NGHP-02-17-C**

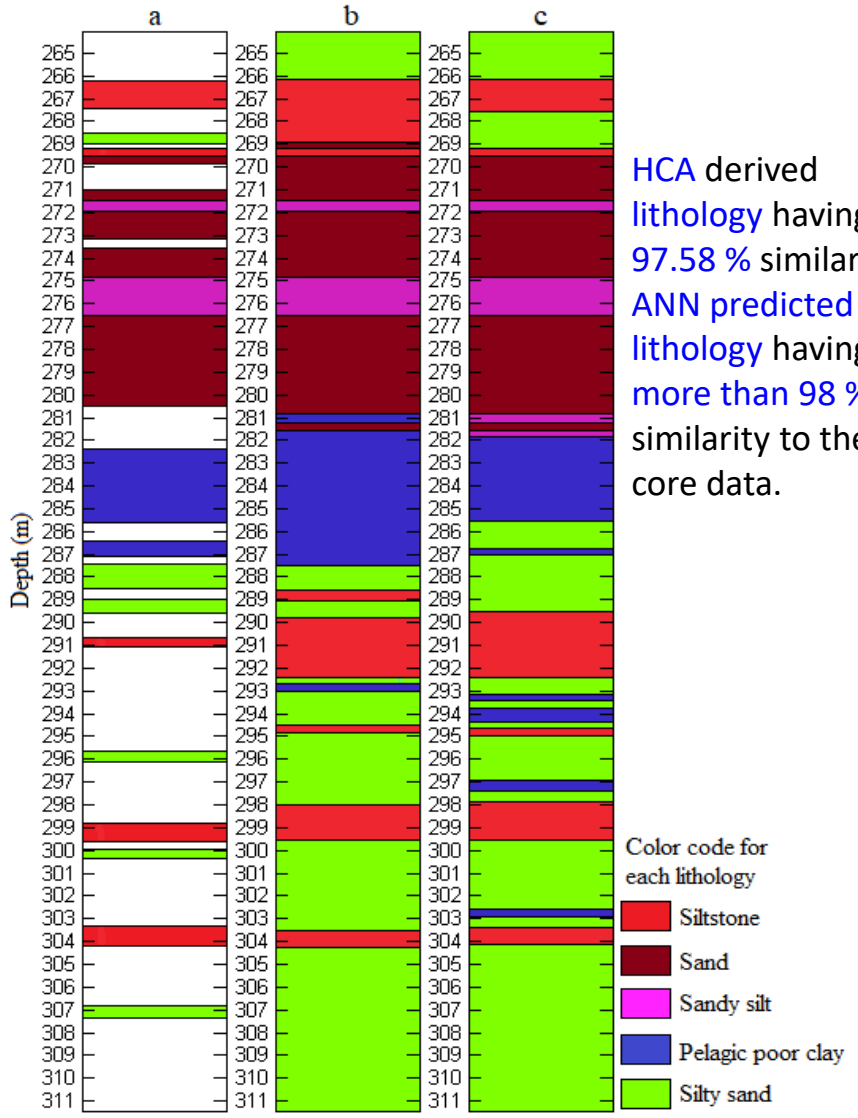


Fig. 107

**(a) core derived lithology, (b) lithology obtained using HCA and (c) ANN predicted lithology at well NGHP-02-23-C**

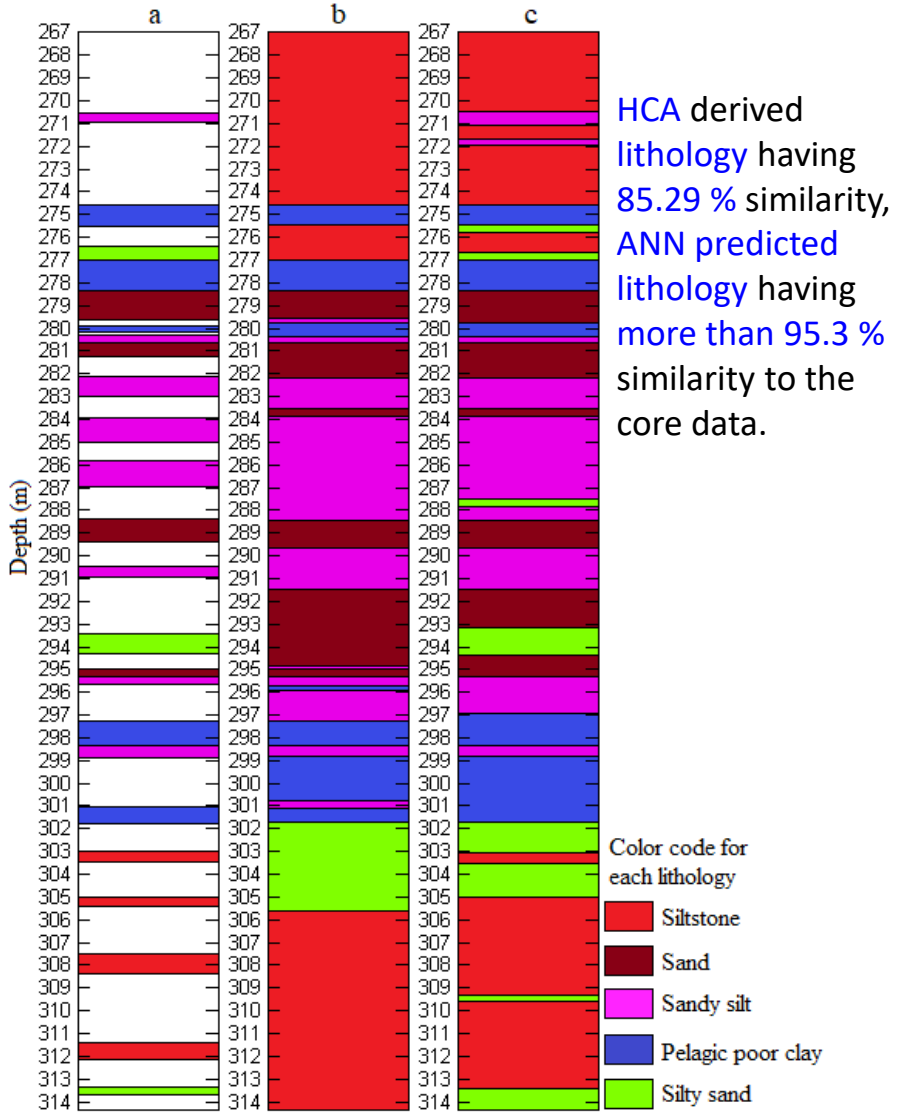


Fig. 108

## Important findings:

- Neural network approach has the ability to identify finer beds that are difficult to be discernible by traditional interpretation using standard industrial geophysical software
- Since the results obtained from the HCA and ANN analysis are almost similar (>85%) at both sites, this supplements traditional wireline log interpretation for lithology identification based on lithification patterns perceived from the core

## Petrophysical parameter prediction using artificial intelligence

# Prediction of Reservoir Parameter using Artificial Intelligence

**Wireline logs at well NGHP-02-17-C**

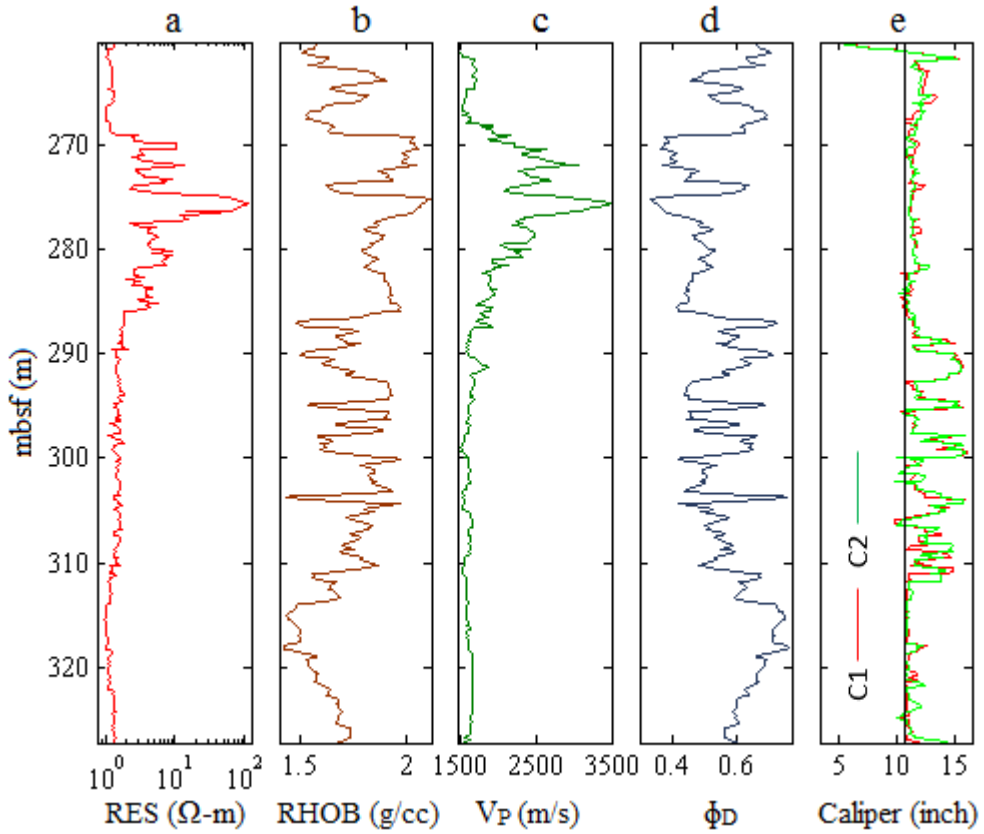


Fig. 109

**Wireline logs at well NGHP-02-19-C**

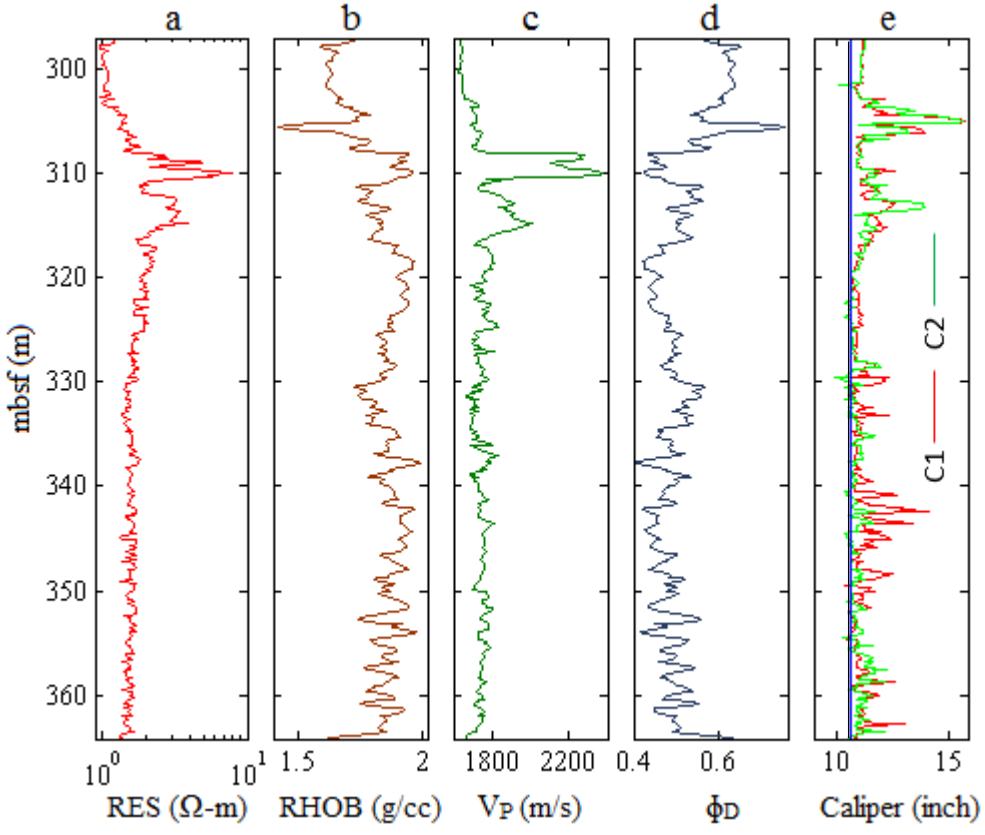


Fig. 110

- Laterolog deep resistivity log – RES,
- Bulk density log – RHOB,
- P-wave velocity log - $V_P$,
- Density porosity log – $\phi_D$,

Reservoir parameters:

- Density porosity,
- Gas hydrate saturation

**(Mukherjee and Sain, 2019)**

# Continued…

**Wireline logs at well NGHP-02-22-C**

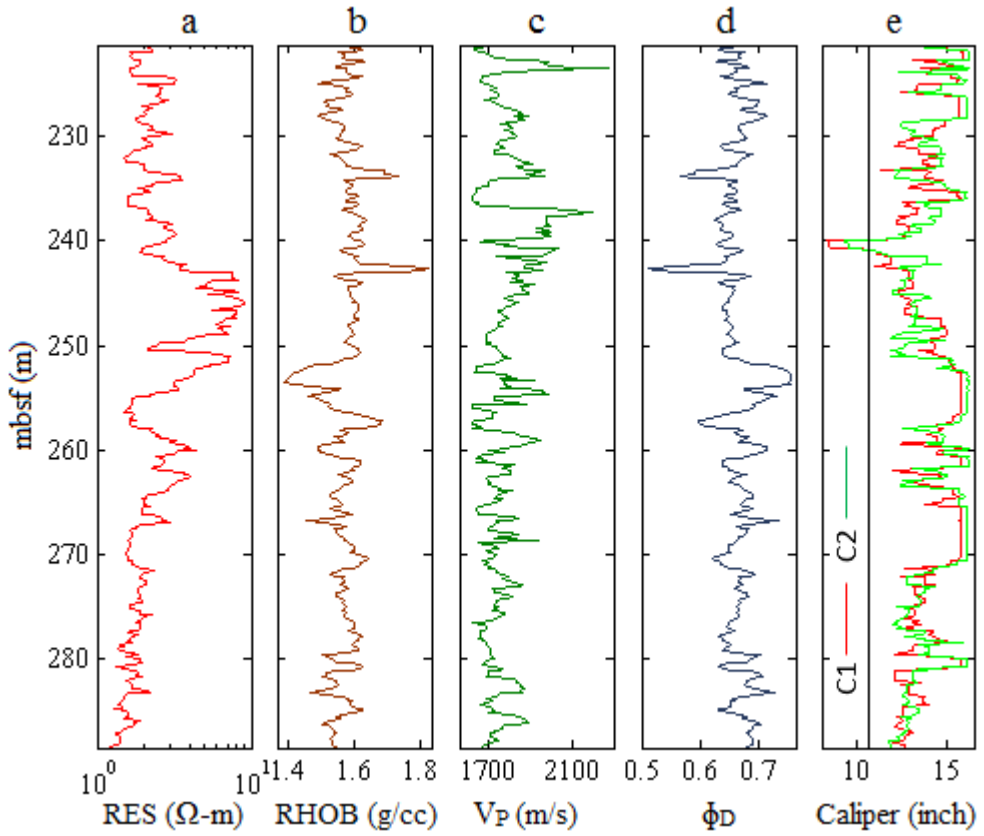


Fig. 111

**(Mukherjee and Sain, 2019)**

- Laterolog deep resistivity log – RES,
- Bulk density log – RHOB,
- P-wave velocity log - $V_P$ and
- Density porosity log – $\phi_D$

# Continued…

## Estimation of gas hydrate saturation using Archie's law:

- As Archie's law was designed to estimate the saturation for conventional hydrocarbon, accumulated in clean sandstone environment.
- Thus, we need to choose all the constants (a, m and n) in such a way that the calibrated values of constants mimic the in-situ environment of the deposition pattern of gas hydrates.

Calibrated values of Archie's constants

| Well ID | a | m | n |
|---|---|---|---|
| NGHP-02-17-C | 1.2 | 2.1 | 2 |
| NGHP-02-19-C | 1.21 | 2.22 | 2.05 |
| NGHP-02-22-C | 1.3 | 2.71 | 1.4 |

- a – constant (lithology dependent)
- m - cementation factor
- n - Archie's saturation exponent

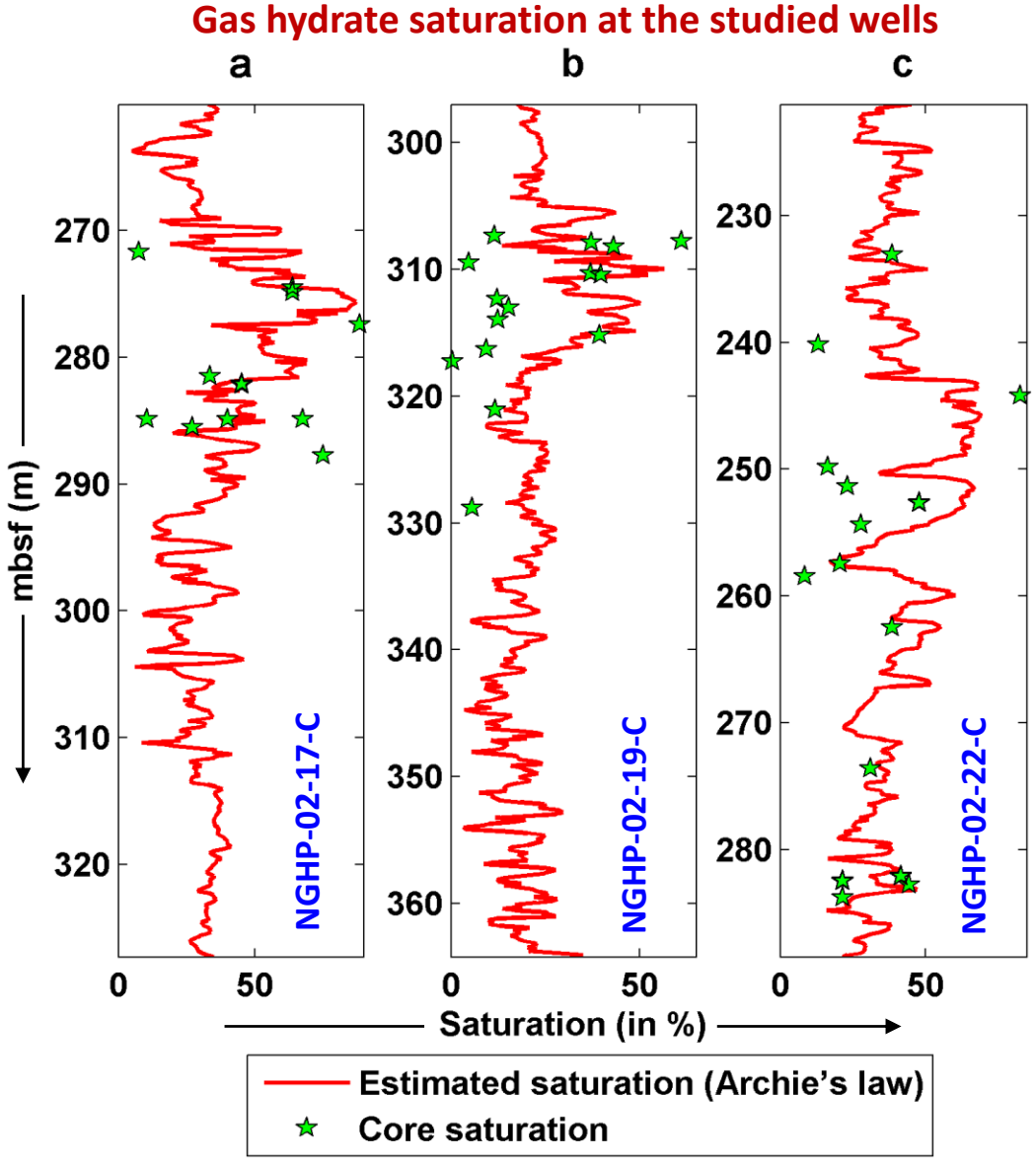


Fig. 112

# Continued… (implementation of AI based approach)

## Designed Networks:

### Porosity Network

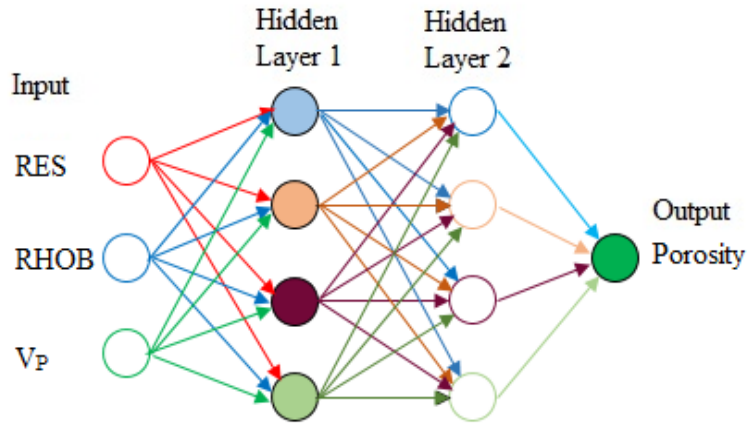


Fig. 113

### Saturation Network

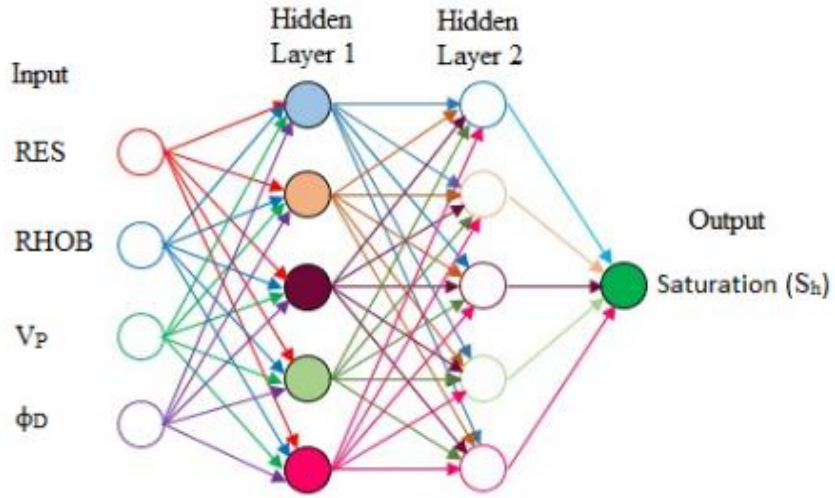


Fig. 114

## Network and learning algorithm:

- The feed-forward BP network is exploited with the gradient descent training function with adaptive learning rate of backpropagation approach and mean square error (MSE) performance function.

## Performance of networks

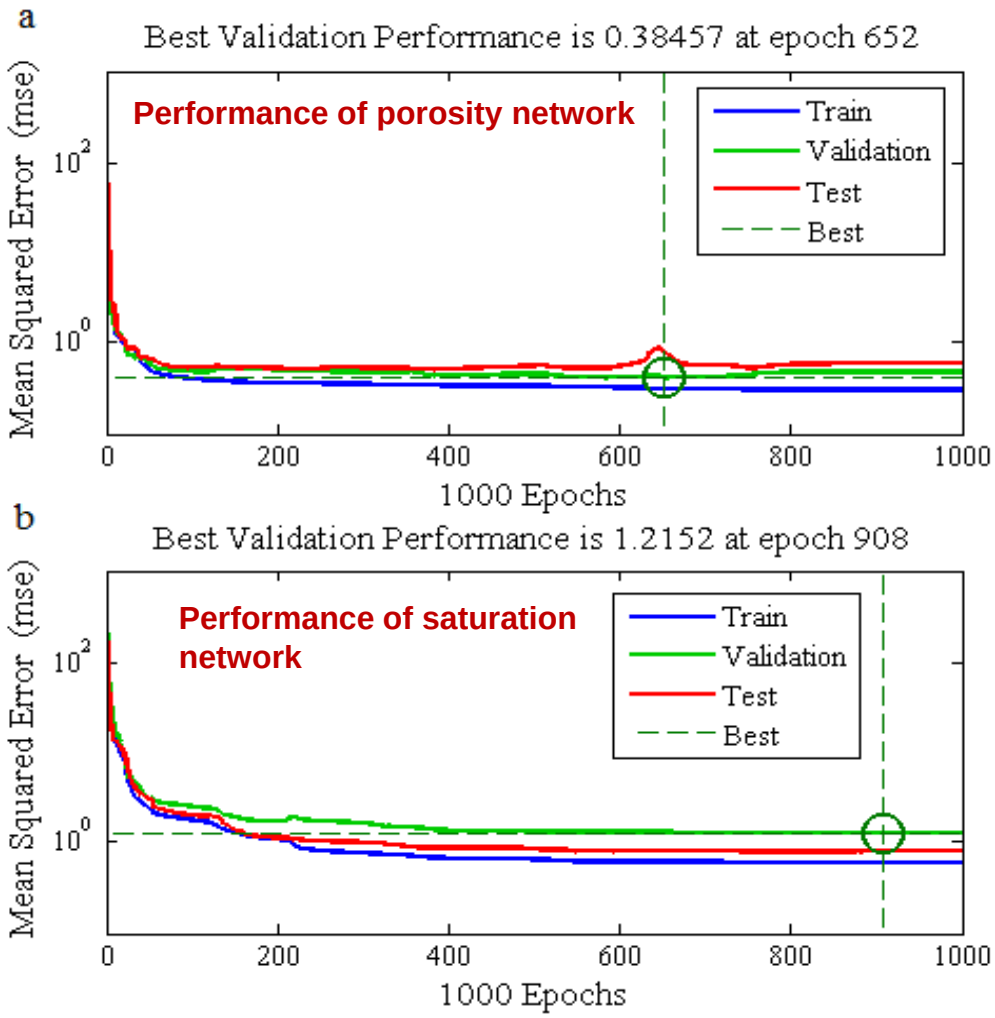


Fig. 115

**(Mukherjee and Sain, 2019)**

# Continued…

**Regression analysis for (a) training, (b) test and (c) validation data set for the porosity network**

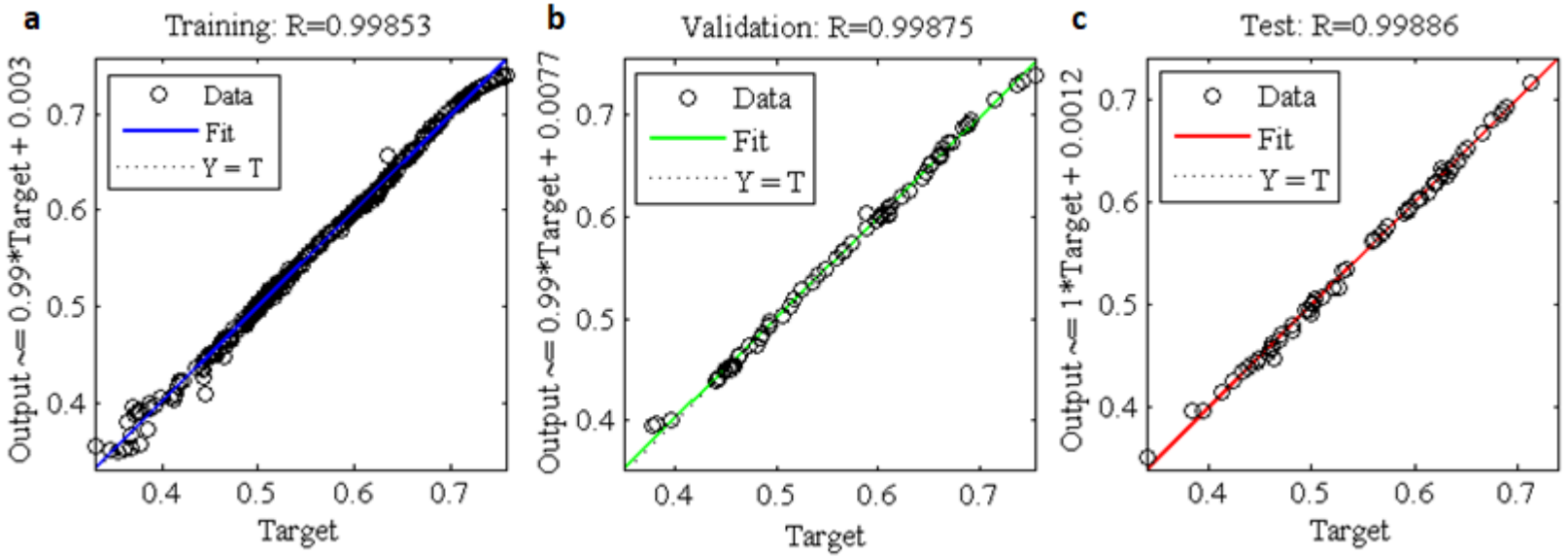


Fig. 116

**Regression analysis for (a) training, (b) test and (c) validation data set for the saturation network**

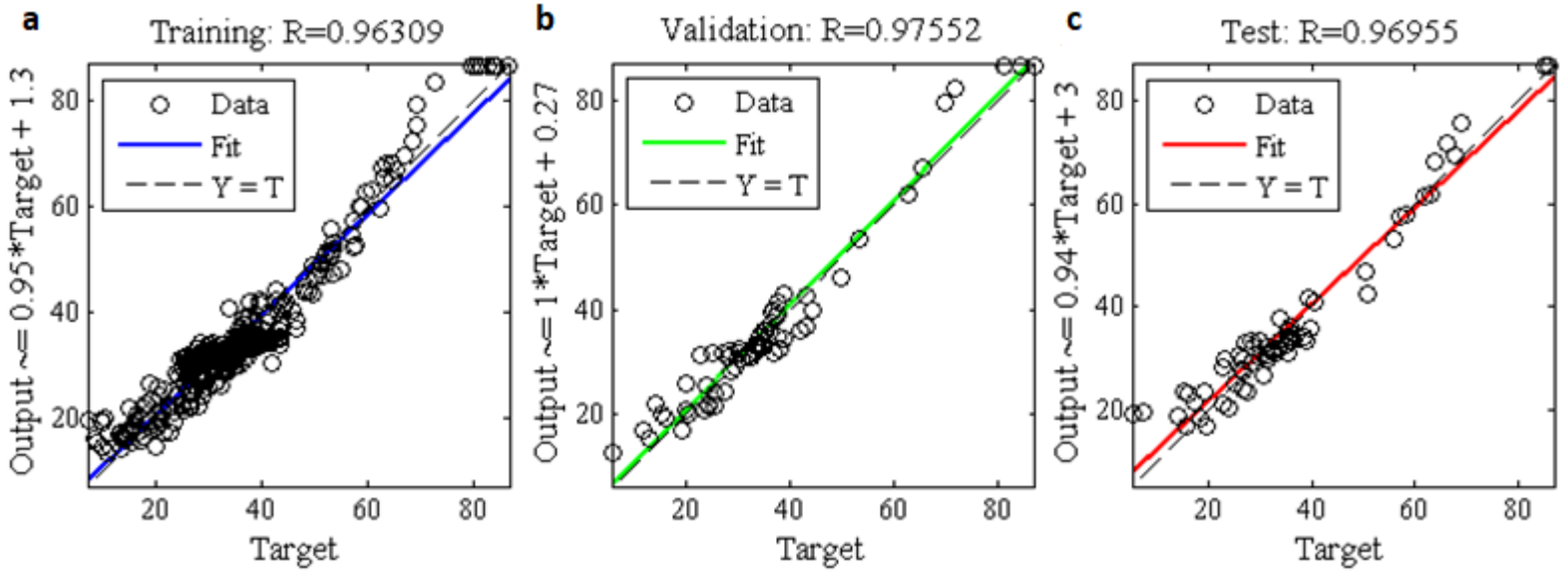


Fig. 117

# Continued…

**Porosity comparison between the traditionally estimated and ANN predicted**

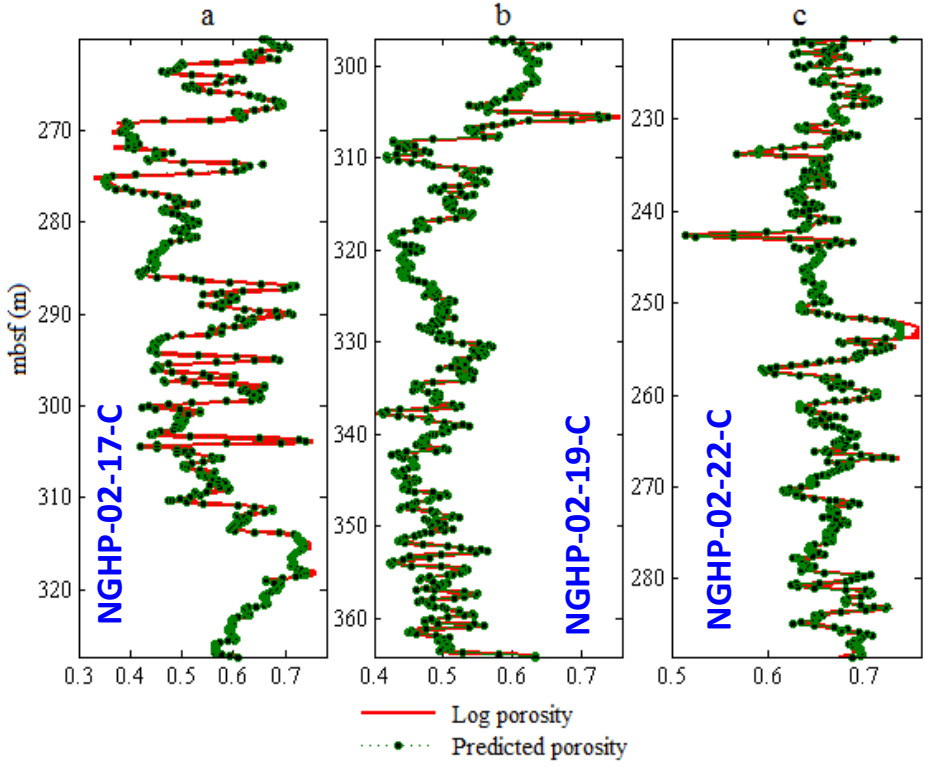


Fig. 118

**Saturation comparison between the traditionally estimated and ANN predicted**

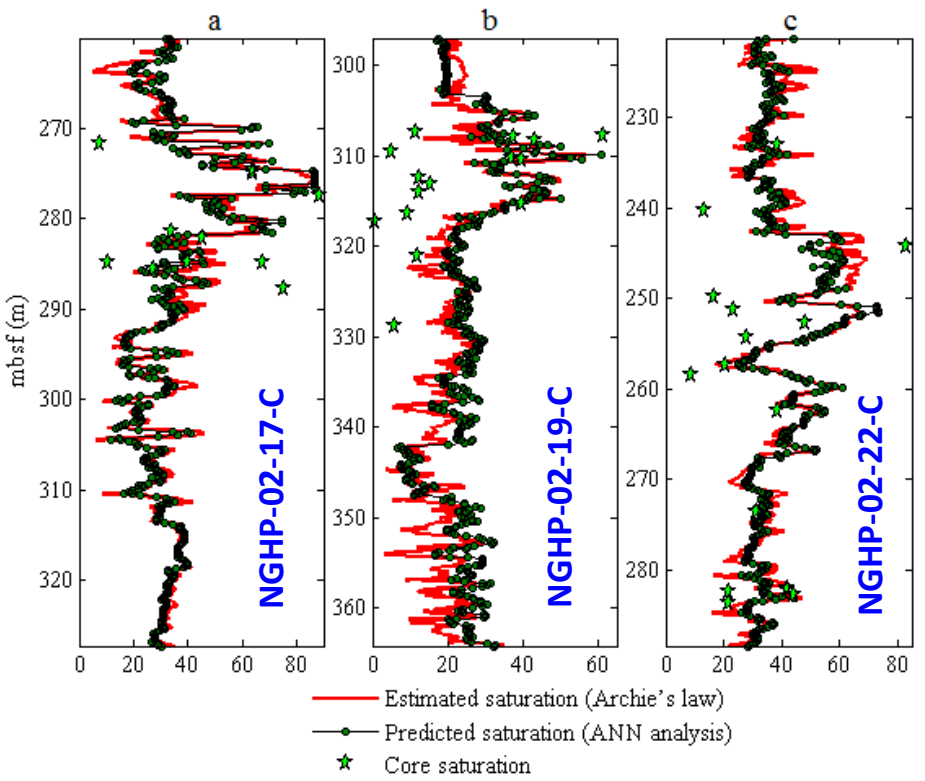


Fig. 119

- The strong correlation (more than 0.7) observed between computed and predicted parameter in both of the cases, shows that the predicted results are reasonable.

**(Mukherjee and Sain, 2019)**

**Important findings:**

- Reasonable correlation have been observed between the traditionally estimated and ANN predicted parameters. Thus, the designed network can be used to assess the petrophysical parameters at any other wells in the same reservoir.
- The Artificial Intelligence (AI) has the ability to predict the saturation of gas hydrates from wireline log data without appropriate calibrations of Archie's constant.

**Automated data-driven way of sonic log data conditioning assisted by recurrent neural network (RNN)**

# Raw logs, conditioned sonic log, and indifference between the raw and conditioned sonic log of well B1

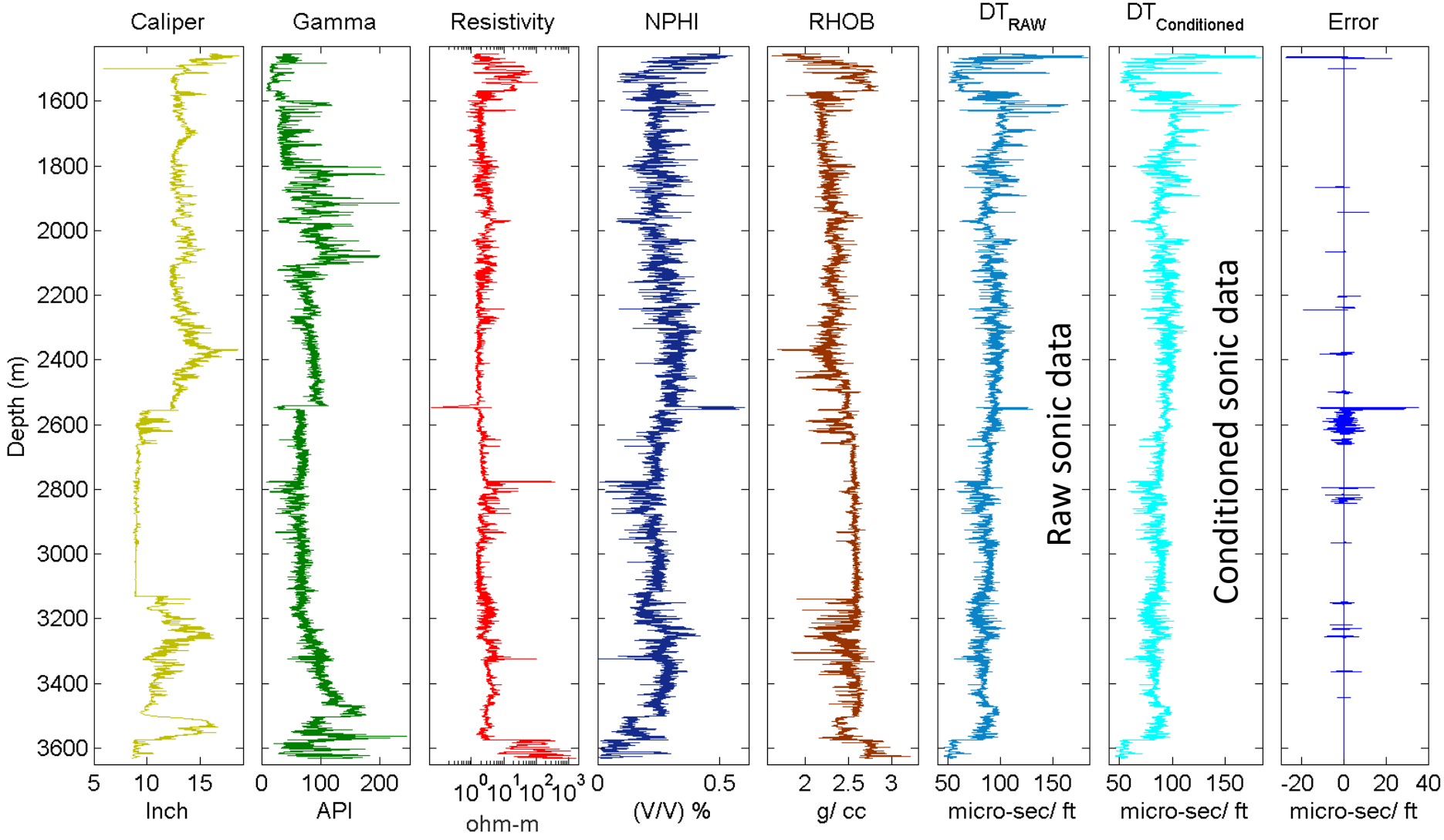


Fig. 120

- Ground truth data Gamma, Resistivity NPHI, RHOB and Raw Sonic log ($DT_{RAW}$) are set as input. Corrected Sonic log ($DT_{Conditioned}$) log set as output of designed network

Error= ( $DT_{RAW}$ ~ $DT_{Conditioned}$ )

# Raw logs, conditioned sonic log, and indifference between the raw and conditioned sonic log of well B2

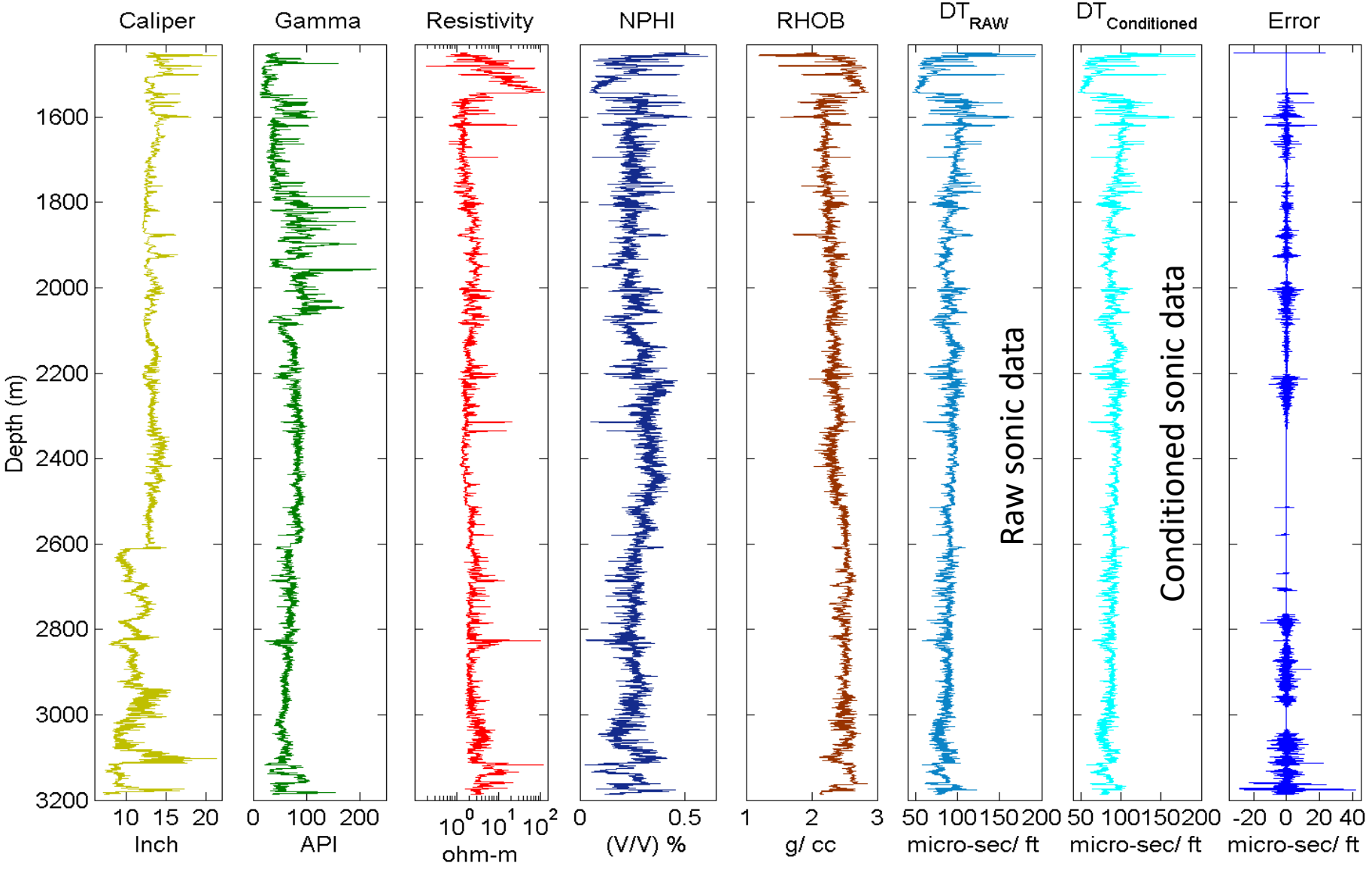


Fig. 121

- Ground truth data Gamma, Resistivity NPHI, RHOB and Raw Sonic log ($DT_{RAW}$) are set as input. Corrected Sonic log ($DT_{Conditioned}$) log set as output of deep learning network

Error= ( $DT_{RAW}$ ~ $DT_{Conditioned}$ )

# Raw logs, conditioned sonic log, and indifference between the raw and conditioned sonic log of well B4

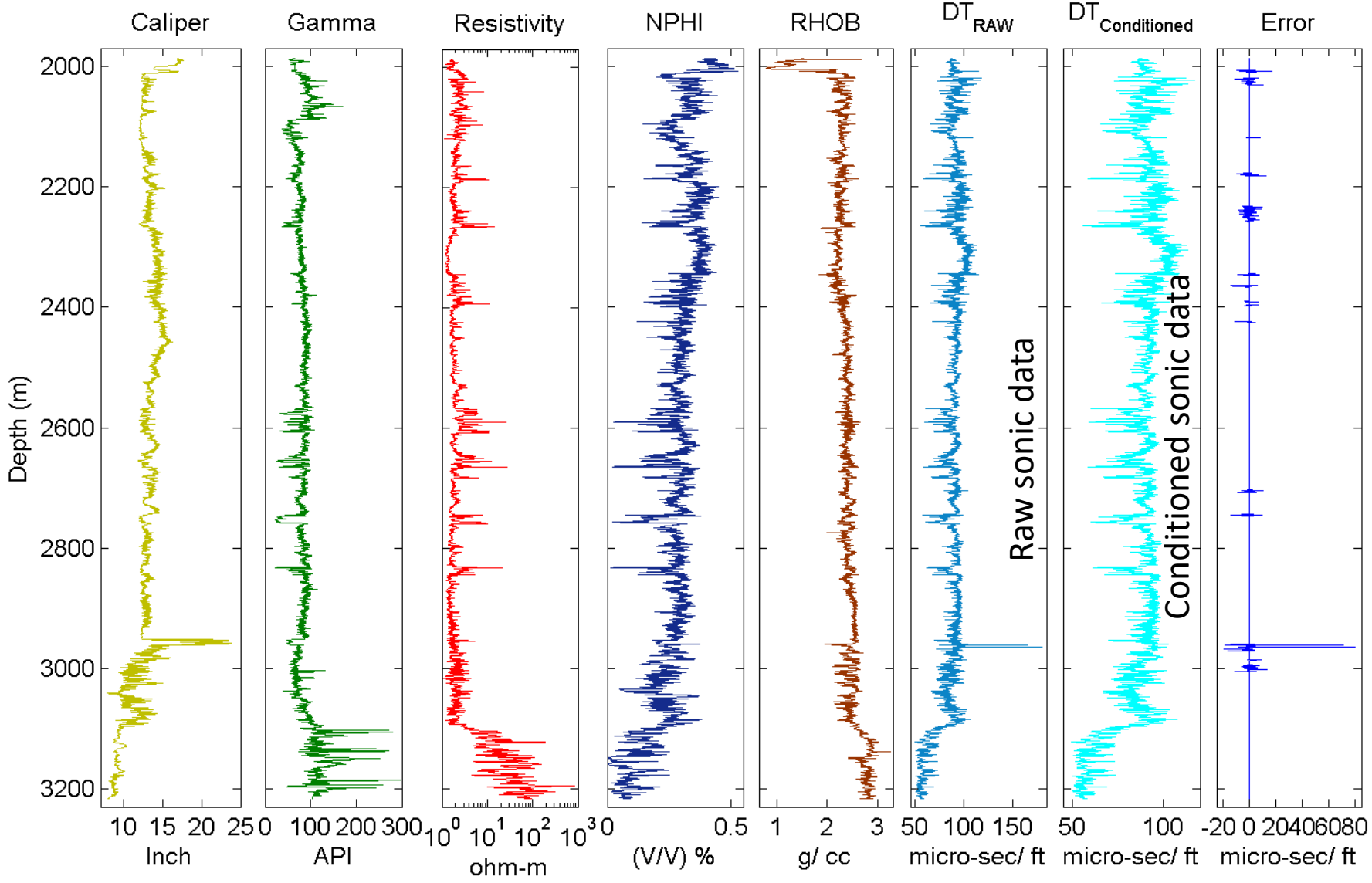


Fig. 122

- Ground truth data Gamma, Resistivity NPHI, RHOB and Raw Sonic log ($DT_{RAW}$) are set as input. Corrected Sonic log ($DT_{Conditioned}$) log set as output of deep learning network

Error= ( $DT_{RAW}$ ~ $DT_{Conditioned}$ )

# Data Normalization & Standardization

## Normalization

- The min-max technique is used
- The advantage is preserving exactly all relationships in the data and it does not introduce any bias

Normalized input is given as,

$$X_i' = \left(\frac{X_i - X_{min}}{X_{max} - X_{min}}\right)(X'_{max} - X'_{min}) + X'_{min}$$

where, $X_i$, $X$min, $X$max are the actual input data, minimum and maximum input data. $X'_{min}$, $X'_{max}$ be the minimum and maximum target value.

## Standardization

- For a better fit and to prevent the training from diverging, standardize the training data to have zero mean and unit variance
- At prediction time, one must standardize the test data using the same parameters as the training data

Standardization is computed as,

1) Mean of the time series
2) Standared deviation of the time series
3) Standardized Data = (time series – mean (time series))/ Standared deviation of the time series

# LSTM unit & how it works

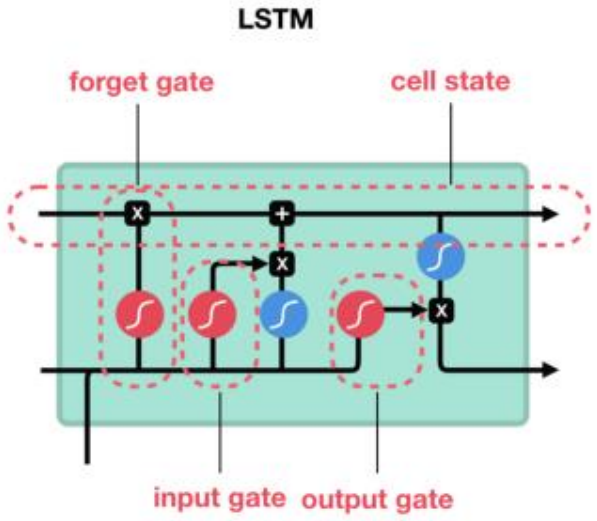


Fig. 123 (a)

Abbreviations

- sigmoid
- tanh
- pointwise multiplication
- Pointwise addition
- Vector concatenation

## Forget gate operations

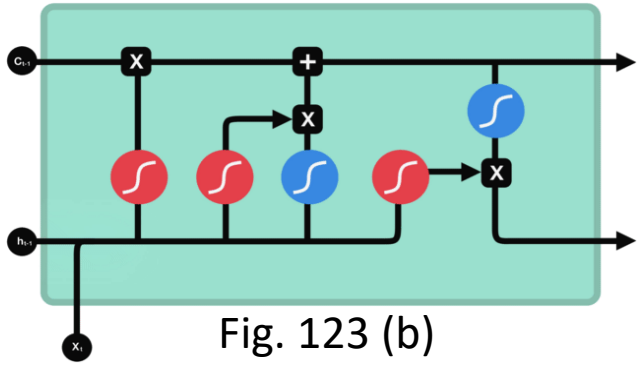

$c_{t-1}$= previous cell state
$h_{t-1}$= out put of previous block
$f_t$= forget get output
$W_{fh}$= weight
$W_{fx}$= weight
$b_f$ = bias

Fig. 123 (b)

$$f_t = \delta[(W_{fh} * h_{t-1}) + (W_{fx} * x_t) + b_f]$$

## Input gate operations

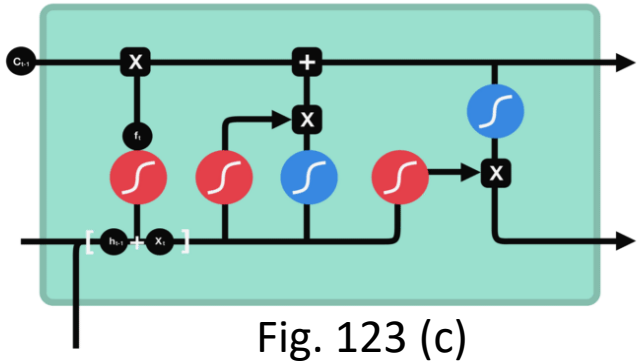

$\tilde{C}_t$= candidate
$i_t$= input get output
$W_{ih}$= weight
$W_{ix}$= weight
$b_i$ = bias

Fig. 123 (c)

$$i_t = \delta[(W_{ih} * h_{t-1}) + (W_{ix} * x_t) + b_i]$$
$$\tilde{C}_t = \delta[(W_{gh} * h_{t-1}) + (W_{gx} * x_t) + b_g]$$

## Calculating cell state

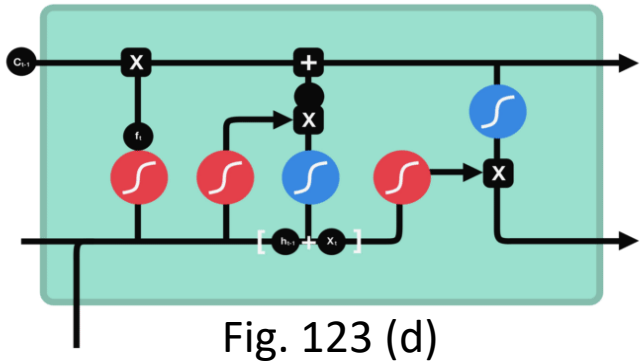

$c_t$= new cell state

Fig. 123 (d)

$$c_t = [c_{t-1} * f_t] + [\tilde{C}_t * i_t]$$

## Output gate operations

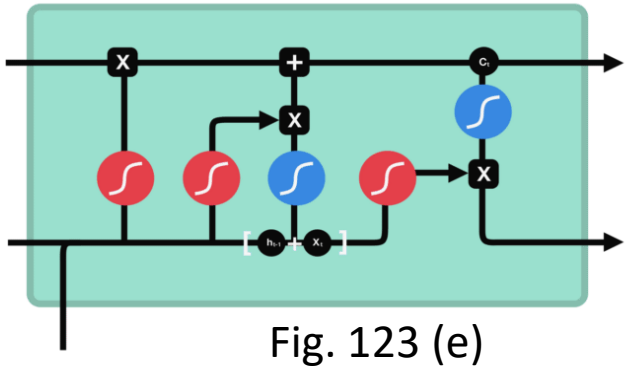

$h_t$= hidden state
$o_t$= output of output gate

Fig. 123 (e)

$$o_t = \delta[(W_{oh} * h_{t-1}) + (W_{ox} * x_t) + b_o]$$
$$y_t = [o_t * tanh c_t] = h_t$$

# Training parameters and training progress

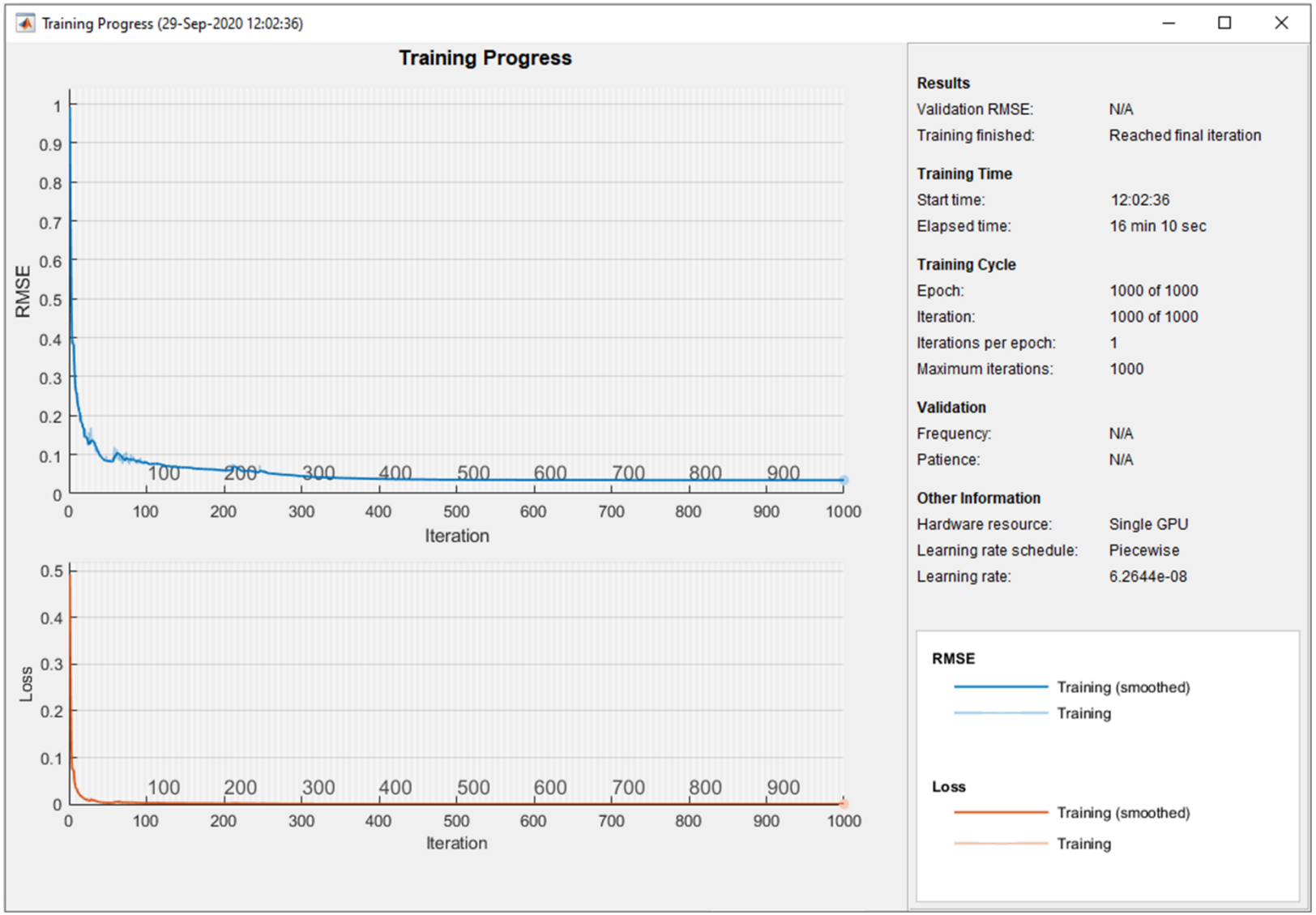


Fig. 124 (a)

```
Training parameter:
numFeatures = 5; %Input
numResponses = 1; %output
numHiddenUnits = 238;
numlayer=1;
```

**Error in the designed network**

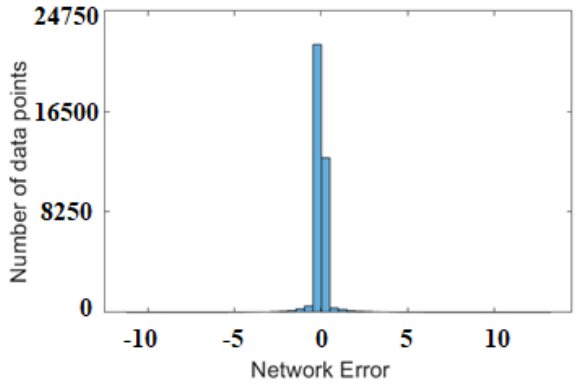


Fig. 124 (b)

# Results for well B1

**(a) raw sonic log, (b) conditioned sonic logs (c) predicted sonic logs (d) overlay plot of conditioned and predicted logs (e) depth-wise mean square deviation between raw and conditioned sonic logs (f) depth-wise mean square deviation between conditioned and predicted sonic logs at well B1.**

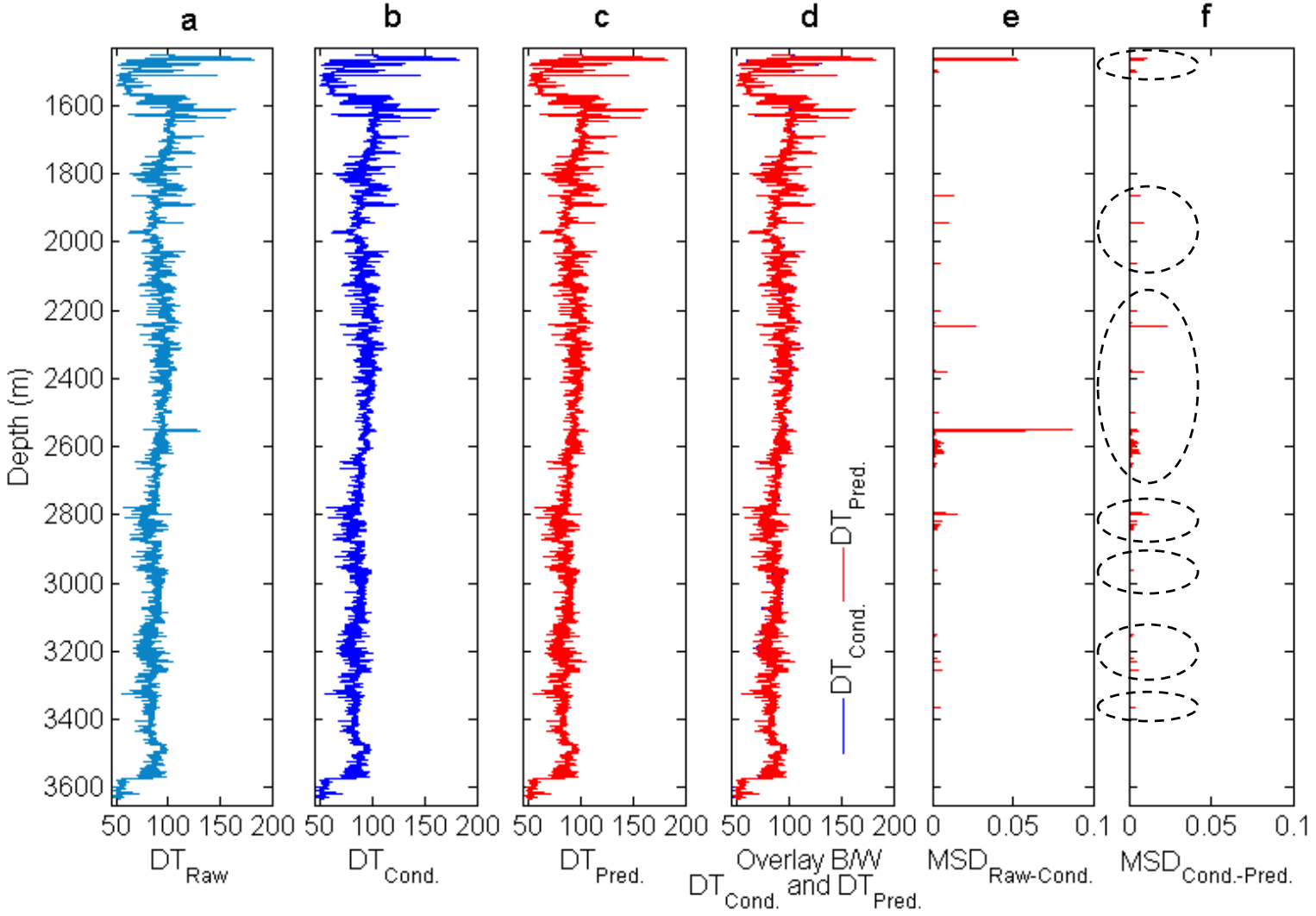


Fig. 125

| Mean Square Error | Value |
|---|---|
| B/W Raw and Conditioned | 1.6535 |
| B/W Conditioned and Predicted | 0. 6165 |

MSD- Mean square difference

$$MSD = \frac{1}{n}\left(y_{cond/raw,i} - y_{pred,i}\right)^2$$

MSE- Mean square error

$$MSE = \frac{1}{n}\sum_{i=1}^{n}\left(y_{cond/raw,i} - y_{pred,i}\right)^2$$

$y_{cond,\,i}$; $y_{raw,\,i}$; $y_{pred,\,i}$ are the conditioned, raw and predicted values at the $i^{th}$ data point

# Results for well B2

**(a) raw sonic log, (b) conditioned sonic logs (c) predicted sonic logs (d) overlay plot of conditioned and predicted logs (e) depth-wise mean square deviation between raw and conditioned sonic logs (f) depth-wise mean square deviation between conditioned and predicted sonic logs at well B2.**

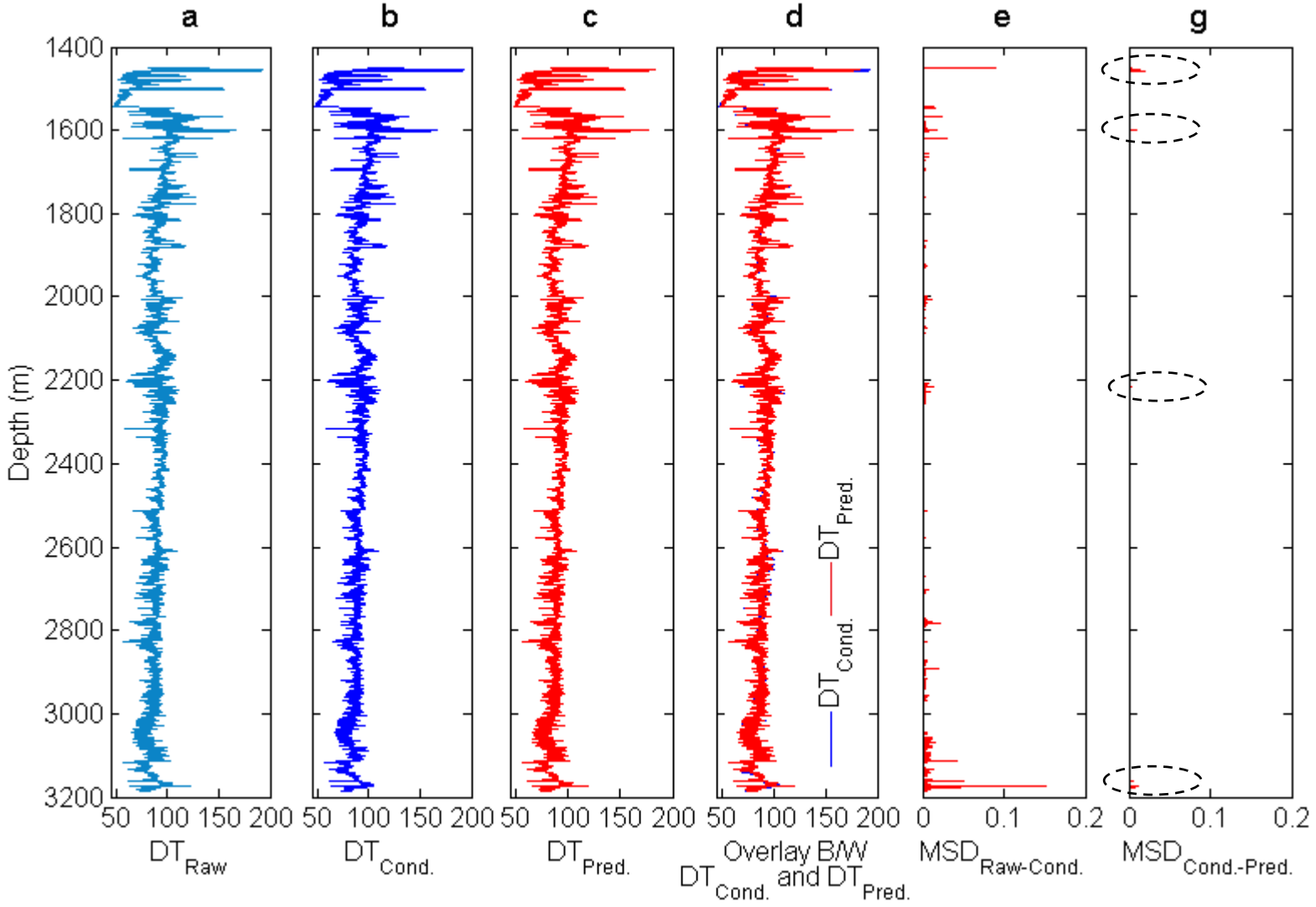


| Mean Square Error | Value |
|---|---|
| B/W Raw and Conditioned | 5.0513 |
| B/W Conditioned and Predicted | 1.1916 |

Fig. 126

# Results for well B4

**(a) raw sonic log, (b) conditioned sonic logs (c) predicted sonic logs (d) overlay plot of conditioned and predicted logs (e) depth-wise mean square deviation between raw and conditioned sonic logs (f) depth-wise mean square deviation between conditioned and predicted sonic logs at well B4.**

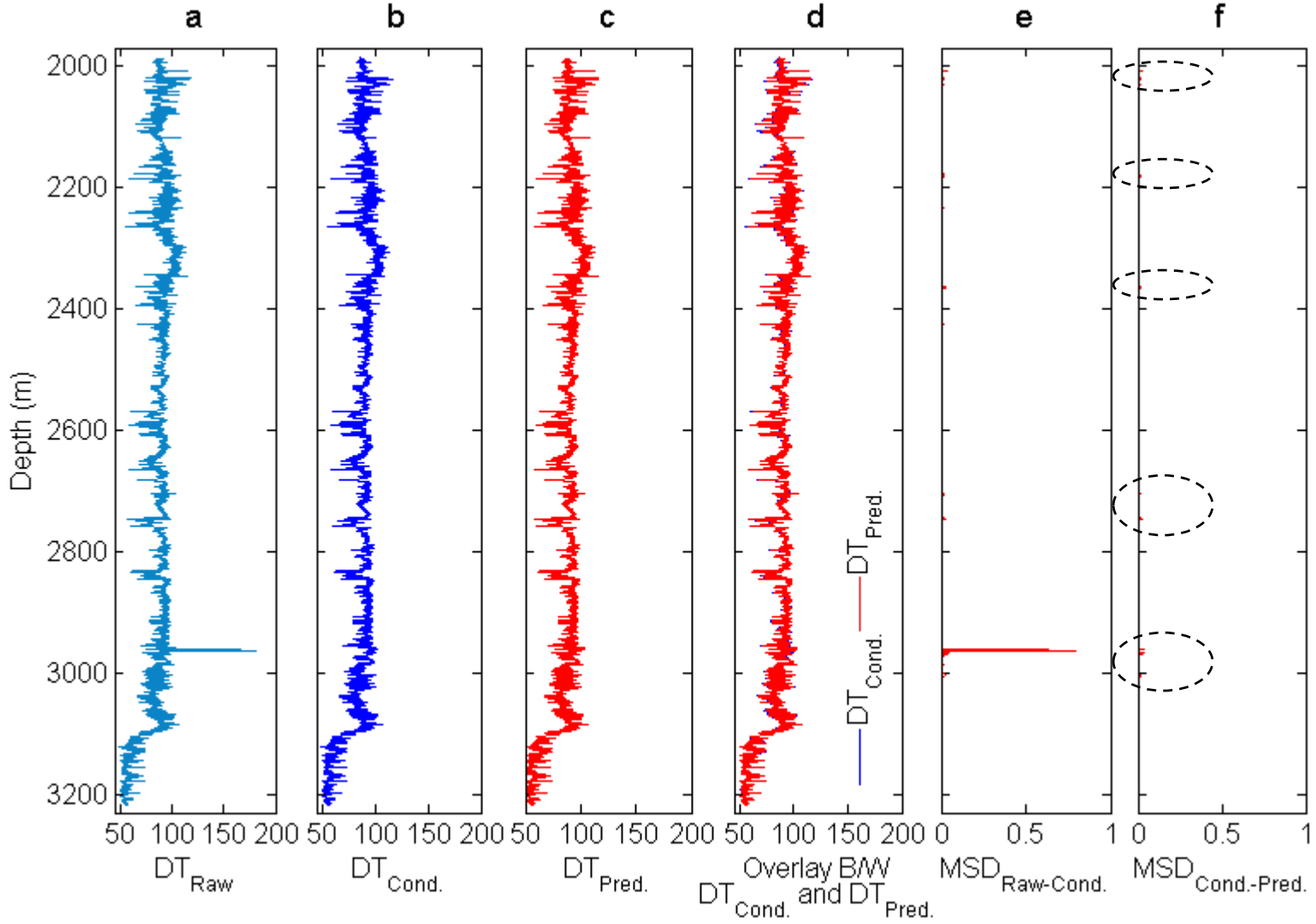


Fig. 127

| Mean Square Error | Value |
|---|---|
| B/W Raw and Conditioned | 3.8769 |
| B/W Conditioned and Predicted | 0.8394 |

Thank you!